Electronic Supplementary Material (ESI) for Catalysis Science & Technology.

Supporting Information

Large Changes in Hydricity as a Function of Charge and Not Metal in (PNP)M-H (De)hydrogenation Catalysts That Undergo Metal-Ligand Cooperativity

Kevin Schlenker, Lillee K. Casselman, Ryan T. VanderLinden, and Caroline T. Saouma*

Department of Chemistry, University of Utah, Salt Lake City, Utah, 84112, U.S.A.

Contents

Section 1: General Considerations

A. Materials and Reagents.

Unless noted, all experiments were performed in a nitrogen-filled glovebox or using standard Schlenk techniques. Experiments performed in air-free conditions outside of the glovebox were conducted utilizing Teflon sealed glassware. Gas additions were done using a Schlenk line and pressure noted with a mercury monometer. J. Young valved NMR tubes were used for ambient pressure and stoichiometric gas addition reactions. Glassware was oven-dried at 160 °C for 24 hours prior to use. Molecular sieves were activated at 180 °C under vacuum for 72 hours and stored in the glovebox. Atmospheric pressure at Salt Lake City, Utah, USA is taken to be 0.85 atm.

All non-deuterated solvents were sparged and stored under nitrogen then collected from a Pure Process Technology solvent purification system to remove oxygen and water, stored over activated 3 Å molecular sieves in the glovebox, and tested with ketyl radical before use. NMR solvents were obtained from Cambridge Isotope Labs, subjected to 3 freeze-pump-thaw cycles, and stored under nitrogen in the glovebox over sieves. Bone-dry CO_2 (99.9%; 10 ppm H_2O) and Ultra-high purity (UHP) H_2 (99.999%; 1 ppm O_2, 1 ppm H_2O, 0.5 ppm THC, 1 ppm CO, 1 ppm CO_2, 5 ppm N_2) gases were purchased from Airgas. $^{15}N_2$ (98%+) was purchased from Cambridge Isotope Laboratories, Inc. in a 1L lecture bottle. **[(3,5-(CF$_3$)$_2$C$_6$H$_3$)$_4$B][Na]**,[1] **[(3,5-(CF$_3$)$_2$C$_6$H$_3$)$_4$B][H(OEt$_2$)$_2$]** (synthesis[2] and purification[3]), **Ph(CH$_3$)C=P(2,4,6-(MeO)$_3$-C$_6$H$_2$)$_3$**,[4] **PNP** ligand [2,6-bis-(di-tert-butylphosphinomethyl)pyridine],[5] **[(PNP)(CO)(H)Ru][BAr$_4^F$]**,[6] **(*PNP)(CO)(H)Ru**,[7] **(PNP)(CO)(H)Ru-H**,[8] **(PNP)(CO)(H)Fe-H**,[9] **(PNP)(CO)(H)Fe-OCHO**,[9] **(*PNP)Co-N$_2$**,[10] **(PNP)Co-H**,[10] **(PNP)Co-OCHO**,[11] and **[(PNP)Co-N$_2$][BAr$_4^F$]**,[12] were prepared according to literature procedures. A*nhydrous* formic acid and **[HBF$_4$][^{tBu}N=P$_4$(Me$_2$N)$_9$]** were prepared as previously reported.[13] The phosphazene bases **^{tBu}N=P$_1$(NC$_4$H$_8$)$_3$** and **^{tBu}N=P$_4$(Me$_2$N)$_9$** were purchased from Sigma Aldrich and used without further purification. All other reagents were purchased commercially and used without further purification.

B. Instrumentation.

Ambient temperature UV-vis measurements were conducted on an Agilent Cary-60 spectrophotometer fitted with a TC-40 cuvette holder (with stirring) equipped with a TC 125 temperature controller or a Q6 sample changer equipped with a Koolance 440 circulator temperature (both from Quantum Northwest). UV-Vis spectra taken at -78°C were done using an Agilent 8453a spectrometer equipped with a Unisoko Cool-Spec cryostat.

NMR spectra were recorded on 300 or 500 MHz instruments. (Bruker Neo Avance 500 or Varian/ Agilent Directdrive VXR-500) ^{1}H and ^{13}C NMR spectra were referenced to their respective deuterated solvents and ^{31}P NMR spectra were referenced externally to H_3PO_4. Delay times were chosen to ensure accurate integrations. Briefly, a series of spectra were collected with different delay times, and the minimum delay at which the relative integrations stopped changing was employed. Analysis of NMR spectra was completed using Mestrenova (Version: 14.1.0-24037).

IR spectra were recorded using an Agilent Cary 630 FTIR spectrometer using ATR or FTIR mode. Solution-phase IR were done using THF solutions of complexes sandwiched between two KBr plates with the instrument in FTIR mode.

C. Error Analysis.

For the determination of K_{eq} values, error bars on individual points correspond to the standard deviation from multiple trials. Weighted linear regression was done with OriginPro 2019b (64-bit) 9.6.5.169.

Unless noted, reported errors are obtained via propagation in uncertainties of established values and/or measurements. All thermochemical data were conducted with multiple equivalence to get an averaged value for each trial, and final values are obtained from several trials.

For every thermochemical measurement, care is taken to ensure that the equilibrium constants we provide arise from true equilibria with no side products. This encompasses:

1. Only doing the thermochemical titrations from material that is stored in a freshly regenerated glovebox. These compounds are highly sensitive and trace moisture impacts stability, particularly for the anionic species. We have an O_2 sensor and have found that keeping a vial open with 1 mL of a stock solution of sodium benzophenone in THF gives us a good indication of when we need to regenerate our glovebox due to moisture concerns. Some of the characterization data shows impurities as these were collected when the box atmosphere was slightly wet and before we knew how to address the issue. With a freshly regenerated glovebox, the impurities (if present) are significantly diminished. We are transparent in showing all the data when we do titrations, including where impurities or side products if competing equilibria are present, such that it is evident the titrations represent true equilibria from clean starting materials.
2. Ensuring that the starting materials are pure. In some instances, the starting material has a minor impurity (less than 5%), and every single spectrum of the titration is analyzed to ensure that the impurity remains constant, ensuring that it is not a part of the equilibrium/reacting with the equilibrium partner. The impurity is taken into account when determining the initial concentrations such that there is not a systematic error. This is true whether the impurity is in the metal complex or titrating partner.
3. Ensuring no side reactions occur. Trials whereby an impurity grows or diminishes are omitted, as these do not represent true equilibria.
4. When using strong bases, we deprotonate the conjugate acid immediately prior to the titrations, to ensure we are not starting with a mixture of base and conjugate acid. We noticed that our starting concentration of base was not what we thought it was as we were getting non-zero intercepts in our plots, and as soon as we switched to this approach, our intercepts became zero.
5. Check if protonated species is due to trace moisture in the system prior to doing reactions. We have found that sometimes trace moisture on the NMR tubes is

sufficient to protonate the anions, so we always collect NMR spectra before adding any reagent to ensure that what we are observing is not due to trace moisture or other impurities. Even if we flame dry a Schlenk line under vacuum, sometimes trace moisture gets into j. young tubes or other glassware when we add gases. This impacts the level of impurities in some analysis, for example when using $^{15}N_2$.

6. When mass balance is assumed, we take care to test this. For example, using an internal standard to ensure that before/after adding the titration partner the overall mass of the species does not change. Sometimes the relative species are integrated against each other to ensure mass balance; in doing titrations with strong bases, we ensure that the overall integration of the base/conjugate base relative to the overall integration of metal containing species is what we expect it to be; deviations would suggest degradation or formation of a paramagnetic species and hence are not used. When possible, we determine the equilibrium constant with and without mass balance assumptions to make sure that the assumption is valid. In the case of not being able to see some of the species, for example if they are too broad to observe by ^{31}P NMR spectroscopy or because they are colorless and so do not appear in the UV-vis spectra, we look for side reactions (new species, loss or formation of unexpected isosbestic points, etc.) and if possible use an internal standard to ensure the species we can observe remains constant and is not reacting in an unexpected way.
7. Data is collected from multiple trials, and within each trial, there are multiple solutions analyzed. For equilibrium studies, we do not use a single point to evaluate *K*. Rather, we collect several points with different equivalents of an equilibrium partner, so that from a plot we obtain *K*. This averages out error. These points are typically collected from different equilibria (i.e., not by sequential addition). Finally, this process is repeated so that the values represent multiple trials, obtained from different batches of material on different days.

D. Crystal Structure Determination.

Single-crystal X-ray diffraction data for **[K(THF)$_3$][(*PNP)(CO)(H)Ru-H]**, **[(*PNP)(CO)(H)Fe]$_2$(μ-N$_2$)** and **[(PNP)(CO)(H)Fe][BAr$_4^F$]** were collected either on a Nonius Kappa CCD diffractometer equipped with a BRUKER APEXII CCD detector (University of Utah) or a Bruker D8 Venture with a Bruker Photon-III detector (Brigham Young University) utilizing Mo K_α radiation (λ = 0.71073 Å), respectively. The APEX3[14] software suite was used to manage data collection, integration (SAINT), absorption correction by the Multi-scan method (SADABS or TWINABS[15] for non-merohedral twinning), structure determination via direct methods (SHELXT[16]), and model refinement (SHELXL[17]) using established refinement strategies[18]. All data was collected either at 100 K (BYU) or 103 K (UofU). Positional disorder was modelled as two-part disorder with appropriate distance, angle, and ADP restraints. All non-hydrogen atoms were refined anisotropically. All hydrogens were calculated geometrically and refined using a riding model except two hydrides coordinated to Ru in **[K(THF)$_3$][(*PNP)(CO)(H)Ru-H]**, which were identified from Q peaks and only restrained to be equidistant from the Ru atom. The

structure of **[K(THF)$_3$][(*PNP)(CO)(H)Ru-H]**, has been deposited with the Cambridge Crystallographic Data Centre (CCDC 2192117).

For **[(PNP)(CO)(H)Fe][BAr$_4^F$]** all non-hydrogen atoms were refined anisotropically. An N_2 molecule was modelled at 50% occupancy on two opposing sides of the Fe center. Our NMR data show a hydride should also be bound to the Fe center, which would likely oppose the N_2 in the structure and explain the partial occupancy. However, the hydride could not be confidently modelled. Positional disorder was observed in the $-CF_3$ groups of the **[(3,5-(CF$_3$)$_2$C$_6$H$_3$)$_4$B]**$^-$ anion and modelled using the PART command as two-part disorder with appropriate distance, angle, and atomic displacement parameter restraints/constraints. The positions of all hydrogen atoms were calculated geometrically and refined using a riding model. This crystal structure has been deposited with the Cambridge Crystallographic Data Centre (CCDC: 2081604).

[(*PNP)(CO)(H)Fe]$_2$(μ-N$_2$) was identified as a non-merohedral twin. We used a large crystal (0.3 Å x 0.2 Å x 0.1 Å) for best resolution data (0.9 Å). Using smaller crystals did not reduce the complexity of the twinning it only reduced resolution. CELL_NOW was used to identify a three-part twin that accounted for 70% of the reflections. Reflection intensities for the three domains were separated during integration. A structure was determined, the anticipated structure was easily modelled, and then all atoms were refined isotopically resulting in R1/wR2 values 28%/55%. Better crystals were unattainable. Due to the low quality of this data set the structure was not deposited with the CCDC but the structure was validated through NMR and IR spectroscopy.

Section 2: Synthesis and Characterization of Compounds

A. Synthesis of (*PNP)(CO)(H)Fe.

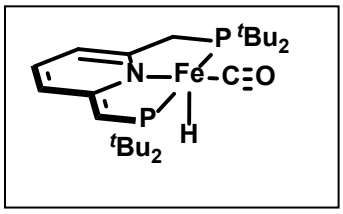

(PNP)(CO)(H)Fe-OCHO (357 mg, 0.68 mmol) was suspended in 10 mL of diethyl ether in a 20 mL scintillation vial containing a stir bar. 76 mg of solid KO^{t}Bu (0.68 mmol) was added all at once to the stirring orange suspension, which immediately gave a dark blue solution. The reaction was left to stir at room temperature for 30 minutes before all volatiles were removed *in vacuo*. The blue residue was extracted with 5 x 20 mL portions of diethyl ether and filtered through celite. Concentration of the blue filtrate and recrystallization at -40°C from diethyl ether yielded material of ~95% purity based on ^{31}P{^{1}H} NMR spectroscopy. Crystals grown from pentanes at -40°C yielded orange blocks. A preliminary crystal structure suggests an N_2 bridged dimer, however, severe twinning and disorder precludes satisfactory refinement. (Yield: 285 mg, 87%). Dissolution of the crystals in THF at room temperature gives a blue solution.

Please see section B for details on the speciation. At room-temperature, we believe the structure shown above may be in equilibrium with a 6-coordinate, THF bound congener. Room temperature NMR data therefore represent averaged signals.

^{1}H (THF-d_8, 25°C, 500 MHz, ppm): -41.57 (1H, br, m, J_{HP} = 51.1 Hz, J_{HP} = 63 Hz, Fe-*H*), 1.19 (9H, d, J_{HP} = 12.6 Hz, -C(C*H*$_3$)$_3$), 1.26 (18H, d, J_{HP} = 13.0 Hz, -C(C*H*$_3$)$_3$), 1.30 (9H, d, J_{HP} = 12.7 Hz, -C(C*H*$_3$)$_3$), 3.00-3.25 (2H, m, -C*HH*-), 3.61 (br, -C*H*- + THF), 5.42 (1H, d, J_{HH} = 6.2 Hz, py), 6.07 (1H, d, J_{HH} = 8.9 Hz, py) 6.22 (1H, t, J_{HH} = 7.8 Hz, py).

^{1}H{^{31}P} (THF-d_8, 25°C, 500 MHz, ppm): -41.57 (1H, s, Fe-*H*), 1.19 (9H, s, -C(C*H*$_3$)$_3$), 1.26 (18H, s, -C(C*H*$_3$)$_3$), 1.30 (9H, s, -C(C*H*$_3$)$_3$), 3.04 (1H, d, J_{HH} = 17.0 Hz, -C*H*H-), 3.20 (1H, d, J_{HH} = 17.0 Hz, -CH*H*-), 3.61 (br, -C*H*- + THF), 5.42 (1H, d, J_{HH} = 6.2 Hz, py), 6.07 (1H, d, J_{HH} = 8.9Hz, py) 6.22 (1H, t, J_{HH} = 7.8 Hz, py).

^{31}P{^{1}H} (THF-d_8, 25°C, 202 MHz, ppm): 96.7 (d, J_{PP} = 112 Hz, -*P*(^{t}Bu)$_2$), 86.9 (d, J_{PP} = 111 Hz, -*P*(^{t}Bu)$_2$).

^{15}N{^{1}H} (THF-d_8, -78°C, 51 MHz, ppm): -43 ppm (br, $\Delta\nu_{1/2}$ = 19.4 Hz).

^{13}C{^{1}H} (THF-d_8, 25°C, 126 MHz, ppm): 220.7 (br, -*C*O), 174.6 (dd, J_{PC} = 22.2, J_{PC} = 6.3 Hz, py), 162.4 (dd, J_{PC} = 6.1 Hz, J_{PC} = 5.9 Hz, py), 132.4 (s, py), 115.2 (d, J_{PC} = 18.3 Hz, py) 98.26 (d, J_{PC} = 11.1 Hz, py) 69.4 (d, J_{PC} = 46.0 Hz, -*C*H-), 39.0 (d, J_{PC} = 19.5 Hz, -P(*C*(CH$_3$)$_3$)$_2$), 35.9 (d, J_{PC} = 14.1 Hz, -P(*C*(CH$_3$)$_3$)$_2$), 35.3 (d, J_{PC} = 17.3 Hz, -*C*HH-), 35.1 (d, J_{PC} = 24.9 Hz, -P(*C*(CH$_3$)$_3$)$_2$), 34.7 (d, J_{PC} = 14.7 Hz, -P(*C*(CH$_3$)$_3$)$_2$), 29.7 (br, -P(C(*C*H$_3$)$_3$)$_2$), 29.1 (m, -P(C(*C*H$_3$)$_3$)$_2$), 29.0 (m, -P(C(*C*H$_3$)$_3$)$_2$), 28.9 (m, -P(C(*C*H$_3$)$_3$)$_2$).

Similar P-C coupling constants are obtained in the analogous **(*PNP)(H)(CO)Ru**.[19]

IR (THF, KBR plate, cm^{-1}): 1878 (*CO*). No N_2 stretches are observed.

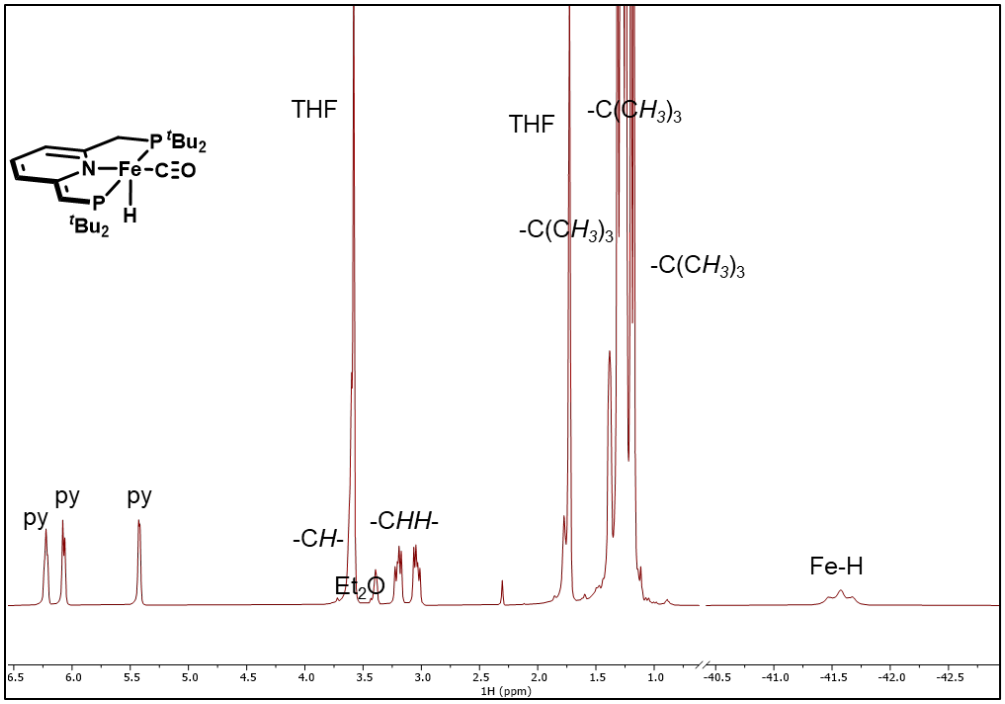

Figure S1. ^{1}H NMR spectrum (500 MHz, 298K, THF-d_8) of **(*PNP)(CO)(H)Fe.**

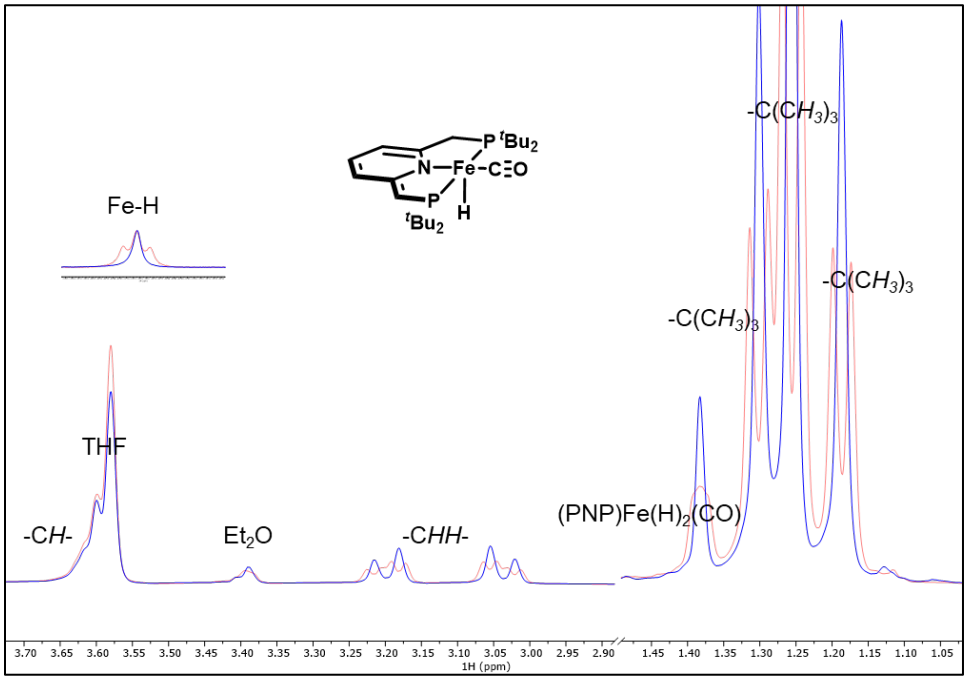

Figure S2. Superimposed ^{1}H NMR (red) and ^{1}H{^{31}P} NMR (blue) spectra (500 MHz, 298K, THF-d_8) of **(*PNP)(CO)(H)Fe**.

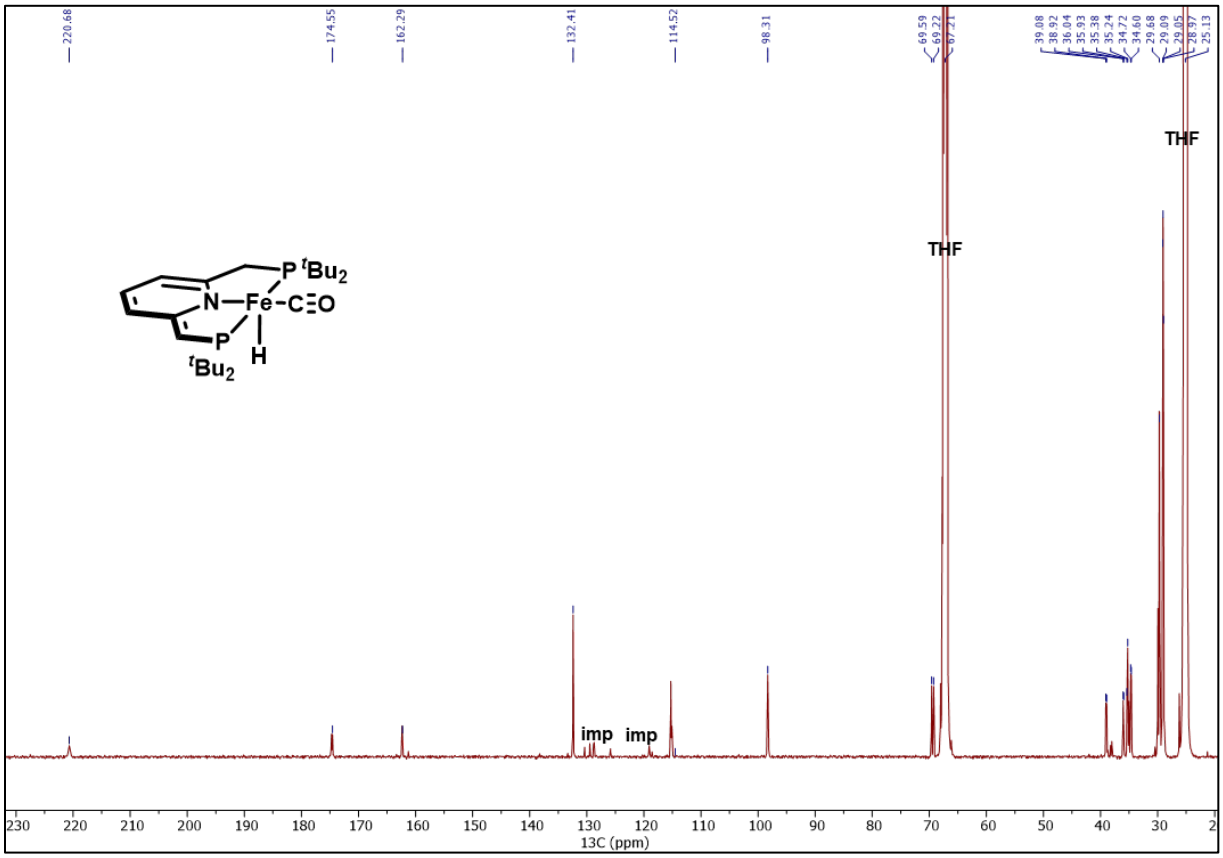

Figure S3. $^{13}C\{^{1}H\}$ NMR (126 MHz, 298K, THF-d_8) spectrum of **(*PNP)(CO)(H)Fe**.

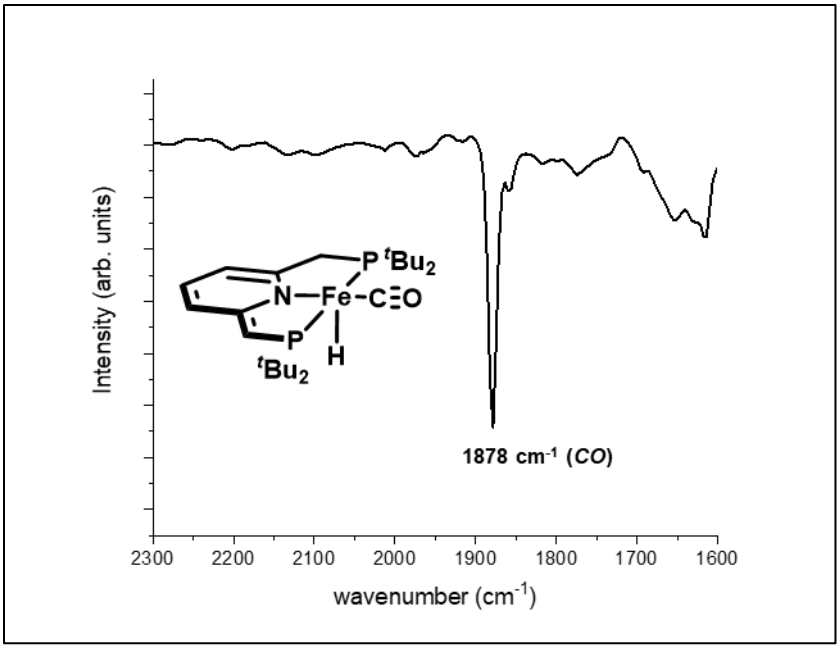

Figure S4. FT-IR spectrum (THF, KBr plate, room temp.) of **(*PNP)(CO)(H)Fe**. The solvent THF is used as the background and subtracted from the final spectrum.

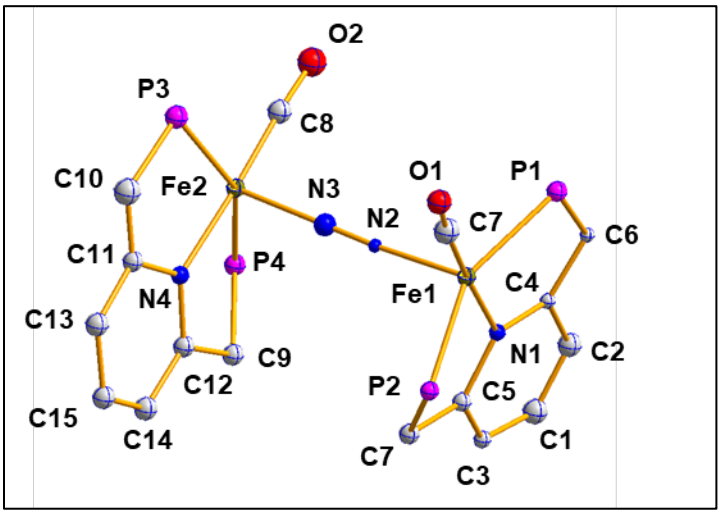

Figure S5. Molecular structure of **[(*PNP)(CO)(H)Fe]$_2$(μ-N$_2$)** with 50% probability thermal ellipsoids. Hydrogen atoms and the tert-butyl substituents on the phosphines were removed for clarity. This structure is not of sufficient quality for publication and is included to simply show connectivity.

B. Characterization of the (*PNP)(CO)(H)Fe Equilibrium.

In solution, **(*PNP)(CO)(H)Fe** exists as an equilibrium mixture of species which is best described as that shown below. For thermodynamic studies (H_2 equilibrium), we assume that structure **A** is correct; inclusion of a THF or N_2 molecule changes the molecular weight and hence molarity of solutions. However, since only the ratio of the product to starting material is required, concentration errors do not impact the final values. Further discussion of concentration error is given in section 4B of this SI.

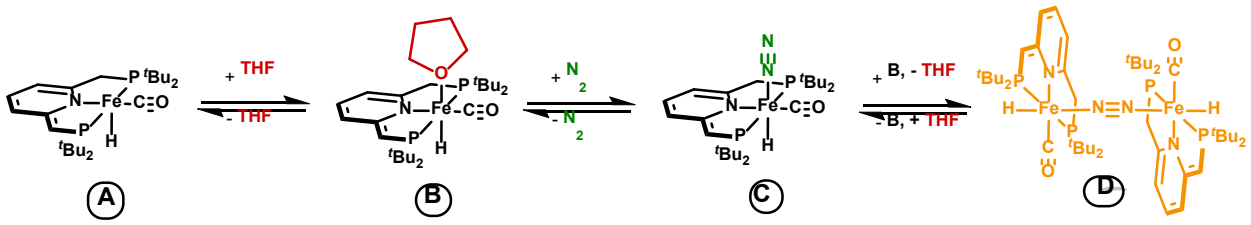

Evidence for this equilibrium is as follows.

First, room temperature solutions of **(*PNP)(CO)(H)Fe** are dark blue, whilst at reduced temperatures, solutions are orange. The color change is reversible and hence is consistent with a change in speciation. The temperature-dependent UV-vis spectra are shown in Figure S6. Second, the preliminary crystal structure is consistent with a dimer that contains a two-atom bridge, with each metal center retaining a 2-atom terminal ligand (presumably CO) (Figure S5). When the crystals are warmed to room temperature, outgassing is evident through bubble formation and crystal cracking. Thus, the solid-state structure is consistent with structure **D**. Given the color of the crystal and the color of solutions at reduced temperatures is the same, structure **D** is likely to be the major isomer at reduced temperatures.

Variable temperature NMR studies were then done under either a $^{14}N_2$ or a $^{15}N_2$ atmosphere. **(*PNP)(CO)(H)Fe** (19 mg, 39 μmol) was dissolved in 0.5 mL of THF-d_8 in a Teflon sealed J Young NMR tube to give a blue solution. The tube was sealed, placed on the Schlenk line, and frozen under lN_2. The atmosphere was evacuated and replaced with 0.65 atm of $^{15}N_2$ while still frozen. After sealing the tube, the reaction was placed at room temperature before collecting the VT NMR spectra. At -78°C, removal of the J Young tube from the NMR spectrometer shows that the blue solution has become dark yellow/orange. During the reaction, the decomposition of (*PNP)Fe(H)(CO) to give (PNP)Fe(H)$_2$(CO), (PNP)Fe(CO)$_2$, and free ligand was observed, similar to that described in the literature for the ^{iPr}PNP variant.[20] The VT NMR study was repeated under $^{14}N_2$ (glovebox) atmosphere.

At room temperature, a single set of resonances is observed in the ^{31}P and ^{1}H NMR spectra. Two broad doublets at 96.7 and 86.9 in the ^{31}P NMR spectrum is consistent with a de-aromatized ligand, while the apparent broad triplet at -41.6 in the ^{1}H NMR spectrum is consistent with a hydride coupling to two phosphorous atoms (upon ^{31}P decoupling, this signal collapses to a singlet). Cooling to -20 °C results in these resonances broadening, which sharpen up as the temperature is further cooled to -78 °C. This is consistent with an averaged "fast-exchange" occurring at room temperature and freezing out of two individual isomers at reduced temperatures (See Figure S9). The ^{31}P NMR

chemical shifts of these resonances are not constant as the temperature is varied, suggesting a complex equilibrium that is proposed to occur between species **A**, **B**, and **C** or that the equilibrium between **A** and **B** is temperature-dependent (Figure S10). The isomers involved in this equilibrium have similar ^{31}P and ^{1}H NMR chemical shifts and are proposed to all be monomeric.

Room temperature solution-phase IR (Figure S4) shows no N_2 stretch, suggesting that **C** is not present at room temperature. The VT ^{15}N NMR studies also show no evidence for a terminal N_2 species, whereby the two N ligands would have distinct chemical shifts. Owing to the complex equilibria observed in the VT NMR spectra, this species is included to account for the shifting of the resonances, and we hypothesize is present in very small amounts. At reduced temperatures, the two "monomeric" isomers are thought to be **A** and **B**. Note, **(*^{i}Pr^{t}PNP)(CO)(H)Fe** coordinates L-type ligands at room temperature, akin to **B**.[20] Structure **A** is invoked by analogy to the 5-coordinate Ru analogue.[19]

Starting at -40 °C, a new set of resonances that are well-shifted from the above-described equilibrium appear and sharpen upon cooling to -78 °C. At -78 °C, this species has two resonances in the ^{31}P NMR spectrum, and an apparent triplet in the ^{1}H NMR spectrum, corresponding to the Fe-H. In the ^{15}N NMR spectrum (Figure S7), a single peak appears at -43.1 ppm. The ^{15}N NMR spectra is internally referenced by the instrument from the lock signal on THF-d_8, and the 0 ppm of the instrument is set as nitromethane. Free $^{15}N_2$ gas ($\delta = -71$ ppm)[21] is not observed. The appearance of a single resonance is consistent with structure **D**. Hence, the resonances that only appear at reduced temperatures (described in this paragraph) are attributed to isomer **D**. This structure gives rise to the orange color. The shift in the ^{31}P NMR resonances upon cooling suggests that **D** is in equilibrium with monomeric species.

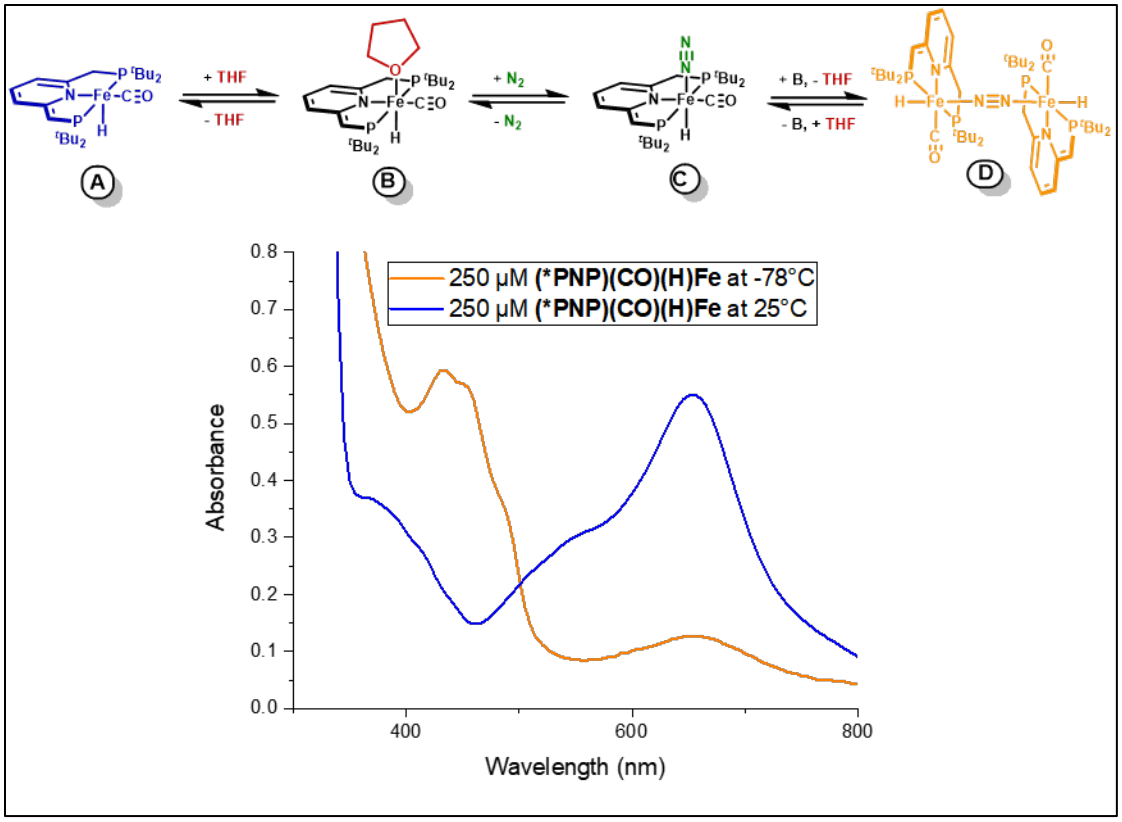

Figure S6. UV-Vis Spectra demonstrating the speciation change and accompanying color change upon cooling **(*PNP)(CO)(H)Fe** at 25°C (blue) and -78°C (orange). When warmed up again, the color reverts to blue.

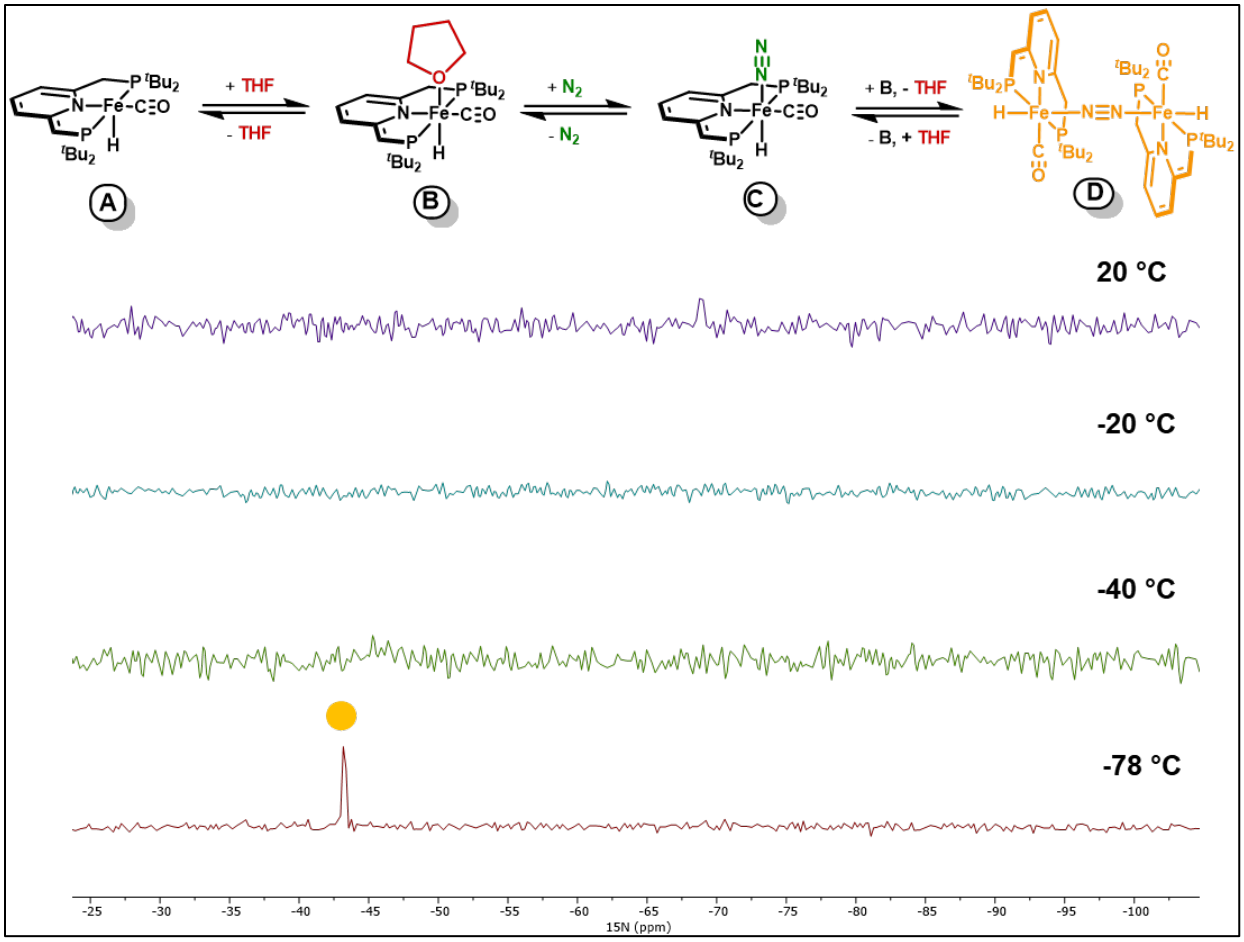

Figure S7. VT $^{15}N\{^{1}H\}$ NMR spectra (51 MHz, VT, THF-d_8) of **(*PNP)(CO)(H)Fe** under $^{15}N_2$ atmosphere. This is consistent with **D** forming at reduced temperatures, and only A/B present at room temperature. If **C** forms, the concentration is too low to be detected.

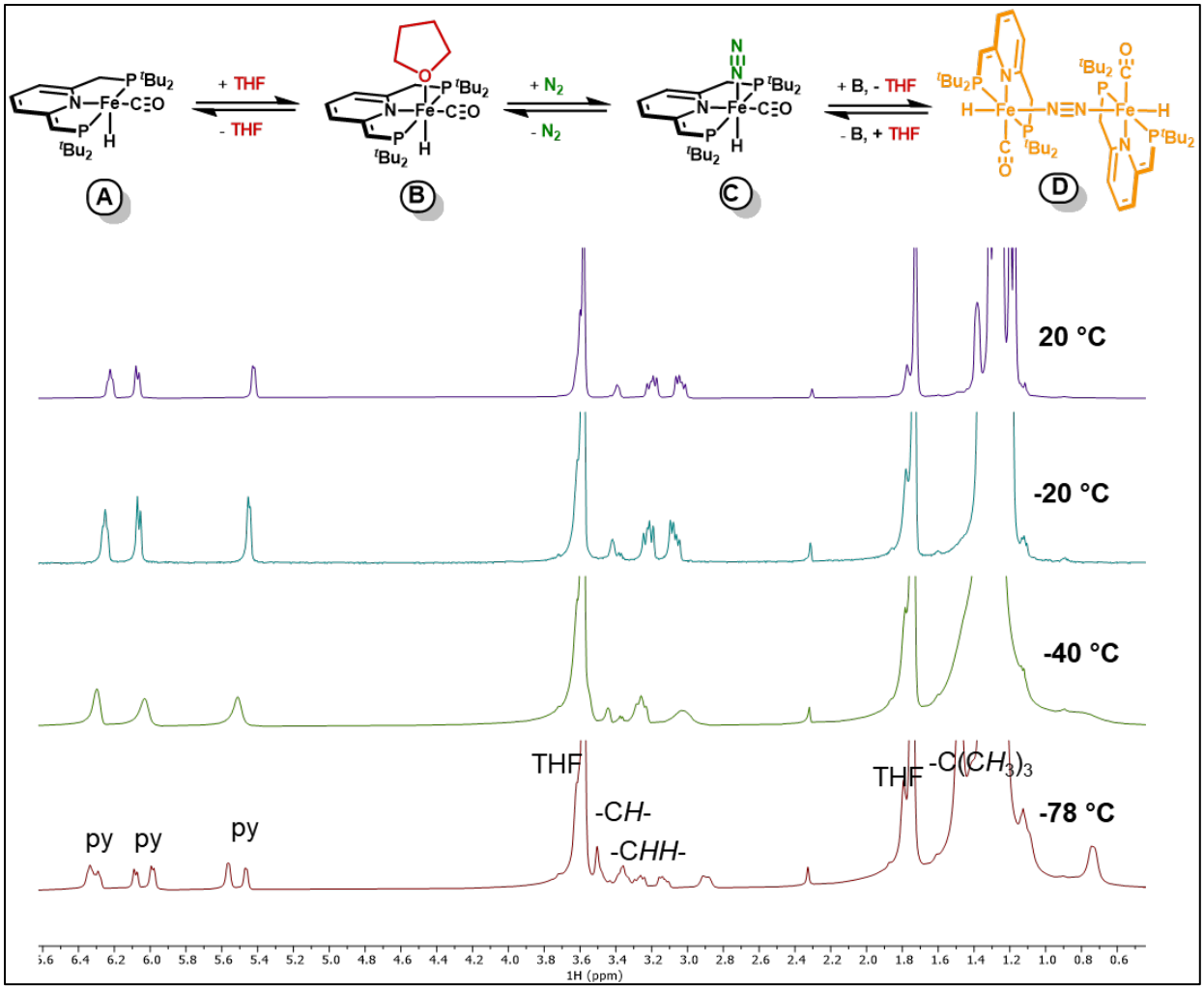

Figure S8. VT ^{1}H NMR spectra (500 MHz, VT, THF-d_8) of **(*PNP)(CO)(H)Fe** under N_2 atmosphere.

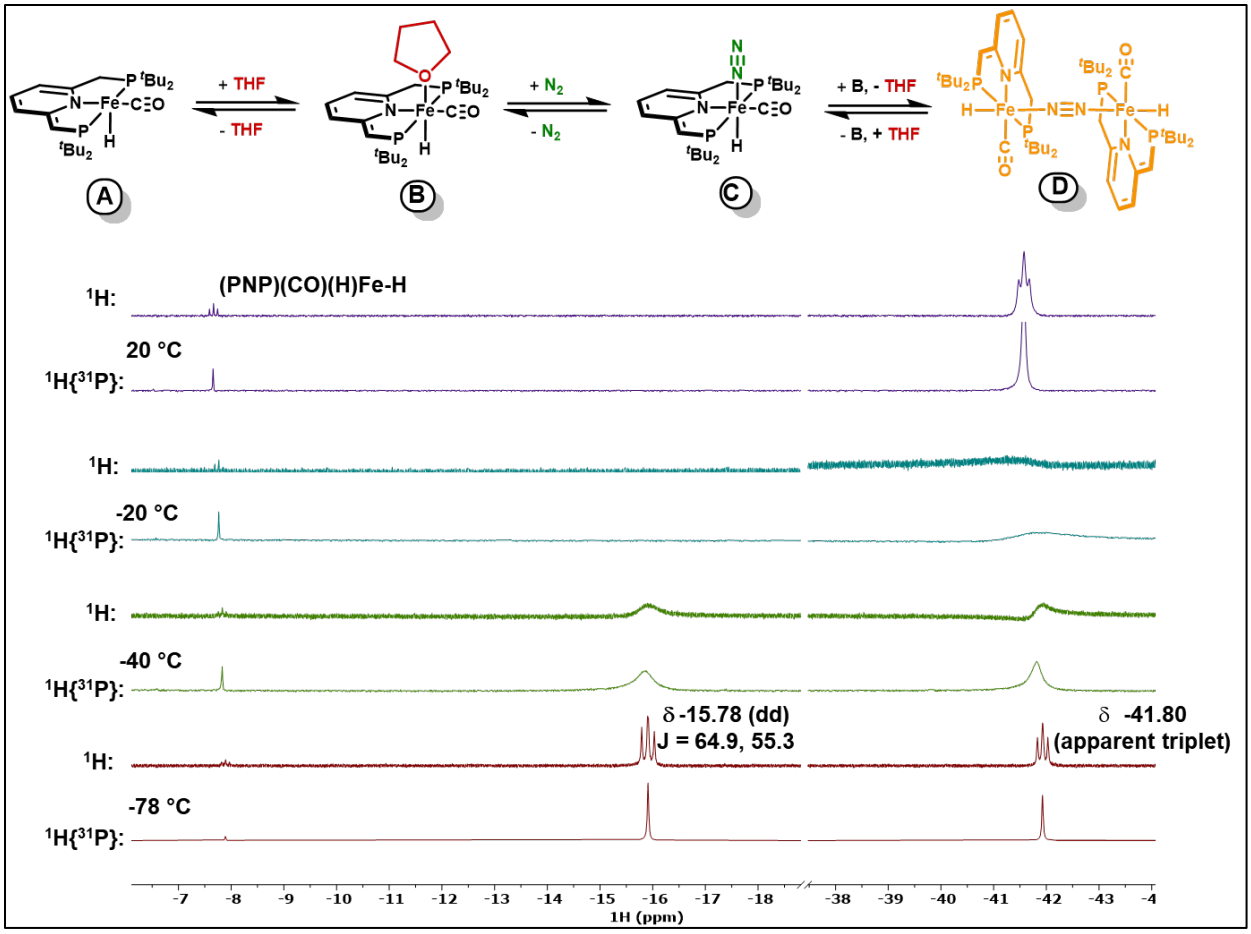

Figure S9. VT ^{1}H/1H{^{31}P} NMR (500 MHz, VT, THF-d_8) spectra of **(*PNP)(CO)(H)Fe** under N_2 atmosphere showing only the hydride region of the ^{1}H NMR spectra. The hydride resonance at -15.78 ppm is attributed to structure **D**, whilst that at -41.80 is attributed to **A**/**B**.

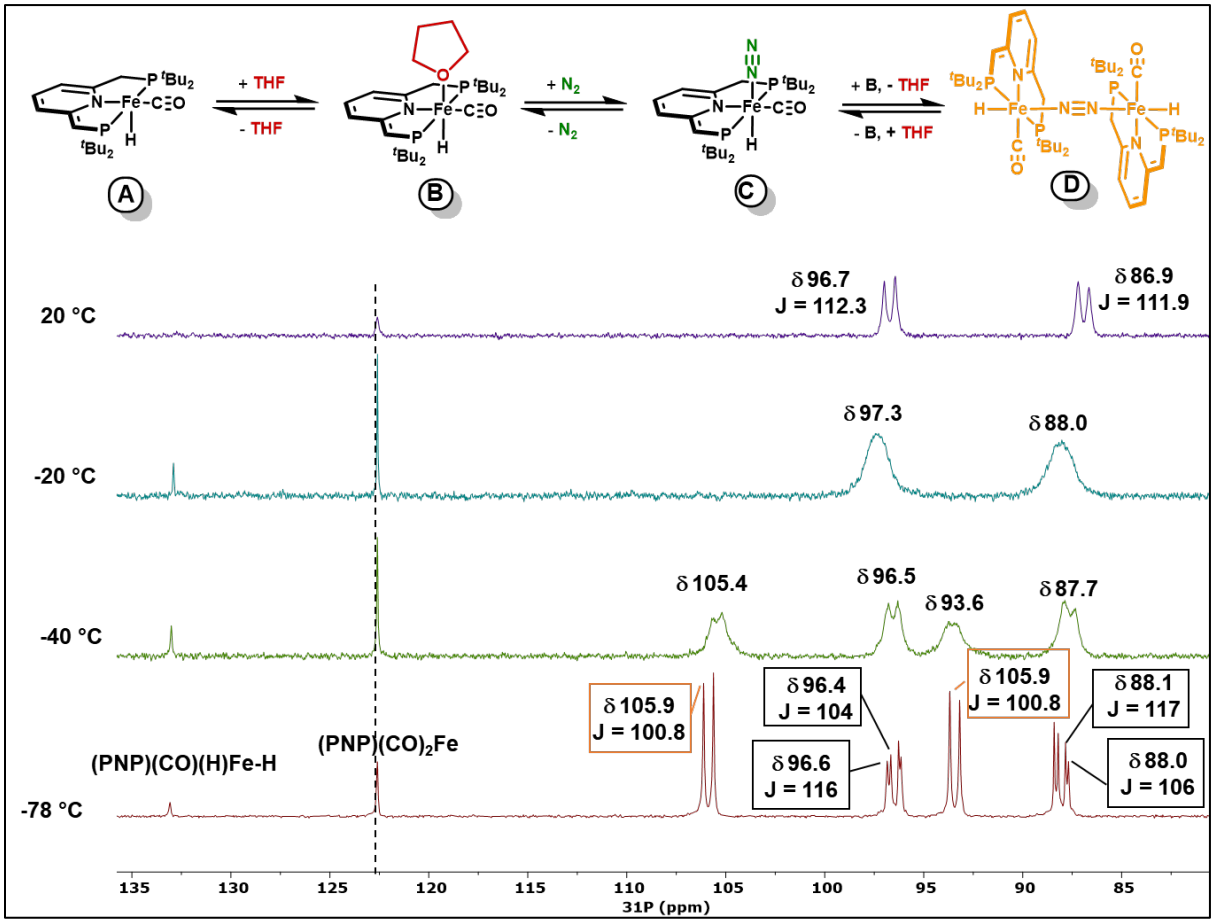

Figure S10. VT $^{31}P\{^{1}H\}$ NMR spectra (202 MHz, VT, THF-d_8) of **(*PNP)(CO)(H)Fe** under N_2 atmosphere. The resonances with orange boxes are attributed to structure **D**, whilst the others are attributed to **A**/**B**.

C. Synthesis of [(PNP)(CO)(H)Fe][BAr_4^F].

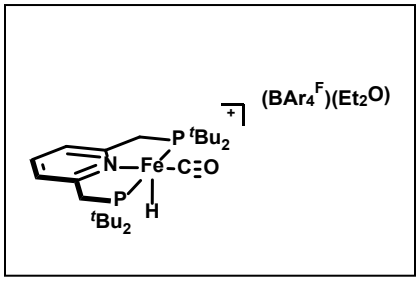

(*PNP)(CO)(H)Fe (61 mg, 0.13 mmol) was dissolved in 10 mL of Et_2O. To the blue solution was added **$H(Et_2O)_2BAr_4^F$** (129 mg, 0.13 mmol) at room temperature. Immediately upon addition of the acid, the dark blue solution became dark purple. The reaction was stirred for ten minutes and all volatiles removed *in vacuo*. The purple residue was dissolved in Et_2O, filtered through celite, and placed in the freezer at -40°C to yield dark red crystals suitable for x-ray diffraction (137 mg, 74% yield). Allowing the crystals to warm to room temperature results in the formation of bubbles in the paraffin oil, likely a result of losing N_2 gas. Hence, collection of the crystals was achieved through decanting the solvent and placing the resulting crystals in paraffin oil at -78°C.

Please see section D for details on the speciation. At room-temperature, we believe the structure shown above may be in equilibrium with a 6-coordinate, N_2 bound congener. Room temperature NMR data therefore represent averaged signals.

^{1}H NMR (THF-d_8, 25°C, 500 MHz, ppm): -15.7 (br, Fe-*H*), 1.11 (6H, t, J_{HH} = 6.8 Hz, (CH_3CH_2)$_2$O), 1.27-1.37 (36H, m, -C(CH_3)$_3$), 3.39 (4H, q, J_{HH} = 6.9 Hz, (CH_3CH_2)$_2$O), 3.91-4.05 (4H, m, -CH_2-), 7.57 (4H, s, BAr_4^F), 7.65 (2H, d, J_{HH} = 7.8 Hz, py), 7.79 (8H, BAr_4^F), 7.93 (1H, t J_{HH} = 7.7 Hz, py).

^{1}H{^{31}P} NMR (THF-d_8, 25°C, 500 MHz, ppm): -15.7 (br, 1H, Fe-*H*), 1.11 (6H, t, J_{HH} = 6.8 Hz, (CH_3CH_2)$_2$O), 1.30 (18H, s, -C(CH_3)$_3$), 1.34 (18H, s, -C(CH_3)$_3$), 3.39 (4H, q, J_{HH} = 6.9 Hz, (CH_3CH_2)$_2$O), 3.98 (4H, m, -CH_2-), 7.57 (4H, s, BAr_4^F), 7.65 (2H, J_{HH} = 7.8 Hz, d, py), 7.79 (8H, BAr_4^F), 7.93 (1H, J_{HH} = 7.7 Hz, t, py).

^{31}P{^{1}H} NMR (THF-d_8, 25°C, 202 MHz, ppm): 100.3 (s, -*P*(^{t}Bu)$_2$)

^{15}N{^{1}H} NMR (THF-d_8, -78°C, 51 MHz, ppm): -30 (br, $\Delta\nu_{1/2}$ = 15.7 Hz), -64 (br, $\Delta\nu_{1/2}$ = 13.8 Hz).

IR (THF, KBR plate, cm^{-1}): 1919 (*CO)*, 1900 *(CO).*

*T*wo -*CO* stretches are observed, and are assigned to either the 6-coordinate THF bound cation or the N_2 bound cation, see section D.

The synthesis of **[(PNP)(CO)(H)Fe-MeCN][BF_4]** was previously reported by Zell et. al.[22] The ^{1}H NMR spectrum of the above reaction in MeCN-d_3 is identical to the literature spectrum.

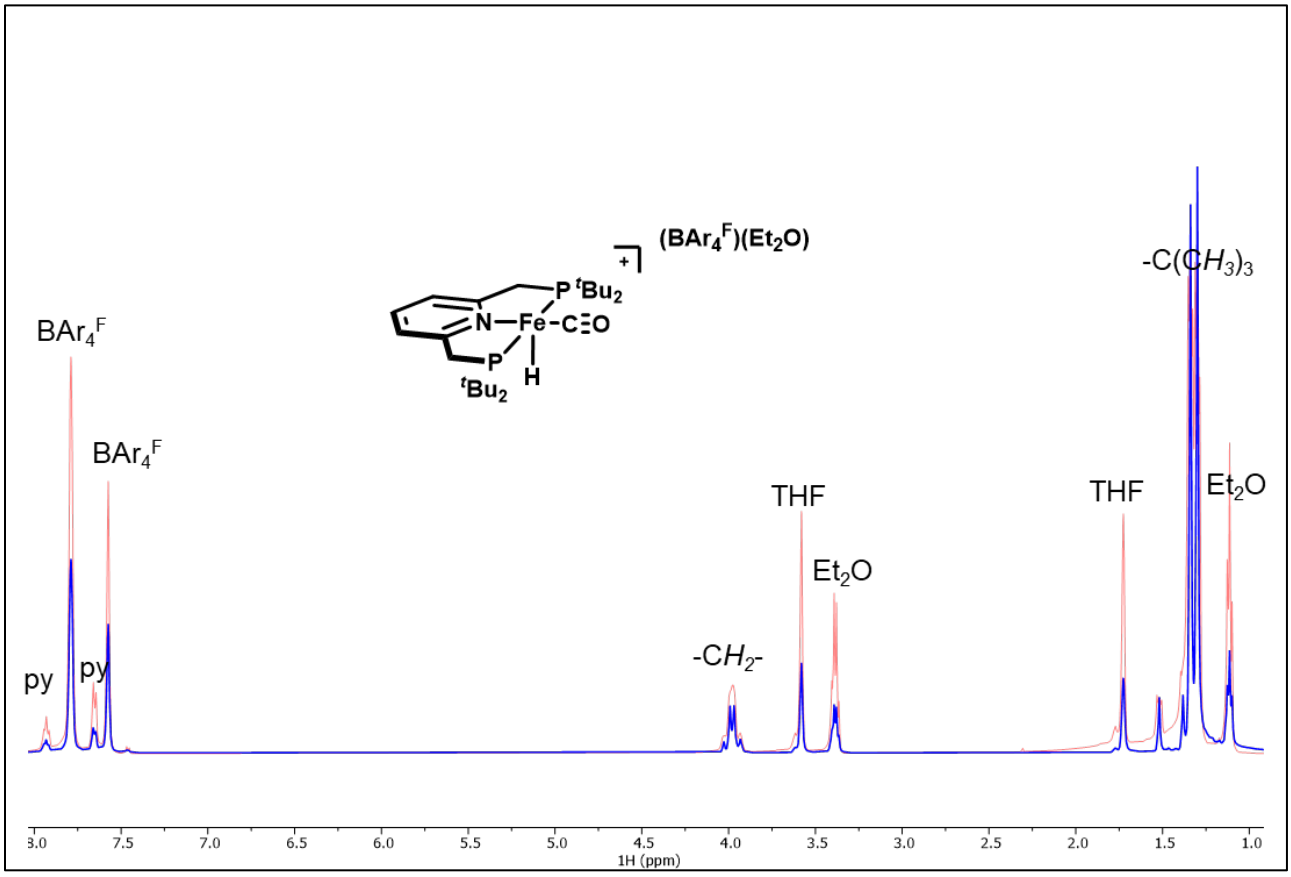

Figure S11. Superimposed ^{1}H NMR (red) and $^{1}H\{^{31}P\}$ NMR (blue) spectra of **[(PNP)(CO)(H)Fe][BAr$_4^F$]** (500 MHz, 298K, THF-d_8).

D. Characterization of the [(PNP)(H)(CO)Fe][BAr$_4^F$] Equilibrium.

The BF_4 salt of **[(PNP)(CO)(H)Fe][BAr$_4^F$]** has previously been characterized in the literature in MeCN.[22] In the absence of a strongly coordinating solvent, **[(PNP)(CO)(H)Fe][BAr$_4^F$]** exists as an equilibrium mixture, proposed to be:

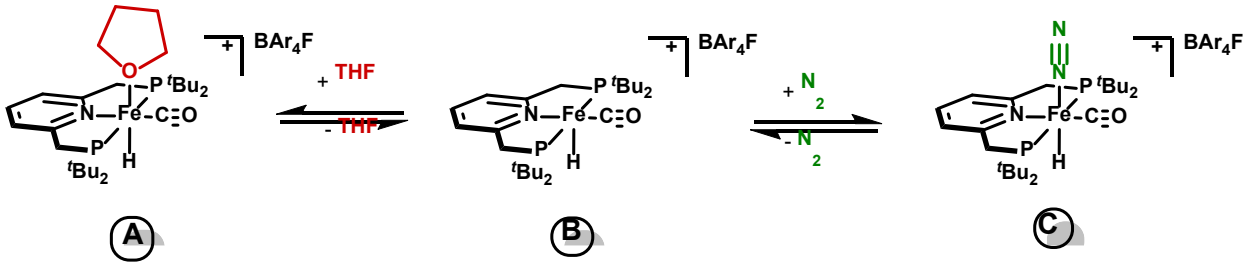

At 25°C, no well-defined peak is observed in the hydride region of the ^{1}H NMR spectra. Addition of one drop of strongly binding MeCN to the NMR sample results in the presence of a triplet at -17.08 ppm (J_{PH} = 54.2 Hz, Fe-*H*) in the ^{1}H NMR spectrum at 25°C; agreeing with the previous literature report of **[(PNP)(CO)(H)Fe-MeCN][BF$_4$]** (-17.12 ppm, J_{PH} = 54.2 Hz, Fe-*H*).[22] The room temperature ^{31}P NMR spectrum (Figure S15) shows a broad resonance at 100.3 ppm (96% of sample), and a minor peak at 113.6 ppm (4% of sample). The two peaks are present when crystals are dissolved in THF, suggesting that the minor peak is part of an equilibrium, or it is an impurity that arises from impurities in the THF. Similarly, addition of strongly coordinating MeCN leads to one major peak in the ^{31}P{^{1}H} NMR spectrum at 107.8 ppm and a minor peak at 113.0 ppm at room temperature. The peak at 113.0 ppm initially integrates to less than 10% of the total integration, however, this value grows over time. Therefore, the peak at 113 ppm is attributed to a yet to be identified impurity resulting from decomposition of **[(PNP)(CO)(H)Fe][BAr$_4^F$]** in THF.

To gain more insight, VT NMR studies were undertaken. **[(PNP)(CO)(H)Fe][BAr$_4^F$]** (33 mg, 24 μmol) was dissolved in 0.5 mL of THF-d_8 in a Teflon sealed J Young NMR tube to give a purple solution. The tube was sealed, placed on the Schlenk line, and frozen under lN_2. The atmosphere was evacuated and replaced with 0.65 atm of $^{15}N_2$ while still frozen. After sealing the tube, the reaction was placed at room temperature before collecting the VT NMR spectra. At -78°C, removal of the J Young tube from the NMR spectrometer shows that the purple solution has become red. The color change was confirmed by VT UV-vis spectroscopy (See Figure S16). VT NMR was repeated under $^{14}N_2$ (glovebox) atmosphere.

The VT ^{15}N{^{1}H} NMR spectra (Figure S14) shows the emergence of two singlets that appear at -40 °C (equal integration) at -30 ppm and -64 ppm, indicating the binding of a terminal N_2 ($N_A \neq N_B$). This is consistent with the crystal structure and isomer **C**. At room temperature, this species is not observed by NMR spectroscopy, and no N_2 stretch is observed in the IR spectrum. Moreover, dissolution of crystals at room temperature results in a color change and outgassing, evidenced by bubbles.

At -40 °C, the ^{31}P NMR spectrum (Figure S15) shows a new singlet at 105.9 ppm assigned as **C** in accordance with the ^{15}N NMR spectra at the same temperature. In the hydride region of ^{1}H NMR spectra at -40°C, two new multiplets are present at -13.72 ppm

(major, J_{PH} = 51.6 Hz) and -24.60 ppm (minor, J_{PH} = 56.0 Hz) in a 5:1 ratio. The peak at -13.73 ppm is assigned to **C** due to the peaks present at the same temperature in the $^{15}N\{^{1}H\}$ NMR spectra. The peak at -24.6 ppm is assigned to either **A** or **B**; it is not an impurity as warming up results in the peak to disappear.

Cooling the sample from 25°C to -78°C increases the broadness of the peaks assigned to **[(PNP)(CO)(H)Fe][BAr$_4^F$]** in the 1.0-8.0 ppm region of the ^{1}H NMR spectrum. These results are consistent with dynamic THF/N_2 binding at room temperature. At 25°C, the cation likely exists as a 6-coordinate species with dynamic coordination of THF/N_2. An assignment which is further supported by the observation of two IR stretches for the bound carbonyl ligand in THF at 1919 cm^{-1} and 1900 cm^{-1} in the FT-IR spectra (Figure S17). IR stretches for transition-metal N_2 complexes appear in the 1800-2300 region;[23] however, due to the presence of several peaks between 1950-2100 cm^{-1} an N_2 peak was not assigned.

For thermodynamic studies, the structure of the cation is taken to be **[(PNP)(CO)(H)Fe][BAr$_4^F$]**. Consideration of an N_2 molecule in the molecular weight leads to 2% error in the initial concentration of **[(PNP)(CO)(H)Fe][BAr$_4^F$]**.

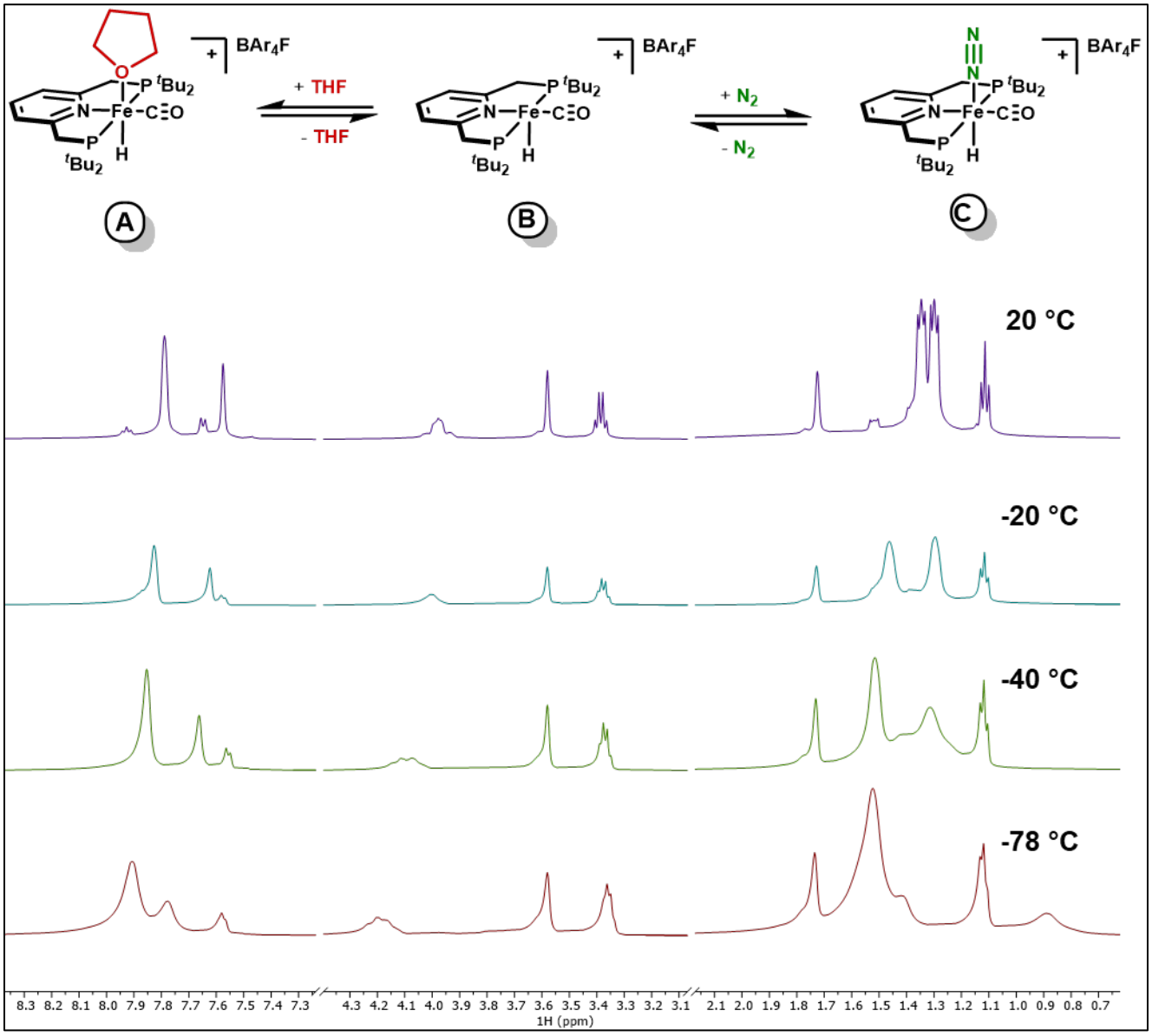

Figure S12. VT ^{1}H NMR spectra (500 MHz, VT, THF-d_8) of **[(PNP)(CO)(H)Fe][BAr$_4^F$]** under $^{15}N_2$ atmosphere.

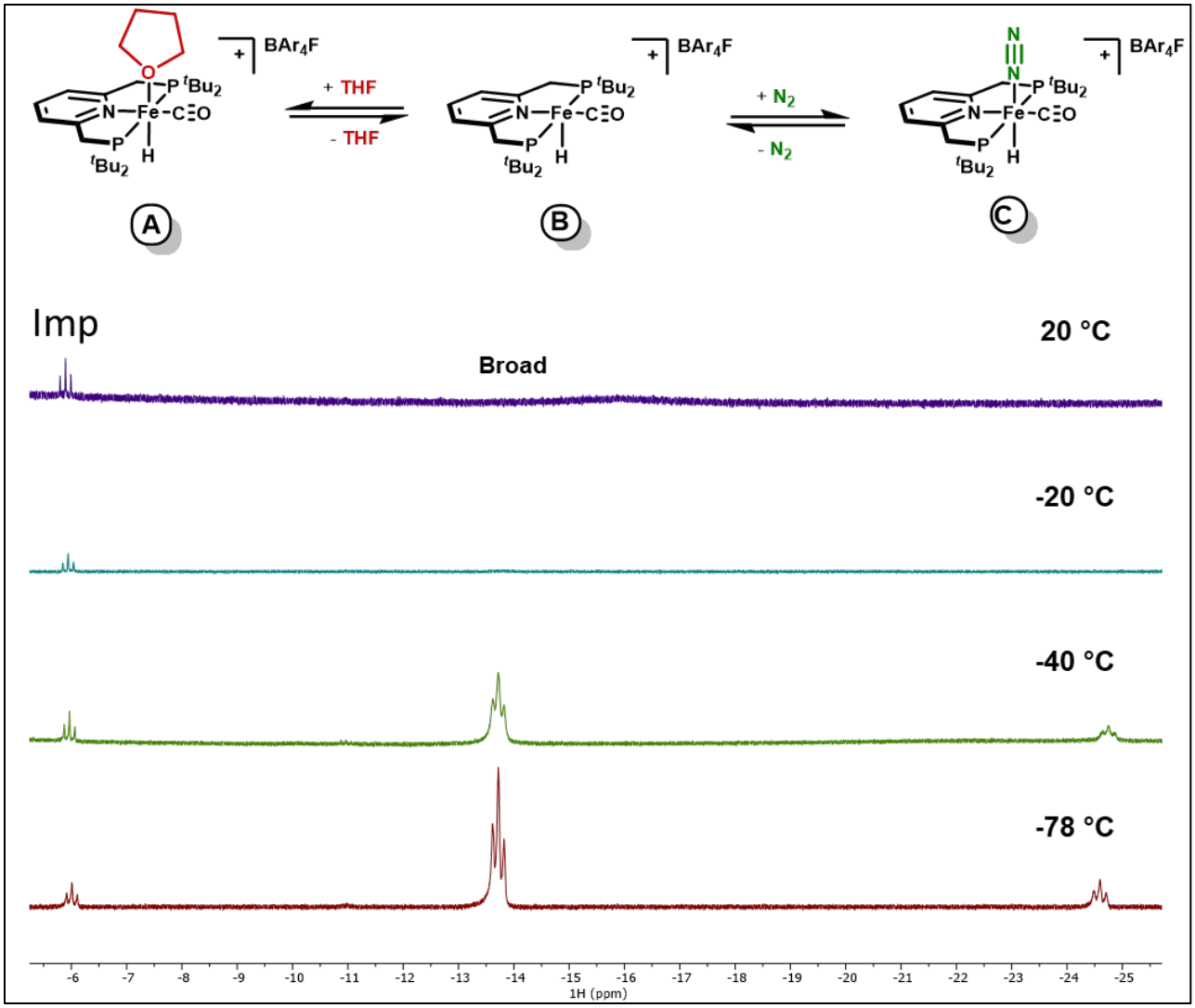

Figure S13. VT ^{1}H NMR spectra (500 MHz, VT, THF-d_8) of the hydride region of **[(PNP)(CO)(H)Fe][BAr$_4^F$]** under $^{15}N_2$ atmosphere.

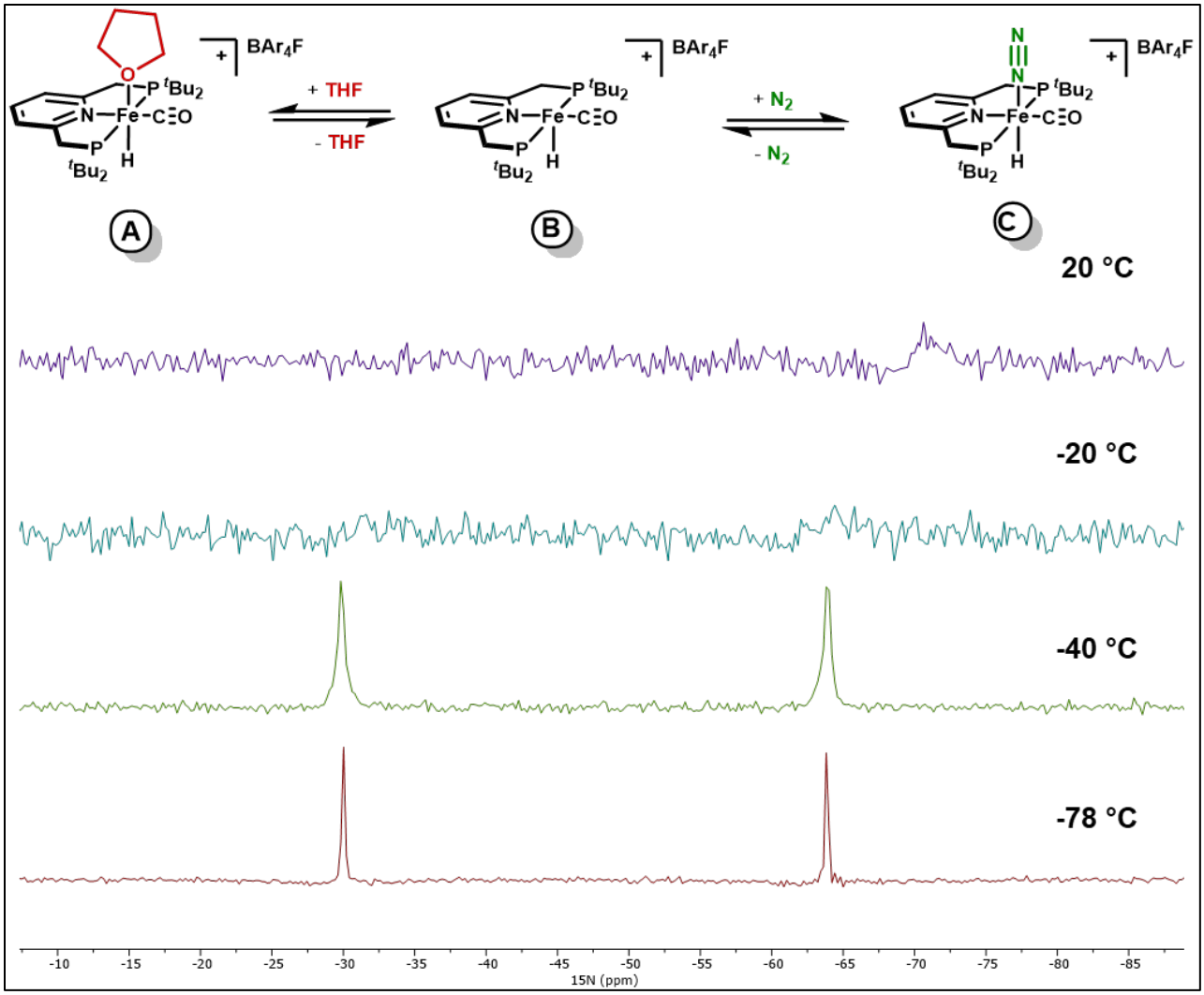

Figure S14. VT $^{15}N\{^{1}H\}$ NMR spectra (51 MHz, VT, THF-d_8) of **[(PNP)(CO)(H)Fe][BAr$_4^F$]** under $^{15}N_2$ atmosphere.

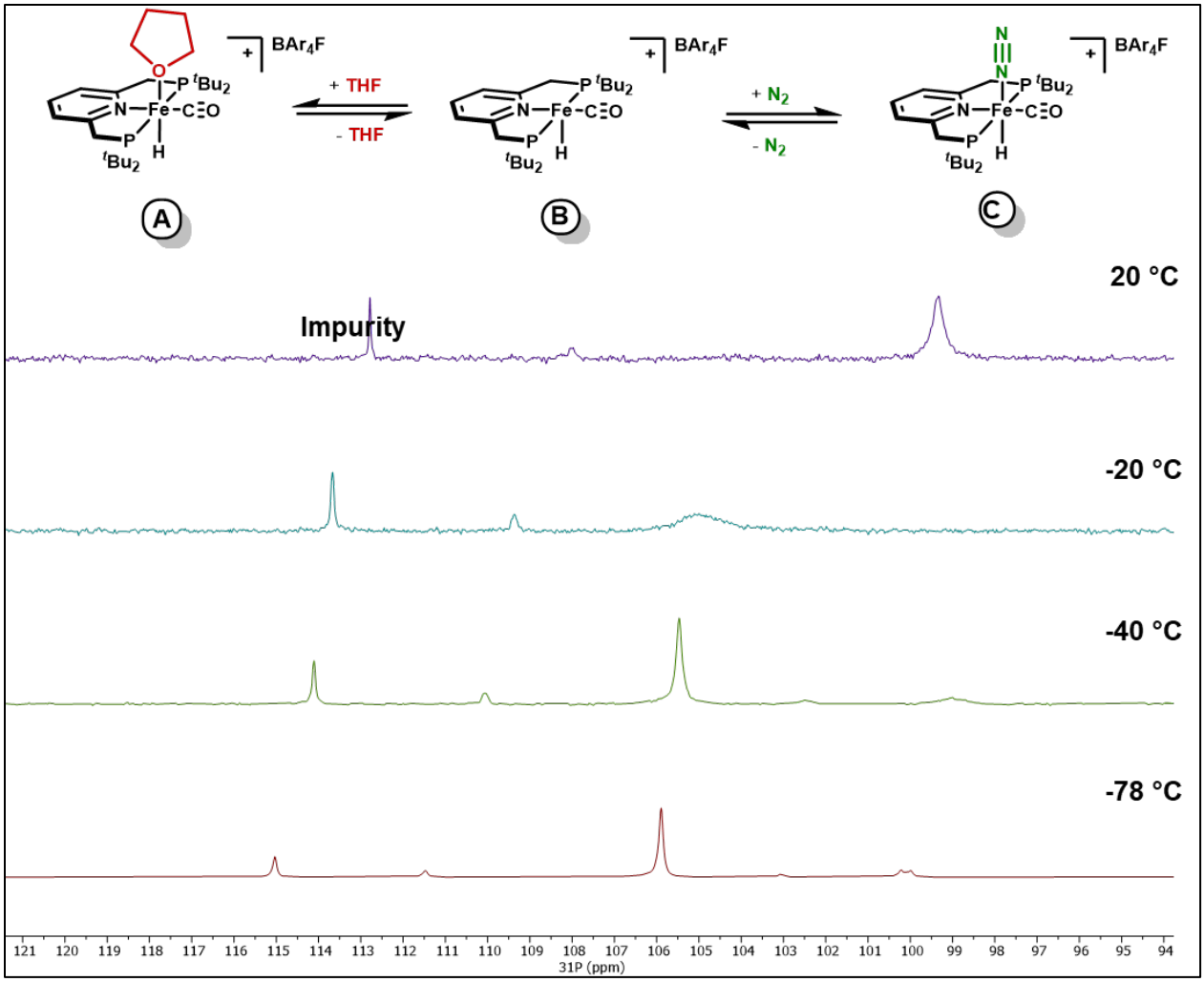

Figure S15. VT $^{31}P\{^{1}H\}$ NMR spectra (202 MHz, VT, THF-d_8) of **[(PNP)(CO)(H)Fe][BAr$_4^F$]** under N_2 atmosphere. Shifting of the signal suggests a temperature-dependent equilibrium between congeners.

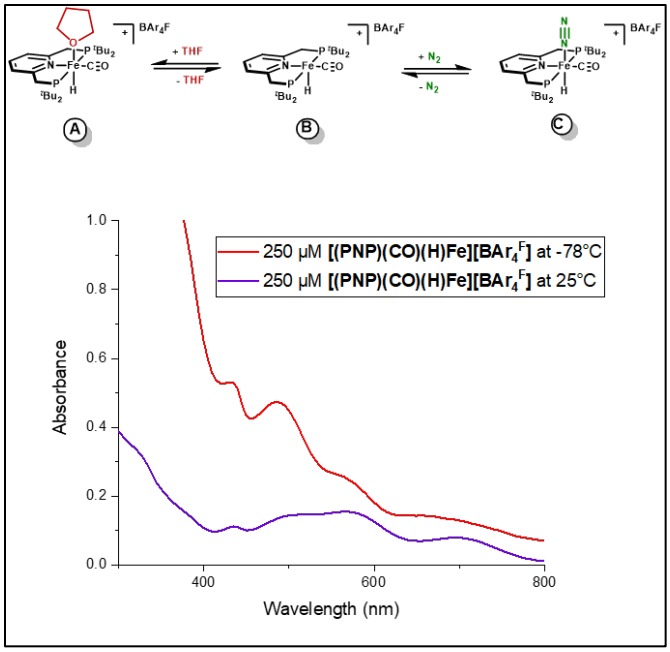

Figure S16. UV-Vis Spectra demonstrating the speciation change and accompanying color change upon cooling **[(PNP)(CO)(H)Fe][BAr$_4^F$]** at 25°C (purple) to -78°C (red).

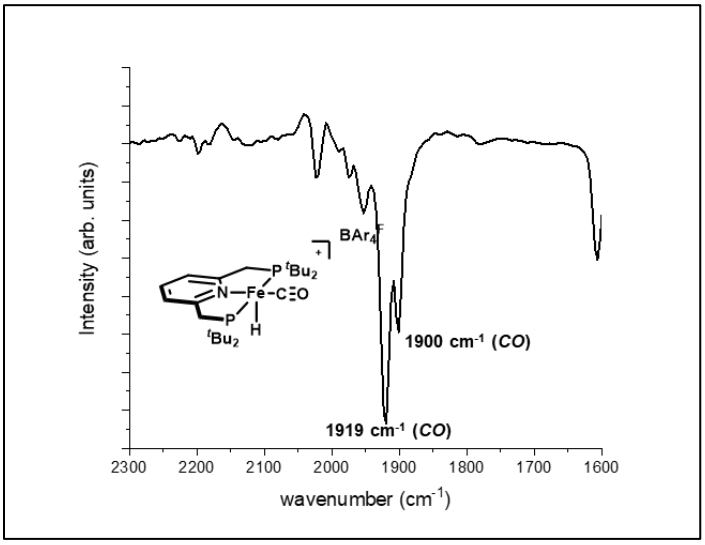

Figure S17. FT-IR (THF, KBr plate, room temp.) spectrum of **[(PNP)(CO)(H)Fe][BAr$_4^F$]**.

E. Synthesis of [Li][(*PNP)(CO)(H)Fe-H].

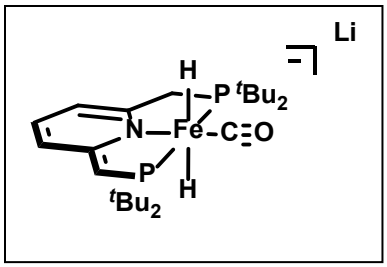

(PNP)(CO)(H)Fe-H (74 mg, 0.15 mmol) was placed into a 20 mL scintillation vial with a stir bar and dissolved in 10 mL of Et_2O. To the stirring yellow solution was slowly added 1.54 mL of 0.1 M *n*-BuLi in pentanes (0.15 mmol) at -78°C, which immediately gave a color change to dark yellow/red. The reaction was stirred for ten minutes after which all volatiles were removed *in vacuo*. The red/brown residue was dissolved in diethyl ether and filtered through celite. Removal of the solvent followed by washing with pentanes gave a product of >93% purity via $^{31}P\{^1H\}$ NMR spectroscopy. (80 mg, 93% yield).

^{1}H NMR (THF-d_8, 25°C, 500 MHz, ppm): -8.73 (2H, m, Fe-*H*), 1.33-1.44 (36H, m, -C(CH_3)$_3$), 2.91-2.99 (2H, m, -C*HH*-), 3.53 (1H, br, -C*H*-), 5.32 (1H, d, J_{HH} = 6.4 Hz, py), 5.80 (1H, d, J_{HH} = 7.8 Hz, py), 6.14 (1H, t, J_{HH} = 7.5 Hz, py).

^{1}H{^{31}P} NMR (THF-d_8, 25°C, 500 MHz, ppm): -8.73 (2H, s, $\Delta\nu_{1/2}$ = 30.8 Hz, Fe-*H*), 1.30-1.40 (36H, m, -C(CH_3)$_3$), 2.95 (2H, s, -C*HH*-), 3.53 (1H, br, -C*H*-), 5.32 (1H, d, J_{HH} = 6.4 Hz, py), 5.80 (1H, d, J_{HH} = 7.8 Hz, py), 6.14 (1H, t, J_{HH} = 7.5 Hz, py).

^{31}P{^{1}H} NMR (THF-d_8, 25°C, 202 MHz, ppm): 118.9 (1P, d, J_{PP} = 110 Hz, -*P*(^{t}Bu)$_2$) 126.1 (1P, d, J_{PP} = 109.7 Hz, -*P*(^{t}Bu)$_2$).

^{13}C{^{1}H} NMR (THF-d_8, 25°C, 126 MHz, ppm): 229.5 (dd, J_{PC} = 34.2, J_{PC} = 25.6, -*C*O), 169.3 (1C, dd, J_{PC} = 21.6, J_{PC} = 6.3 Hz, py), 160.1 (1C, dd, J_{PC} = 9.0 Hz, J_{PC} = 5.2 Hz, py), 129.4 (1C, s, py), 108.6 (1C, d, J_{PC} = 16.3 Hz, py), 97.1 (1C, d, J_{PC} = 9.4 Hz, py), 63.8 (1C, d, J_{PC} = 35.6 Hz, -*C*H-), 38.9 (1C, d, J_{PC} = 10.7 Hz, -*C*HH-), 36.5 (2C, d, J_{PC} = 17.4 Hz, -P(*C*(CH$_3$)$_3$)$_2$), 35.5 (2C, d, J_{PC} = 11.1 Hz, -P(*C*(CH$_3$)$_3$)$_2$), 31.4 (12C, d, J_{PC} = 4.4 Hz, -P(C(*C*H$_3$)$_3$)$_2$), 30.4 (12C, d, J_{PC} = 4.3 Hz, -P(C(*C*H$_3$)$_3$)$_2$).

IR (ATR, KBr pellet, cm^{-1}): 1801 (*CO*).

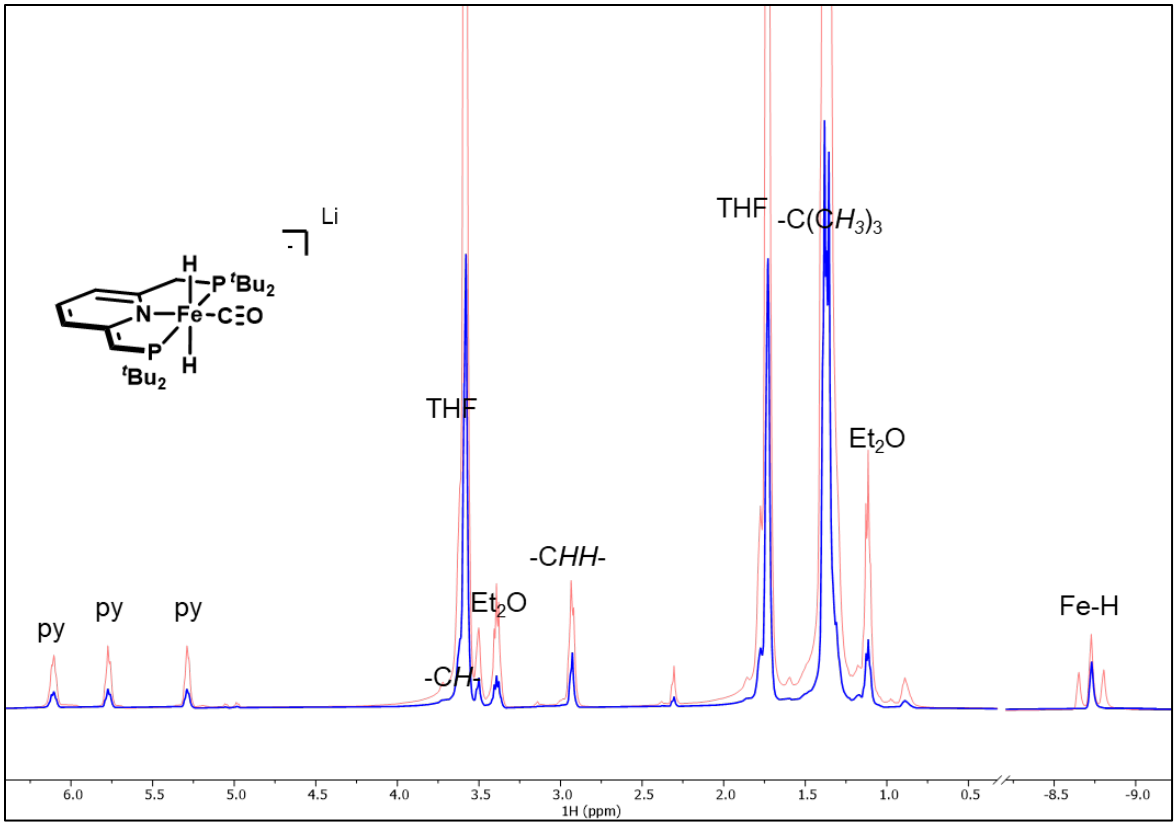

Figure S18. Superimposed ^{1}H NMR (red) and $^{1}H\{^{31}P\}$ NMR (blue) spectra of **[Li][(*PNP)(CO)(H)Fe-H]** (500 MHz, 298K, THF-d_8).

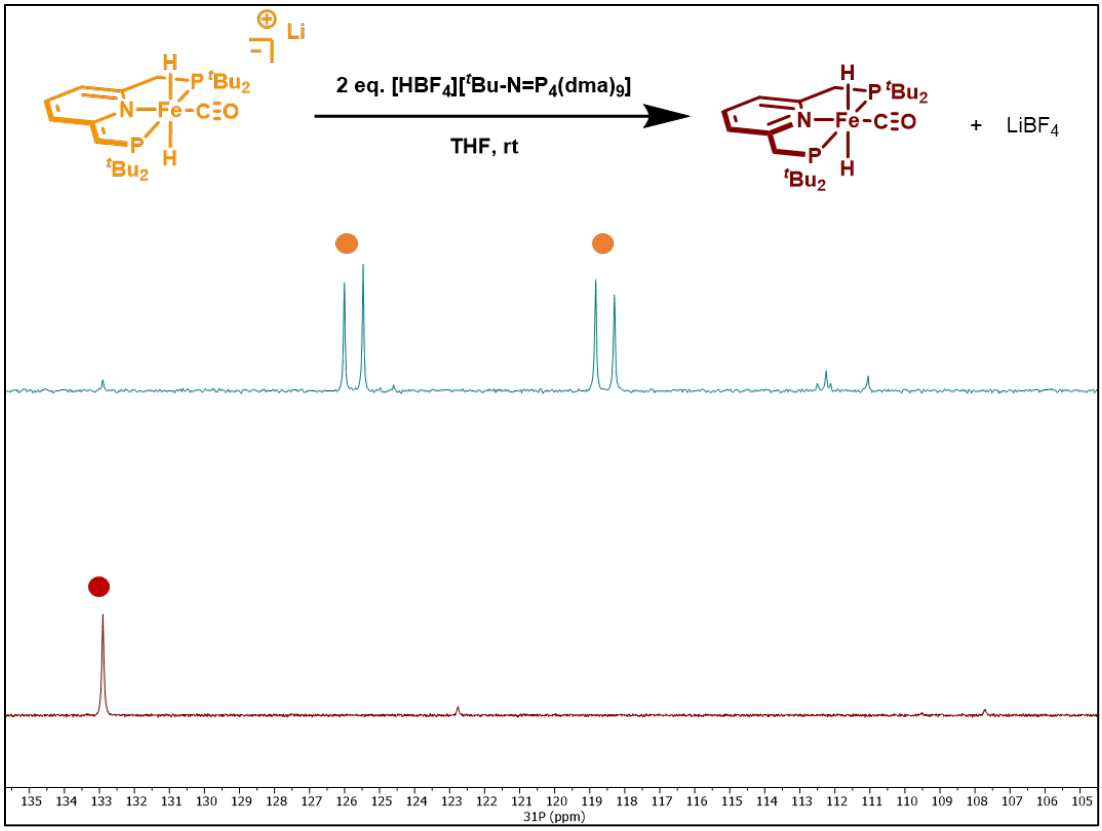

Figure S19. Stacked $^{31}P\{^{1}H\}$ NMR spectra (202 MHz, 298K, THF) of **[HBF$_4$][^{tBu}N=P$_4$(Me$_2$N)$_9$]** (8 µmol, 320 µL of a 29 mM stock solution in THF) addition to **[Li][(*PNP)(CO)(H)Fe-H]** (4 µmol, 409 µL of a 10 mM stock solution in THF). This shows that the deprotonation is reversible.

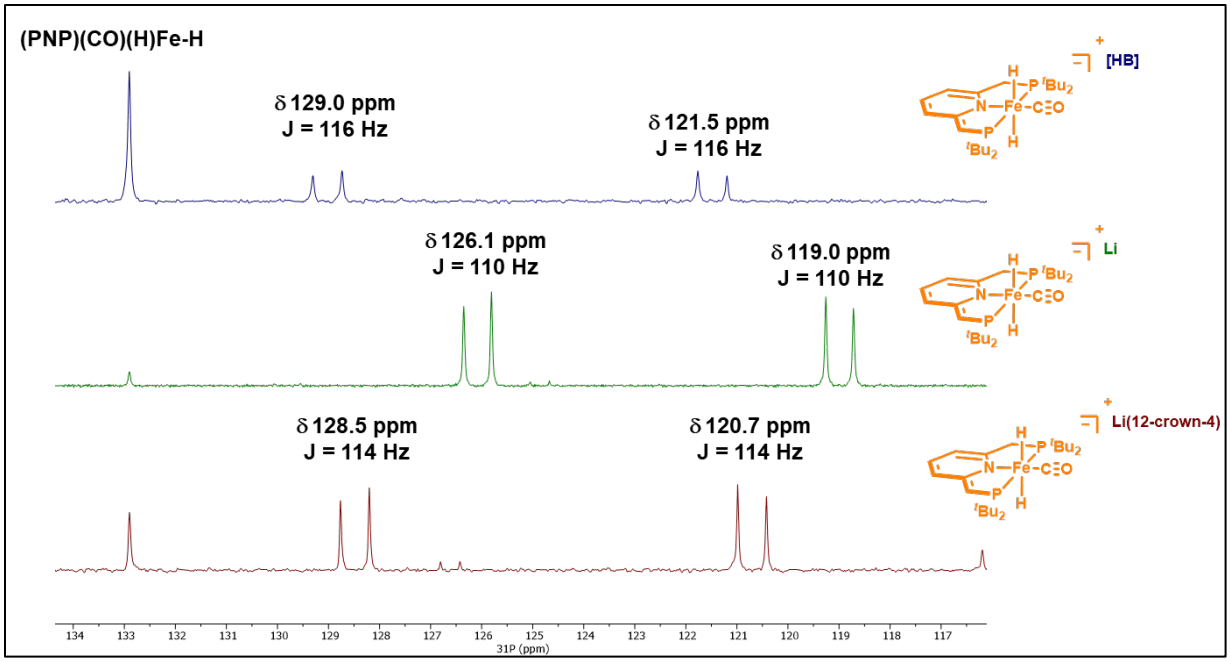

Figure S20. Stacked $^{31}P\{^{1}H\}$ NMR spectra (202 MHz, 298K, THF) of the anion **[(*PNP)(CO)(H)Fe-H]**$^{-}$ with differing counter cations. Top: **[HB][(*PNP)(CO)(H)Fe-H] (B = Ph(CH$_3$)C=P(2,4,6-(MeO)$_3$-C$_6$H$_2$)$_3$)** generated during the titration of (**PNP)(CO)(H)Fe-H** with 4.0 eq. of the wittig base as described in section 3C. Middle: **[Li][(*PNP)(CO)(H)Fe-H]** (32 mM in THF). Bottom: **[Li(12-crown-4)][(*PNP)(CO)(H)Fe-H]** generated from the addition of 12-crown-4 (10 µmol, 0.8 mL of a 0.11 M stock solution in THF) to **[Li][(*PNP)(CO)(H)Fe-H]** (2 µmol, 340 µL of a 55 mM stock solution in THF).

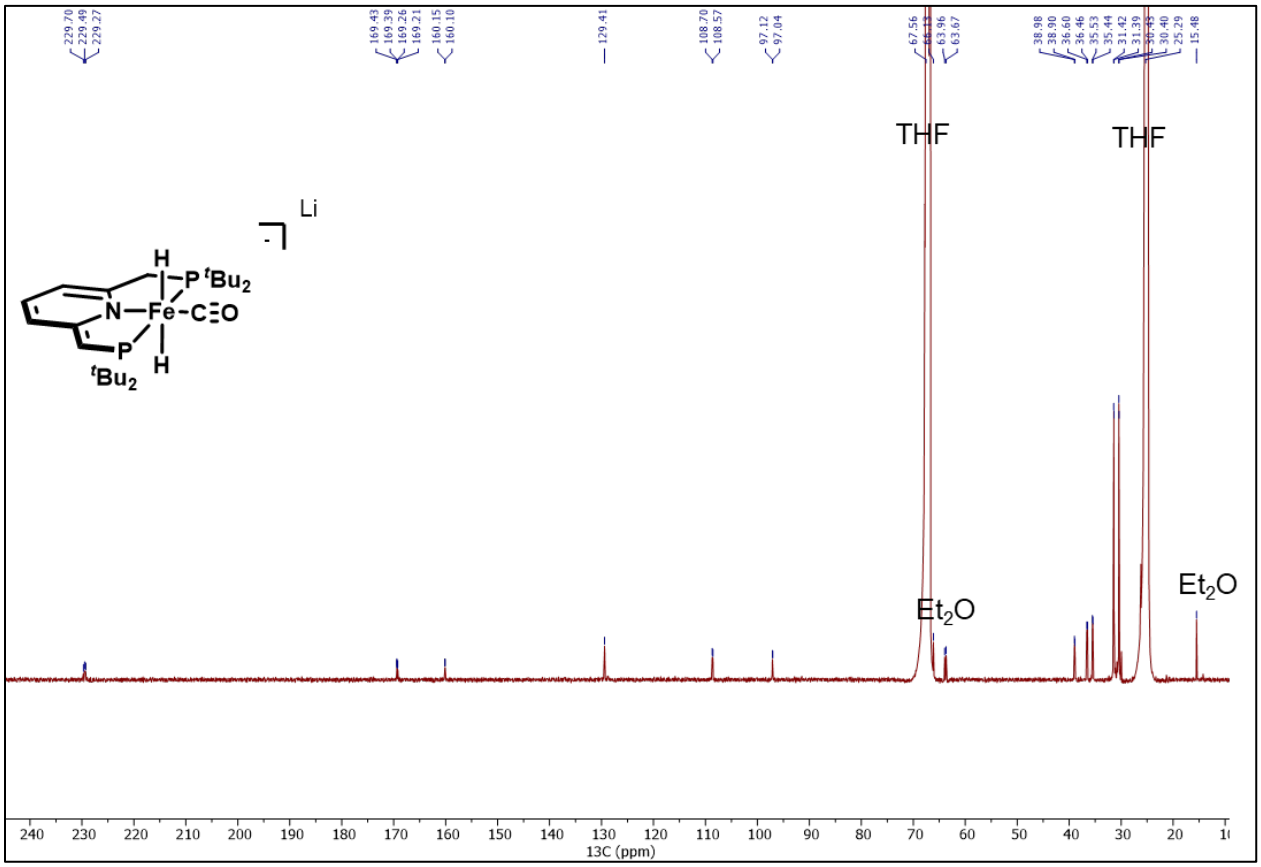

Figure S21. $^{13}C\{^{1}H\}$ NMR spectrum (126 MHz, 298K, THF-d_8) of **[Li][(*PNP)(CO)(H)Fe-H]**.

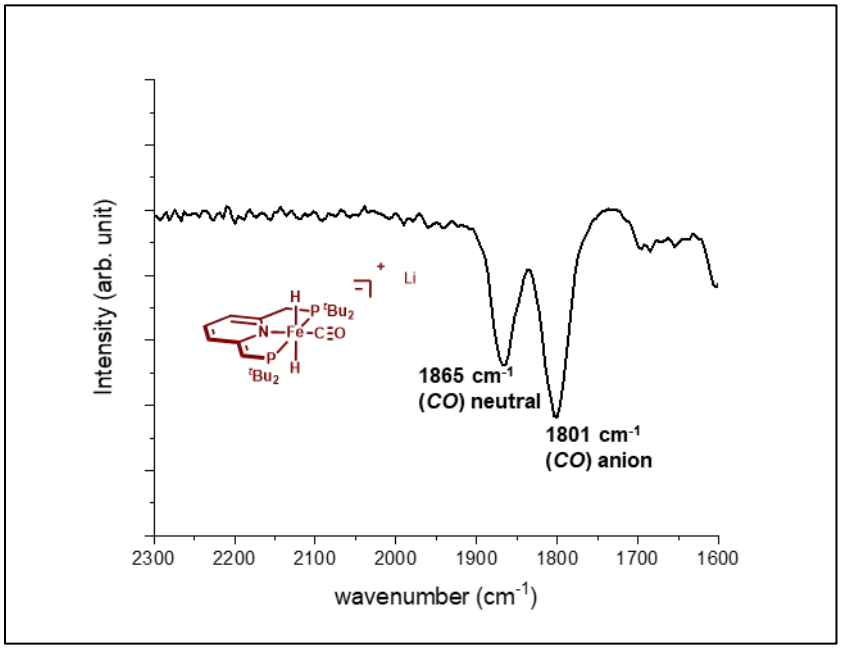

Figure S22. FT-IR (KBr pellet) of **[Li][(*PNP)(CO)(H)Fe-H]**, the peak at 1865 cm^{-1} agrees with the literature value for **(PNP)(CO)(H)Fe-H**.[9] Protonation may have occurred from trace moisture in the KBr and/or upon removing the sample from the glovebox atmosphere.

F. Synthesis of [Li][(*PNP)(CO)(H)Ru-H].

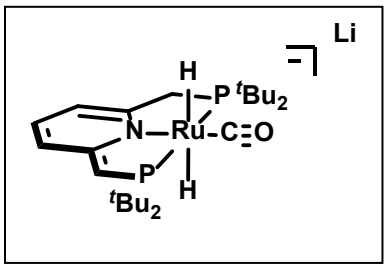

(*PNP)(CO)(H)Ru (50 mg, 0.10 mmol) was dissolved in 10 mL of Et_2O and placed into a 50 mL Schlenk tube with a stir bar. The tube was placed on the Schlenk line and frozen at -196 °C at which point the atmosphere was removed and replaced with H_2. Upon warming to room temperature, a color change from green to yellow occurs indicating formation of **(PNP)(CO)(H)Ru-H**. The Schlenk tube was taken into the glovebox. The tube was opened and 0.95 mL of 0.1 M *n*-BuLi in pentanes (0.10 mmol) was added dropwise at -78°C giving a color change to a vibrant yellow/orange color. The reaction was stirred for ten minutes and all volatiles removed *in vacuo*. The yellow residue was dissolved in diethyl ether and filtered through celite. Removal of the solvent followed by washing with pentanes gave material of >95% purity from integration of the $^{31}P\{^1H\}$ NMR spectrum. **[Li][(*PNP)(CO)(H)Ru-H]** is protonated by trace moisture to give **(PNP)(CO)(H)Ru-H** which loses H_2 to form **(*PNP)(CO)(H)Ru**; therefore, NMR spectra were recorded under an H_2 atmosphere to prevent H_2 loss. (38 mg, 75% yield).

^{1}H NMR (THF-d_8, 25°C, 500 MHz, ppm): -5.91 (2H, dd, J_{HP} = 16.7 Hz, J_{HP} = 19.5 Hz, Ru-*H*), 1.36 (18H, d, J_{HP} = 12.0 Hz, -C(CH_3)$_3$), 1.39 (18H, d, J_{HP} = 12.4 Hz, -C(CH_3)$_3$), 2.91-2.95 (2H, d, J_{PH} = 8.3 Hz, -C*H*H-), 3.36 (br, -C*H*- + (CH_3CH_2)$_2$O), 5.22 (1H, d, J_{HH} = 6.5 Hz, py), 5.77 (1H, d, J_{HH} = 8.7 Hz, py), 6.08 (1H, t, J_{HH} = 7.6 Hz, py).

^{1}H{^{31}P} NMR (THF-d_8, 25°C, 500 MHz, ppm): -5.90 (2H, s, $\Delta\nu_{1/2}$ = 29.4 Hz, Ru-*H*), 1.37 (18H, s, -C(CH_3)$_3$), 1.39 (18H, s, -C(CH_3)$_3$), 2.93 (2H, s, -C*H*H-), 3.38 (br, -C*H*- + (CH_3CH_2)$_2$O), 5.22 (1H, d, J_{HH} = 6.5 Hz, py), 5.77 (1H, d, J_{HH} = 8.7 Hz, py), 6.08 (1H, t, J_{HH} = 7.6 Hz, py).

^{31}P{^{1}H} NMR (THF-d_8, 25°C, 202 MHz, ppm): 98.0 (1P, d, J_{PP} = 241 Hz, -*P*(^{t}Bu)$_2$), 101.2 (1P, d, J_{PP} = 2401 Hz, -*P*(^{t}Bu)$_2$).

^{13}C{^{1}H} NMR (THF-d_8, 25°C, 126 MHz, ppm): 215.7 (dd, J_{PC} = 12.9, J_{PC} = 13.8, -*C*O), 168.9 (dd, J_{PC} = 19.4, J_{PC} = 4.6 Hz, py), 159.6 (dd, J_{PC} = 7.3 Hz, J_{PC} = 4.2 Hz, py), 129.8 (s, py), 109.9 (d, J_{PC} = 15.7 Hz, py), 96.5 (d, J_{PC} = 9.5 Hz), 64.1 (d, J_{PC} = 41.3 Hz, -*C*H-), 39.7 (d, J_{PC} = 13.7 Hz, -*C*HH-), 35.5 (dd, J_{PC} = 17.9 Hz, J_{PC} = 3.1 Hz, -P(*C*(CH_3)$_3$)$_2$), 34.6 (dd, J_{PC} = 11.2 Hz, J_{PC} = 3.0 Hz, -P(*C*(CH_3)$_3$)$_2$), 31.6 (J_{PC} = 5.7 Hz, -P(C(*C*H_3)$_3$)$_2$), 30.5 (d, J_{PC} = 5.6 Hz, -P(C(*C*H_3)$_3$)$_2$).

IR (KBr Pellet, cm^{-1}): 1826 (*CO*).

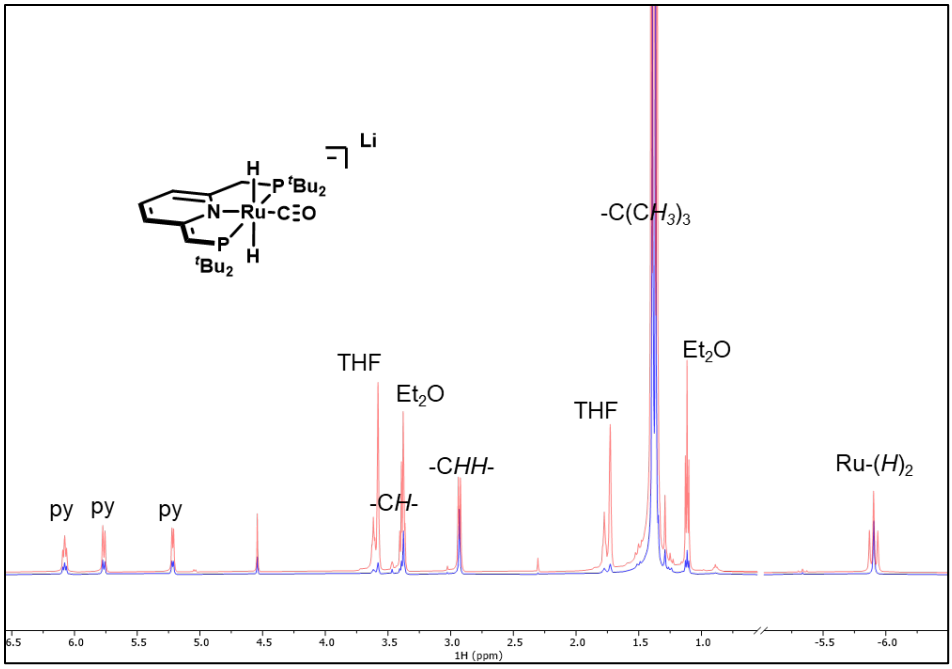

Figure S23. Superimposed ^{1}H (red) and $^{1}H\{^{31}P\}$ (blue) NMR spectra of **[Li][(*PNP)(CO)(H)Ru-H]** (500 MHz, 298K, THF-d_8).

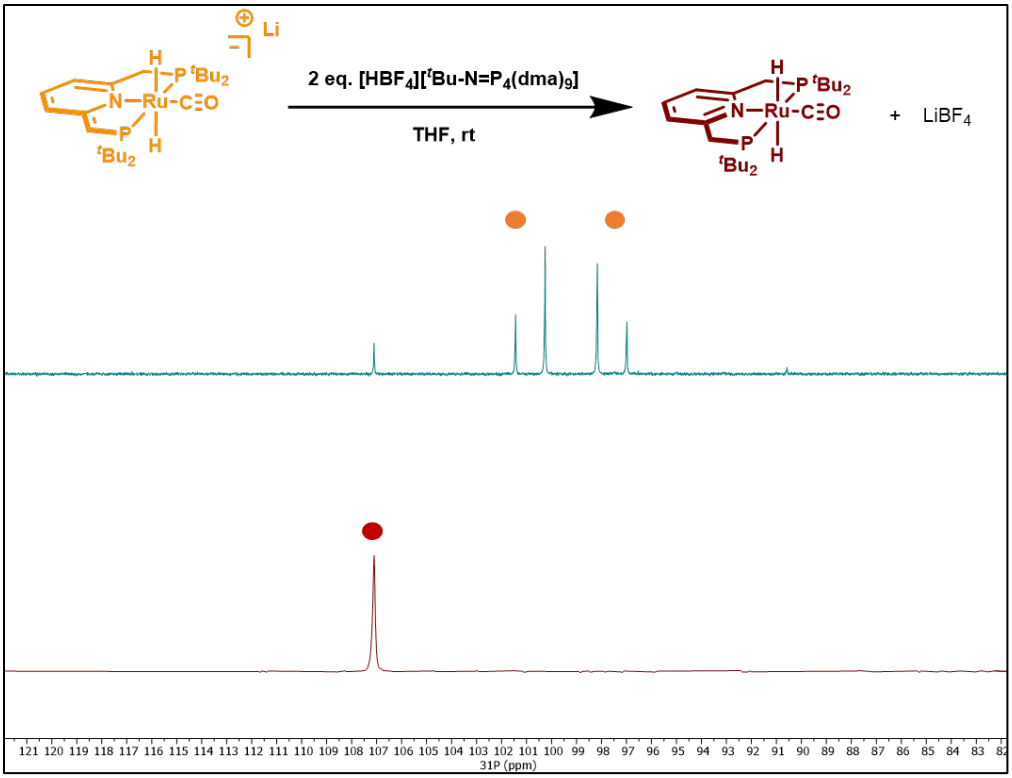

Figure S24. Stacked $^{31}P\{^{1}H\}$ NMR spectra (202 MHz, 298K, THF) of **[^{tBu}N=P$_4$(Me$_2$N)$_9$][HBF$_4$]** (4 µmol, 160 µL of a 29 mM stock solution in THF) addition to **[Li][(*PNP)(CO)(H)Ru-H]** (2 µmol, 417 µL of a 6 mM stock solution in THF). This shows that the deprotonation is reversible.

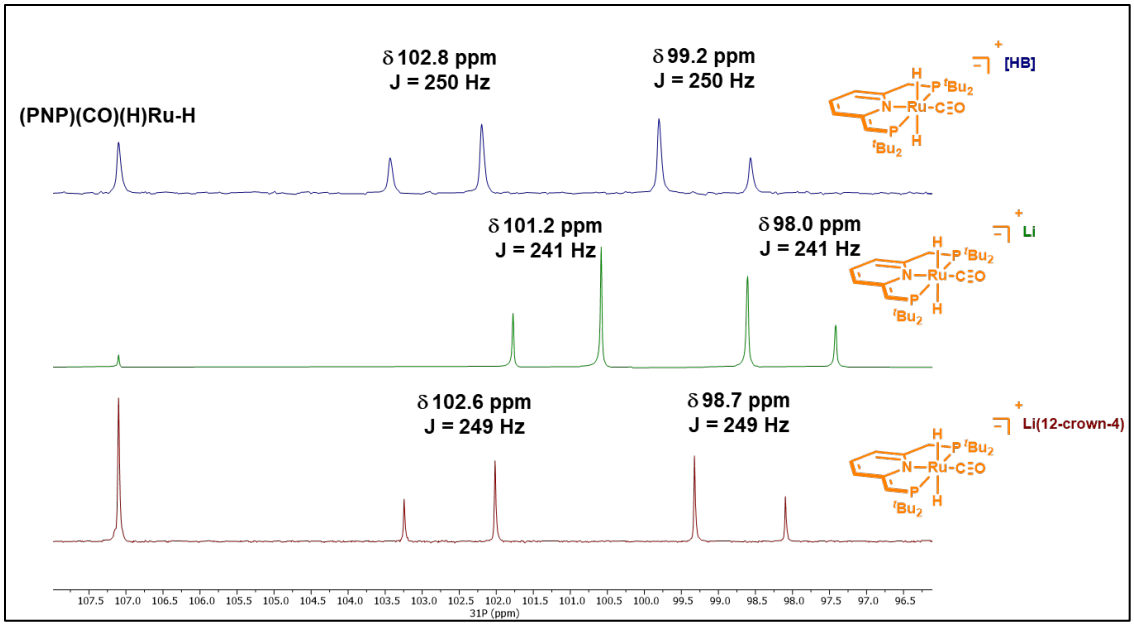

Figure S25. Stacked $^{31}P\{^{1}H\}$ NMR spectra (202 MHz, 298K, THF) of the anion **[(*PNP)(CO)(H)Ru-H]$^-$ with** differing counter cations. **Top: [HB][(*PNP)(CO)(H)Ru-H]** (B = $Ph(CH_3)C{=}P(2,4,6\text{-}(MeO)_3\text{-}C_6H_2)_3$) generated during the titration of (PNP)(CO)(H)Ru-H with 1.5 eq. of the wittig base as described in section 3D. **Middle: [Li][(*PNP)(CO)(H)Ru-H]** (37 mM in THF). **Bottom: [Li(12-crown-4)][(*PNP)(CO)(H)Ru-H]** generated from the addition of 12-crown-4 (10 µmol, 0.9 mL of a 0.11 M stock solution in THF) to **[Li][(*PNP)(CO)(H)Ru-H]** (2 µmol, 340 µL of a 55 mM stock solution in THF).

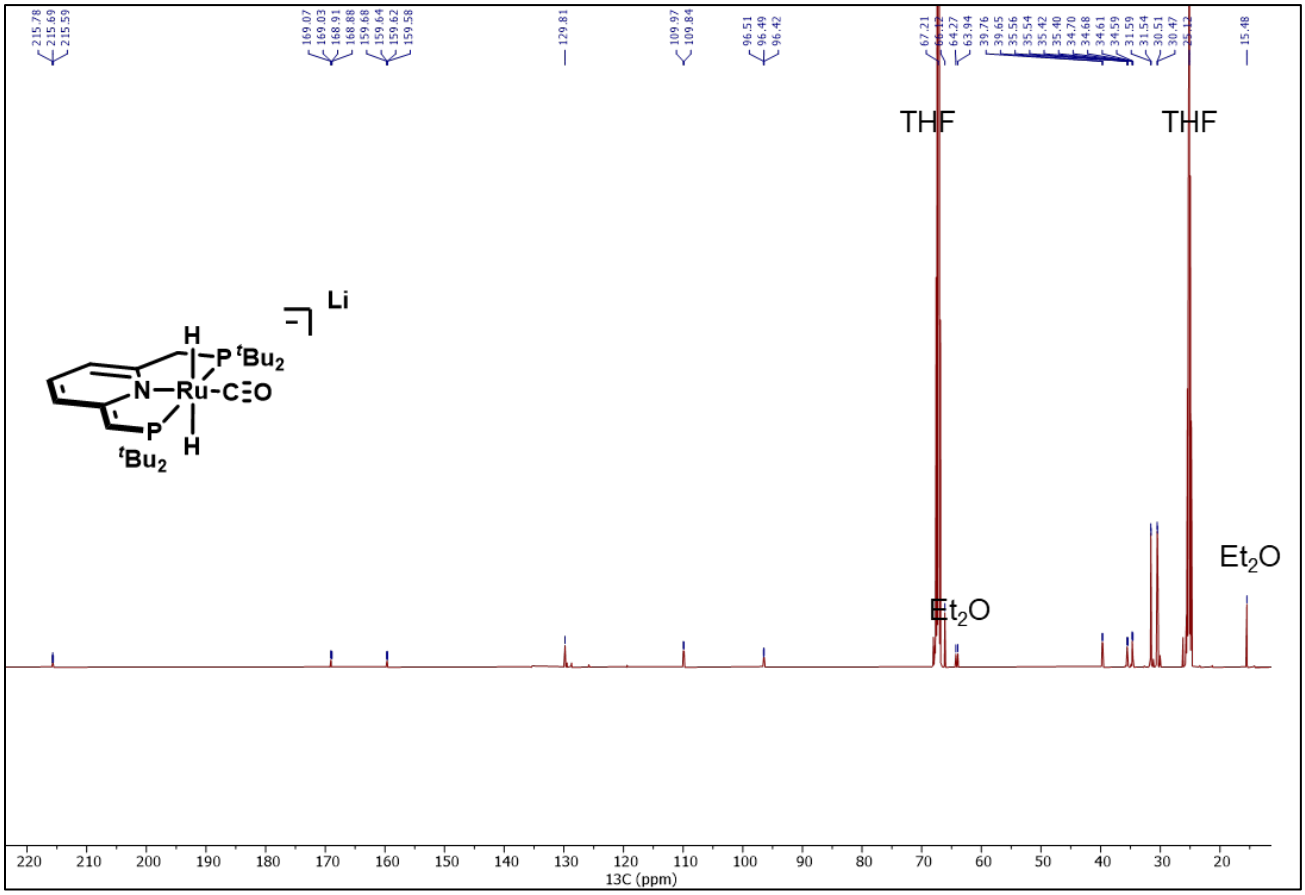

Figure S26. $^{13}C\{^{1}H\}$ NMR spectrum (126 MHz, 298K, THF-d_8) of **[Li][(*PNP)(CO)(H)Ru-H]**.

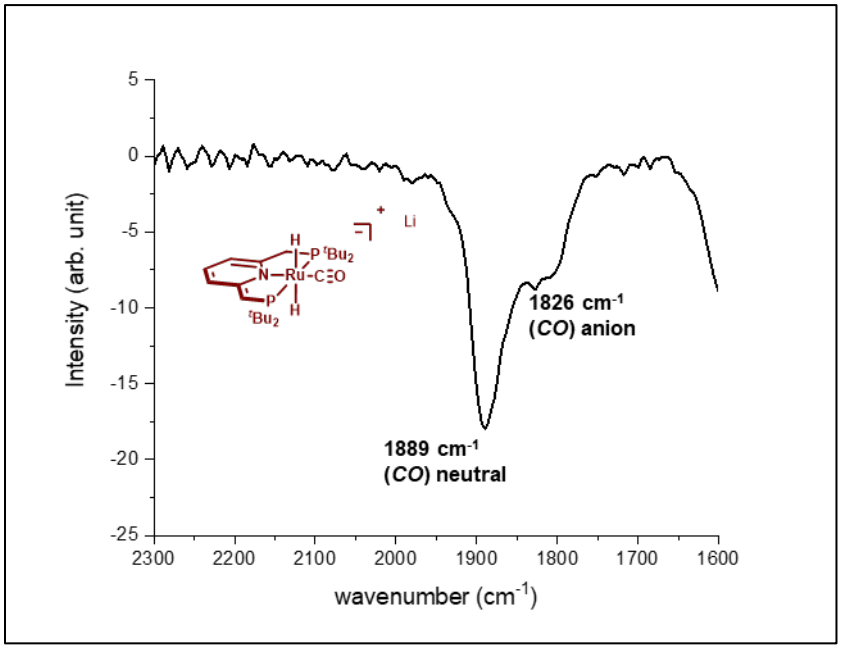

Figure S27. FT-IR (KBr pellet) of **[(*PNP)(CO)(H)Ru-H][Li]**, the peak at 1889 cm^{-1} agrees with the literature value for **(PNP)(CO)(H)Ru-H**.[19] Due to the moisture sensitivity of the anion, protonation from trace moisture in the KBr likely led to the protonation.

G. Synthesis of [K][(*PNP)(CO)(H)Ru-H].

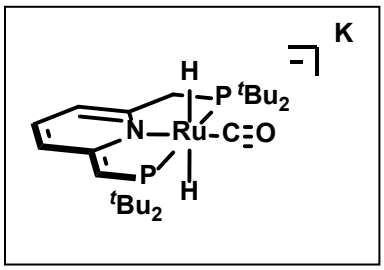

(*^{tBu}PNP)(CO)(H)Ru (502 mg, 0.95 mmol) was added to a 1 L Teflon valved round bottom flask containing a stir bar and dissolved in 200 mL of THF. The flask was placed on the Schlenk line, freeze-pump-thawed three times and the atmosphere replaced with H_2 while still frozen. The reaction was warmed to room temp at which point the green reaction mixture becomes yellow, indicating the formation of **(^{tBu}PNP)(CO)(H)Ru-H** (confirmed via $^{31}P\{^1H\}$ NMR).[7] The reaction was allowed to stir for an additional hour before returning to the glovebox, where it was cooled to -78°C and 1 eq. of solid KO^{t}Bu (0.95 mmol, 107 mg) was added all at once. The reaction was stirred for ten minutes at which point 100 mL of a 10 mM *n*-BuLi solution in pentanes (0.95 mmol, 10 mM solution made by diluting 381 µL of a 2.5 M *n*-BuLi solution in hexanes) was added in portions over ~20 minutes. Upon addition of *n*-BuLi, a slight color change to a brighter orange/red color occurs. The reaction was sealed and stirred for 1 hour at -78°C, removed from the glovebox, and exposed to 0.85 atm of H_2. After stirring for 48 hours at room temperature, the reaction was heated at 55°C for 12 hours. The flask was returned to room temperature at which point the orange/red THF solution was filtered through celite, and the reaction solution concentrated to ~20 mL followed by the addition of ~100 mL of pentanes. Placement of the red/orange solution at -35°C in the freezer yielded yellow/orange prisms suitable for single crystal x-ray diffraction which were of >98% purity as assessed via $^{31}P\{^1H\}$ NMR. The crystals were dried under vacuum for ~1 hour upon collection.

^{1}H NMR (THF-d_8, 25°C, 500 MHz, ppm): -6.61 (2H, dd, J_{PH} = 16.6 Hz, J_{PH} = 16.7 Hz, Ru-H_2), 1.37 (18H, d, J_{PH} = 12.5 Hz, -C(CH_3)$_3$), 1.40 (18H, d, J_{PH} = 12.4 Hz, P(C(CH_3)$_3$)), 2.93 (2H, d, J_{PH} = 8.2 Hz, -C*HH*-), 3.55 (1H, d, J_{PH} = 3.8 Hz, -C*H*-), 5.32 (1H, d, J_{HH} = 6.5 Hz, Py), 5.83 (1H, d, J_{HH} = 8.7 Hz, Py) 6.19 (1H, dd, J_{HH} = 8.6, J_{HH} = 6.5 Hz, py).

^{1}H{^{31}P} NMR (THF-d_8, 25°C, 500 MHz, ppm): -6.61 (2H, s, Ru-H_2), 1.37 (18H, s, -C(CH_3)$_3$), 1.40 (18H, s, P(C(CH_3)$_3$)), 2.93 (2H, s, -C*HH*-), 3.55 (1H, s, -C*H*-), 5.32 (1H, d, J_{HH} = 6.5 Hz, Py), 5.83 (1H, d, J_{HH} = 8.7 Hz, Py) 6.19 (1H, dd, J_{HH} = 8.6, J_{HH} = 6.5 Hz, py).

^{31}P{^{1}H} NMR (THF-d_8, 25°C, 202 MHz, ppm): 101.2 (d, J_{PP} = 242.7 Hz, -P(^{t}Bu)$_2$), 97.2 (d, J_{PP} = 242.8 Hz, -P(^{t}Bu)$_2$)

^{13}C{^{1}H} (THF-d_8, 126 MHz, ppm): 213.1, 168.4, 160.2, 130.4, 109.4, 96.8, 39.4, 38.6, 35.7, 35.6, 34.7, 34.7, 31.4, 30.4.

IR (THF, KBR plate, cm^{-1}): 1871 (*CO*).

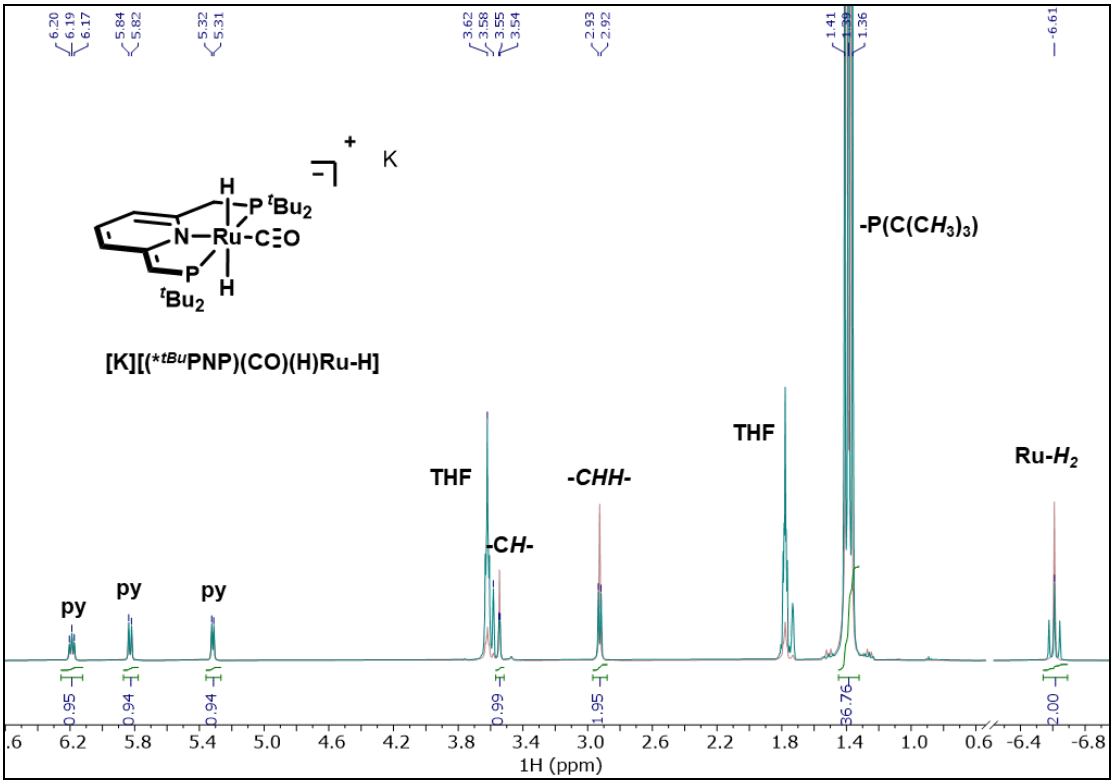

Figure S28. Superimposed ^{1}H NMR (blue) and $^{1}H\{^{31}P\}$ NMR (red) spectra of **[K][(*^{tBu}PNP)(CO)(H)Ru-H]** (500 MHz, 298K, THF-d_8).

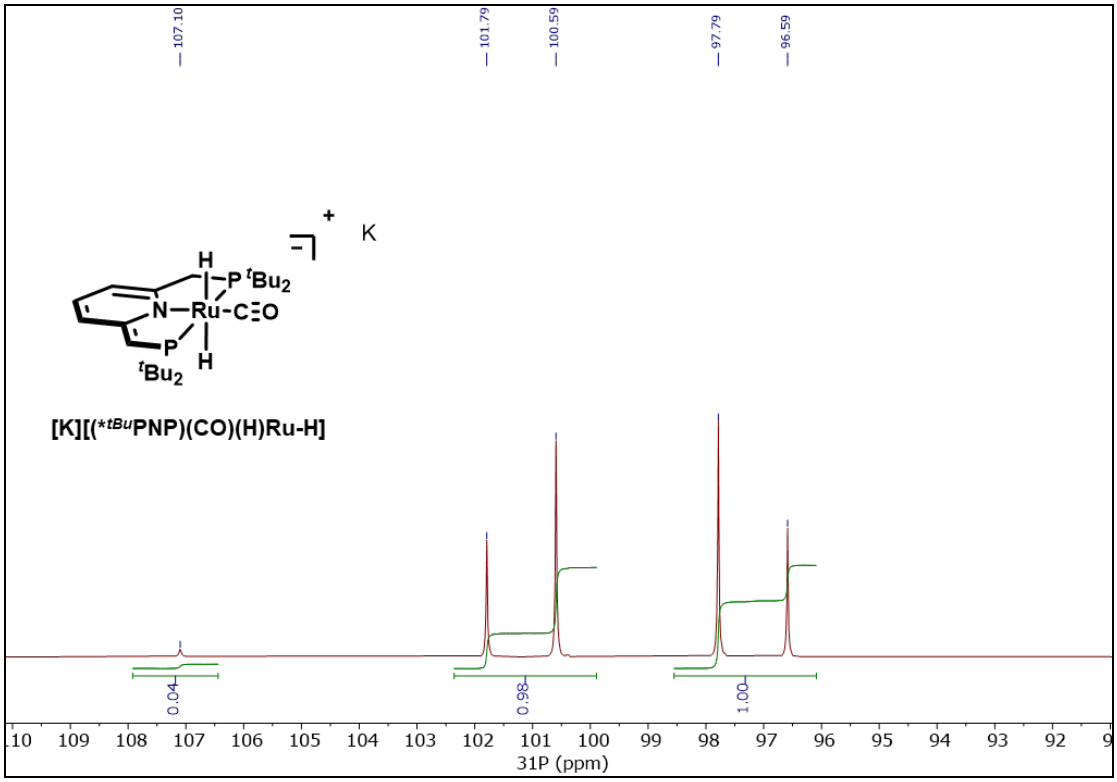

Figure S29. $^{31}P\{^{1}H\}$ NMR (202 MHz, 298K, THF-d_8) spectrum of **[K][(*^{tBu}PNP)(CO)(H)Ru-H]**. The peak at 107.1 ppm corresponds to **(^{tBu}PNP)(CO)(H)Ru-H**.

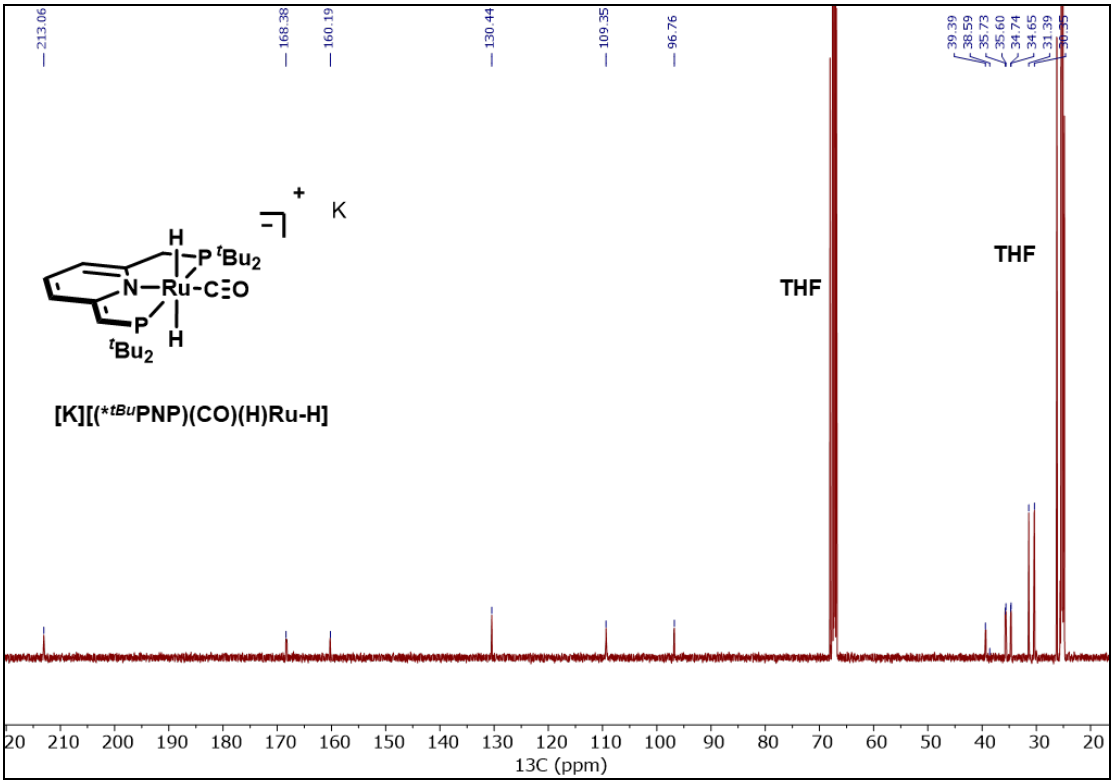

Figure S30. $^{13}C\{^{1}H\}$ NMR (126 MHz, 298K, THF-d_8) spectrum of **[K][(*^{tBu}PNP)(CO)(H)Ru-H]**.

Section 3: pK_{ip} Measurements.

A. pK_{ip} of [(PNP)Co-N_2][BAr_4^F].

In a typical experiment, a 11 mM stock solution of **[(PNP)Co-N_2][BAr_4^F]** was prepared in THF as was a 42 mM stock solution of **$^{tBu}P_1$(pyrr)$_3$**, (pK_{ip}= 20.2 in THF)[24] in THF. 380 µL (4 µmol) of the **[(PNP)Co-N_2][BAr_4^F]** solution was transferred to each of 4 NMR tubes. Varying equivalents of the phosphazene base was then added to each tube from the stock solution (1, 1.5, 2, and 2.5 equiv.). After addition, the tubes were inverted and the $^{31}P\{^1H\}$ NMR spectrum of each sample was recorded. The titration was done in triplicate so that the overall pK_{ip} is determined from three independent trials.

To ensure accurate integration, a relaxation delay of 10 seconds (d1 = 10 s) was used; increasing the delay time did not change any of the relative integrations. The phosphazene base has a peak at -9.4 ppm in the $^{31}P\{^1H\}$ spectrum; after protonation, the peak shifts to 22.5 ppm. The ratio of the protonated:deprotonated base was determined from the relative integrations of the two peaks. The concentrations of **[(PNP)Co-N_2][BAr_4^F]** and **(*PNP)Co-N_2** were determined from mass balance, assuming the amount of **(*PNP)Co-N_2** present is equivalent to the amount of protonated base. The peaks for both **(*PNP)Co-N_2** and **[(PNP)Co-N_2][BAr_4^F]** are broad, precluding accurate integration. To confirm the assumption of mass balance, a 44 mM stock solution of triphenyl phosphate (6 µmol) was added as an internal ^{31}P standard during the addition of 1 equiv. of **$^{tBu}P_1$(pyrr)$_3$**. Integration of the triphenyl phosphate relative to the two phosphazene peaks (HP_1 + P_1) yields >95% of the expected concentration, indicating only proton transfer to the phosphazene occurs. Once the concentration of the four reactants were known, the equilibrium expression can be obtained by using eq. 1.

$$K_{eq} = \frac{[(^*\mathbf{PNP})\mathbf{Co}-\mathbf{N_2}][\mathrm{HP_1}]}{[(\mathbf{PNP})\mathbf{Co}-\mathbf{N_2}][\mathrm{P_1}]} \quad (1)$$

Rearrangement to eq. 2 allows for the equilibrium constant to be determined from the slope of the plot of $\frac{[(^*\mathbf{PNP})\mathbf{Co}-\mathbf{N_2}][\mathbf{HP_1}]}{[(\mathbf{PNP})\mathbf{Co}-\mathbf{N_2}]}$ vs. [P_1] .

$$[\mathrm{P_1}] \cdot K_{eq} = \frac{[(^*\mathbf{PNP})\mathbf{Co}-\mathbf{N_2}][\mathrm{HP_1}]}{[(\mathbf{PNP})\mathbf{Co}-\mathbf{N_2}]} \quad (2)$$

Since the pK_{ip} of the phosphazene base is known, the final pK_{ip} of **[(PNP)Co-N_2][BAr_4^F]** is obtained using eq. 3.

$$\mathrm{p}K_{ip}[(\mathbf{PNP})\mathbf{Co}-\mathbf{N_2}] = \mathrm{p}K_{ip}(\mathrm{HP_1}) - \log K_{eq} \quad (3)$$

The pK_{ip} (pK_a = pK_{ip}) of the phosphazene base is 20.2,[24] giving a final pK_{ip} of 20.4 ± 0.2 for **[(PNP)Co-N_2][BAr_4^F]**.

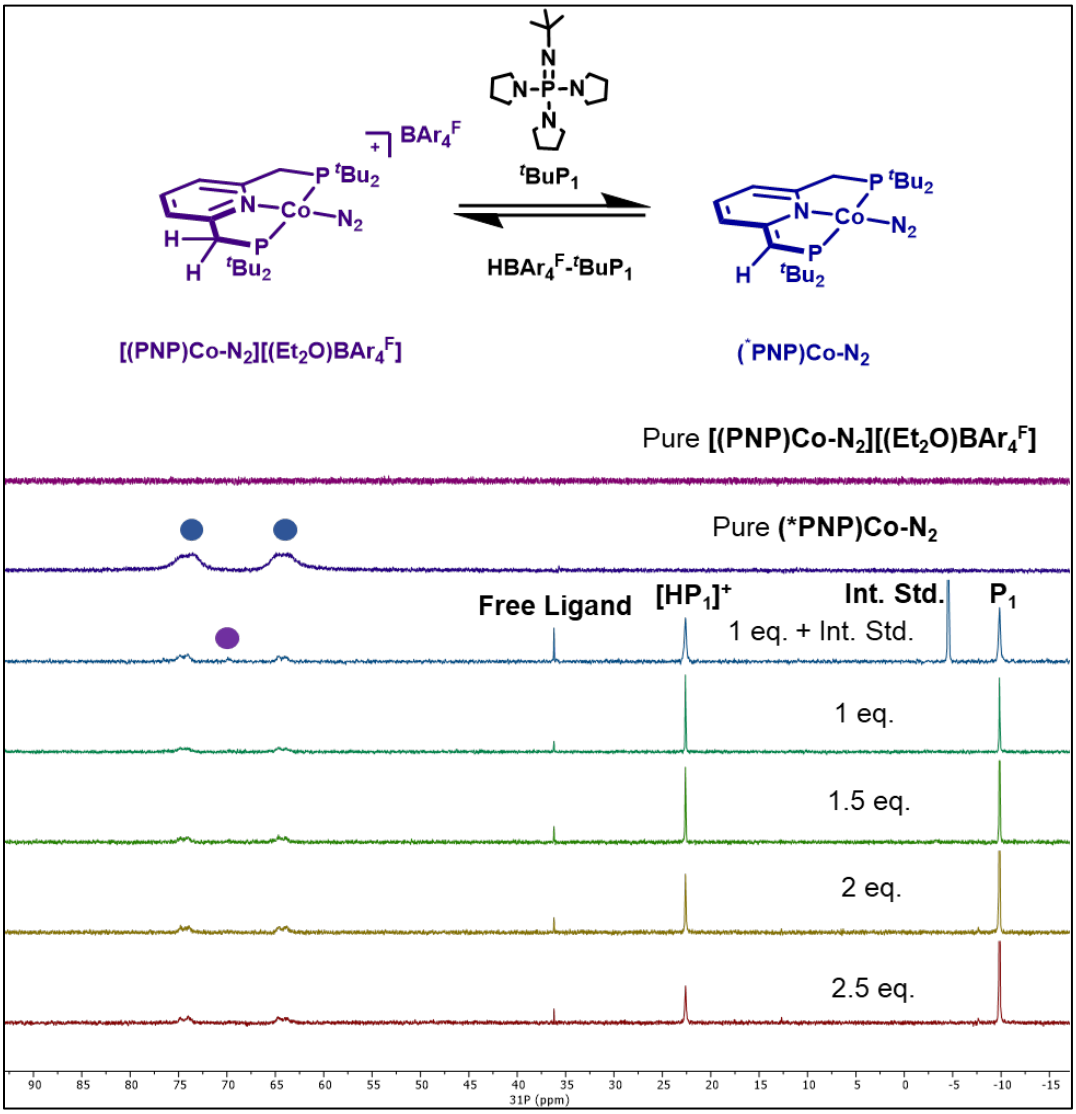

Figure S31. Stacked $^{31}P\{^{1}H\}$ NMR spectra (202 MHz, 298K, THF) of $^{tBu}P_1(NC_4H_8)_3$ addition to **[(PNP)Co-N_2][(Bar$_4^F$]**. Assuming mass balance the relative integration of the protonated phosphazene base versus free base allows for the determination of the pK_{ip}. The peaks for both **(*PNP)Co-N_2** and **[(PNP)Co-N_2][Bar$_4^F$]** are broad, precluding accurate integration. This broadening is present in pure samples; see top two spectra of product (6 mM in THF) and starting material (4 mM in THF). Addition of an internal standard triphenylphosphate indicates that all mass is accounted for. Integration of the free ligand is consistent throughout.

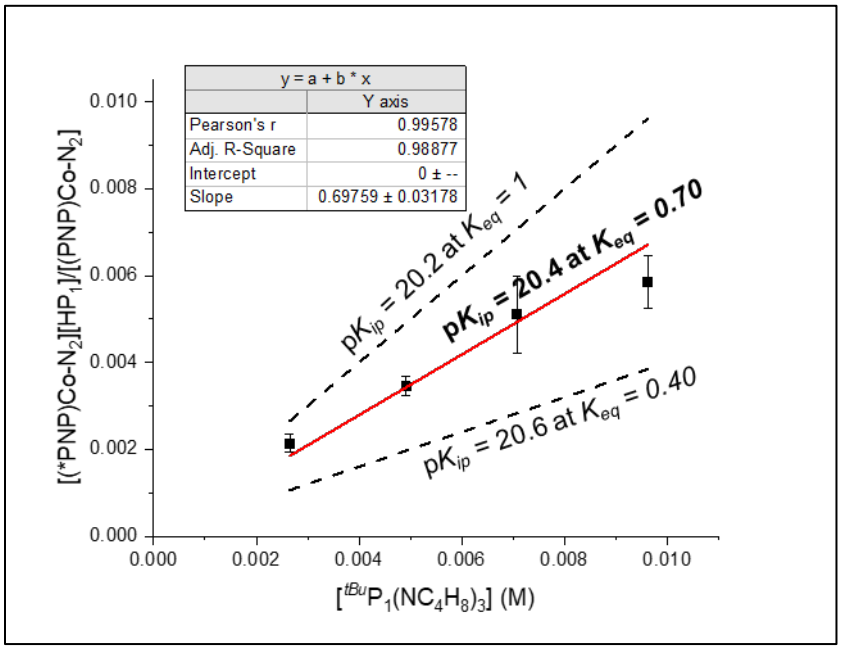

Figure S32. Plot of $\frac{[(^{*}\mathbf{PNP})\mathbf{Co}-\mathbf{N_2}][\mathbf{HP_1}]}{[(\mathbf{PNP})\mathbf{Co}-\mathbf{N_2}]}$ vs. [^{tBu}**P$_1$(NC$_4$H$_8$)$_3$**], giving a K_{eq} value of 0.70 ± 0.03 yielding a pK_{ip} of 20.4 ± 0.2 for **[(PNP)Co-N$_2$][BAr$_4^F$]**. Dashed lines show the expected fit for the upper and lower pK_{ip} bounds of the error.

B. pK_{ip} of [(PNP)(CO)(H)Fe][BAr_4^F].

In a typical experiment, a 6 mM stock solution of **[(PNP)(CO)(H)Fe][BAr_4^F]** was prepared in THF and aliquoted into 5 separate NMR tubes (654 µL, 4 µmoles). To each NMR tube was added varying equivalents (0.5, 0.75, 1, 1.25, and 1.5) of the phosphazene base, **$^{tBu}P_1(NC_4H_8)_3$**, (pK_{ip} = 20.2 in THF)[24] from a 54 mM stock solution in THF. After addition, the $^{31}P\{^1H\}$ NMR spectrum of each sample was recorded. Data analysis was done analogously to that described above for **[(PNP)Co-N_2][BAr_4^F]**. However, unlike the titration of **[(PNP)Co-N_2][BAr_4^F]**, peaks for both the protonated and deprotonated iron species are observed; therefore, the relative integrations of all four species were used to determine equilibrium concentrations. For each trial, only **[(PNP)(CO)(H)Fe][BAr_4^F]** with purity >98% from $^{31}P\{^1H\}$ NMR was used, and the impurity accounted for in determining initial concnetrations. Stock solutions of **[(PNP)(CO)(H)Fe][BAr_4^F]** were made and used on the same day.

A pK_{ip} of 19.8 ± 0.2 is obtained for **[(PNP)(CO)(H)Fe][BAr_4^F]**.

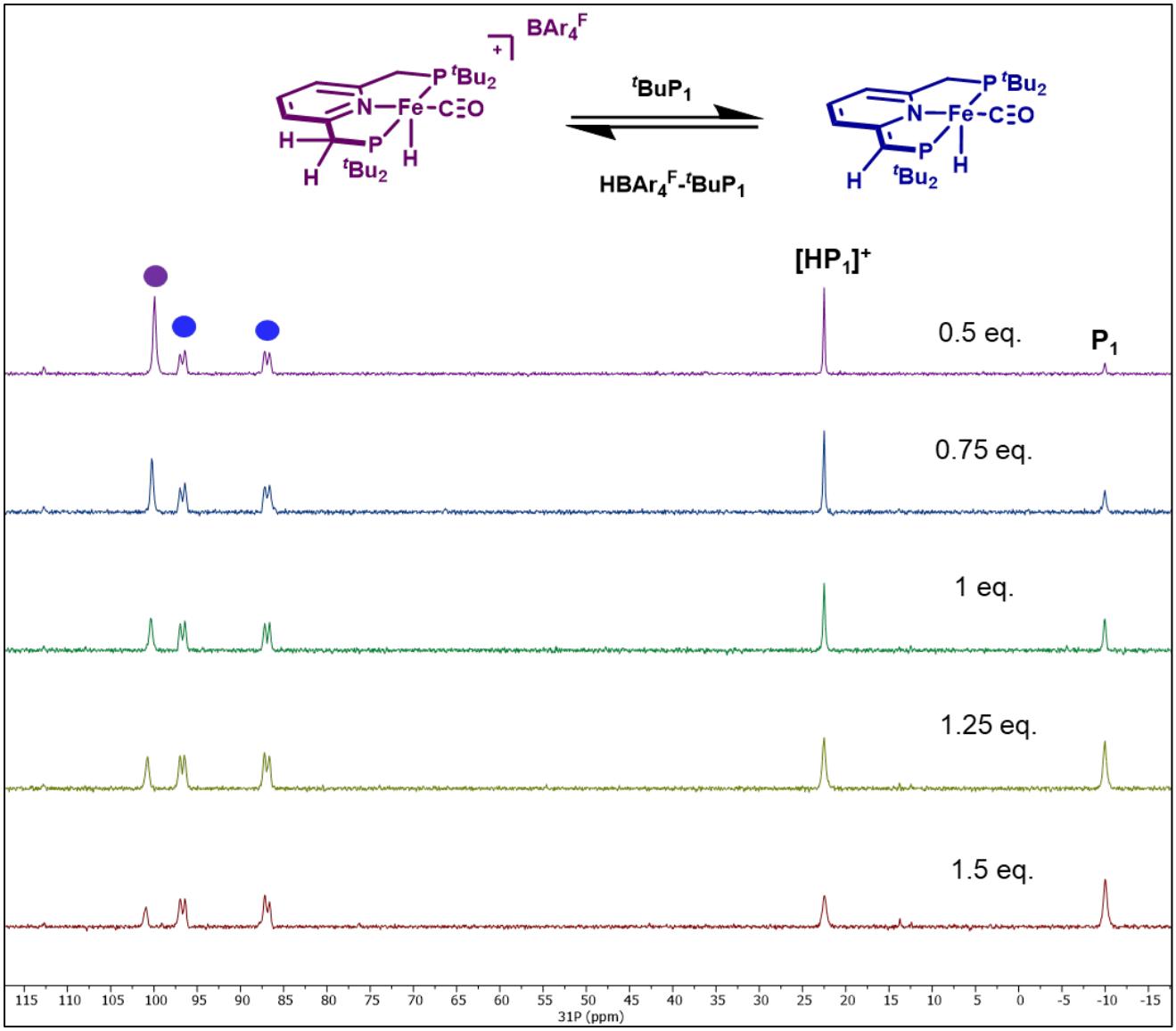

Figure S33. $^{31}P\{^{1}H\}$ NMR spectra (202 MHz, 298K, THF) of $^{tBu}P_1(NC_4H_8)_3$ addition to **[(PNP)(CO)(H)Fe][BAr$_4^F$]**.

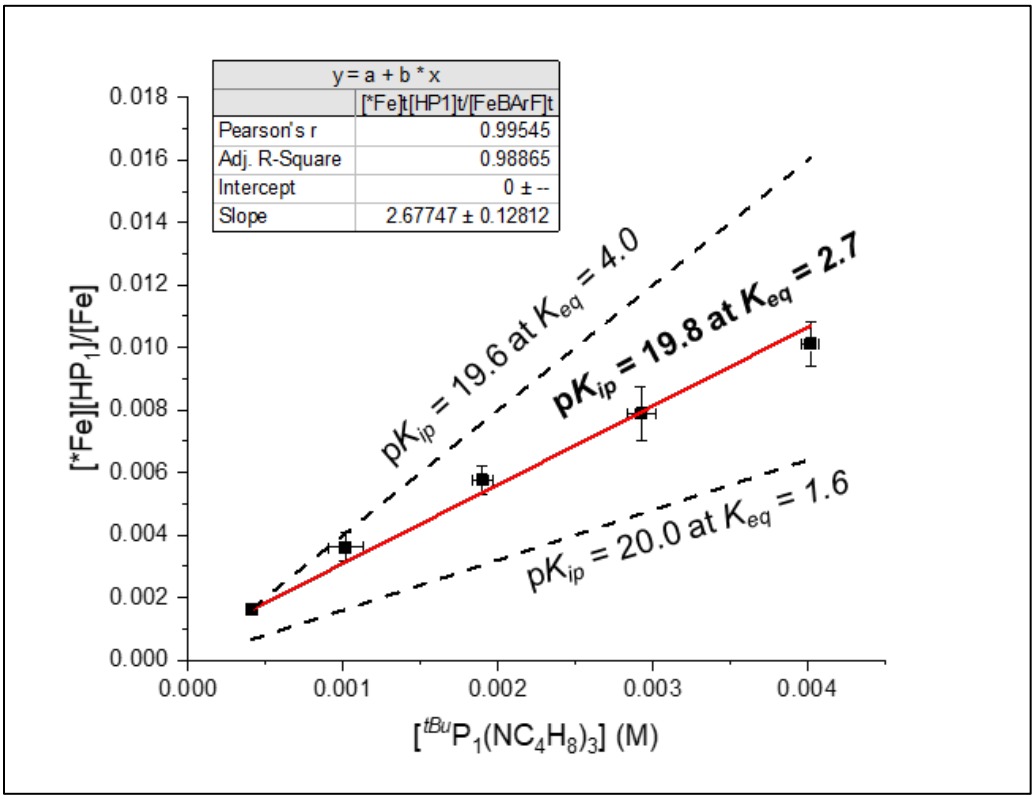

Figure S34. Plot of $\frac{[(^{*}\mathbf{PNP})\mathbf{Fe(H)(CO)}][\mathbf{HP_1}]}{[(\mathbf{PNP})\mathbf{Fe(H)(CO)}]}$ vs. [^{tBu}**P$_1$(NC$_4$H$_8$)$_3$**], giving a K_{eq} value of 2.7 ± 0.1 yielding pK_{ip} = 19.8 ± 0.2 for **[(PNP)(CO)(H)Fe][BAr$_4^F$]**. Dashed lines show the expected fit for the upper and lower pK_{ip} bounds of the error.

C. pK_{ip} of (PNP)(CO)(H)Fe-H.

In a typical experiment, 194 µL of a 25 mM stock solution of **(PNP)(CO)(H)Fe-H** (5 µmol) in THF was placed into a J Young NMR tube. To the solution was added varying equivalents (1, 2, 3, 4) of the Wittig Base, **Ph(CH$_3$)C=P(2,4,6-(MeO)$_3$-C$_6$H$_2$)$_3$**, from a 35 mM stock solution in THF. Additional THF was added to ensure a minimum solvent level of 0.5 mL. After combination, the ^{31}P{^{1}H} NMR spectrum was recorded. The reactions were repeated in triplicate so that the overall pK_{ip} is determined from three independent trials. The Wittig base was prepared immediately prior to use in titrations by addition of KO^{t}Bu to **[Ph(CH$_3$)C=P(2,4,6-(MeO)$_3$-C$_6$H$_2$)$_3$][HBr]** in THF, filtration through celite, and removal of all volatiles *in vacuo*.[4] Purity was confirmed via ^{1}H and ^{31}P{^{1}H} NMR in C_6D_6, and only base with >95% purity was used in the titration, and the purity was taken into account when calculating the concentrations. Stock solutions were made only on the day of preparation. Stock solutions of **(PNP)(CO)(H)Fe-H** were used within two days of preparation; this species is stable under an N_2 atmosphere. Data analysis was done analogously to that described above.

The pK_{ip} of the Wittig base is 32.1,[4] giving a final pK_{ip} of 32.8 ± 0.2 for **(PNP)(CO)(H)Fe-H**.

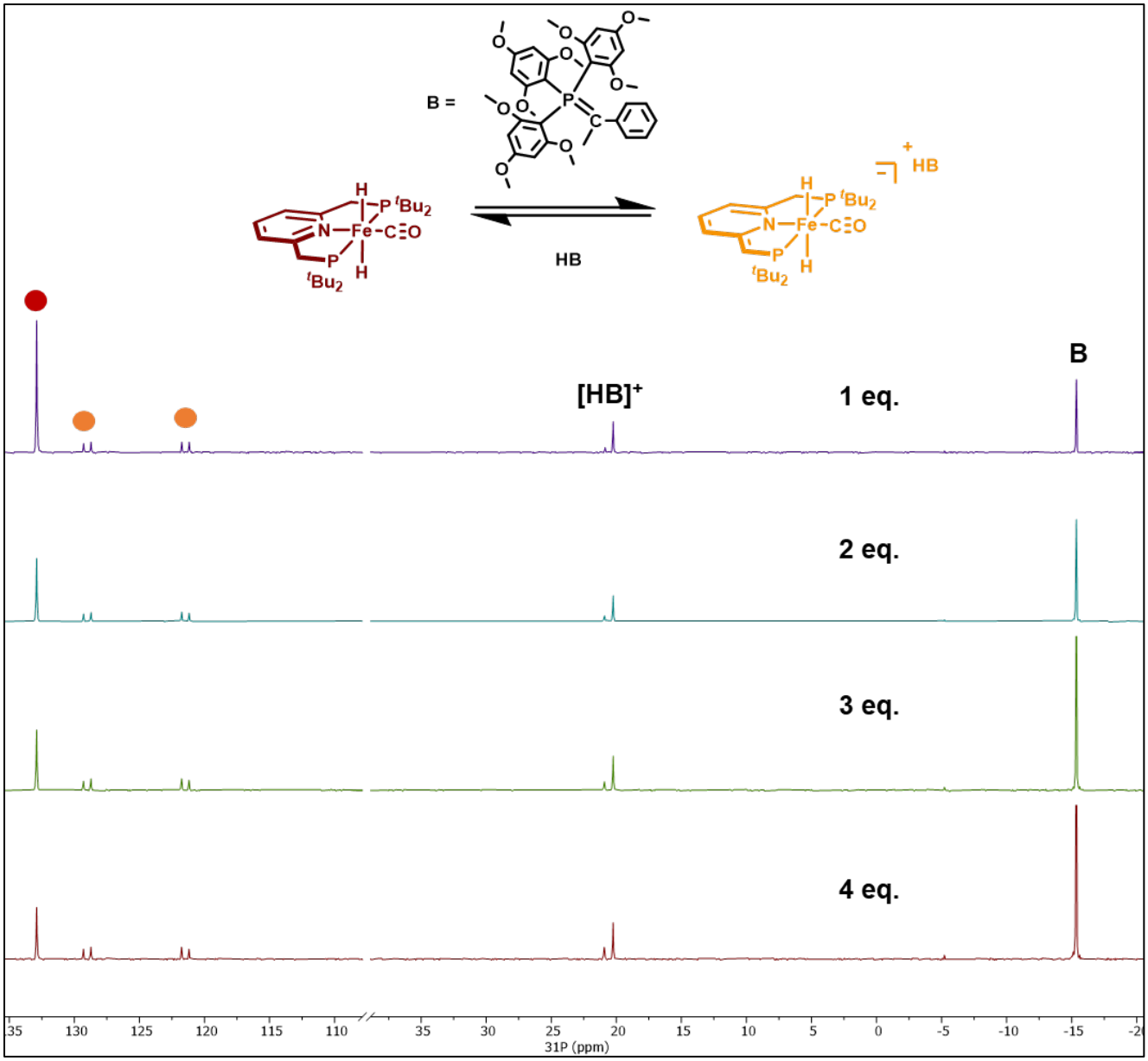

Figure S35. $^{31}P\{^{1}H\}$ NMR spectra (202 MHz, 298K, THF) of **$Ph(CH_3)C=P(2,4,6\text{-}(MeO)_3\text{-}C_6H_2)_3$** addition to **(PNP)(CO)(H)Fe-H**. Integration of all four species were used to determine the equilibrium concentration of reactants. The peak at 20.9 ppm is attributed to a residual impurity in the Wittig base (trace moisture) accounting for less than 5% of the total integration; integration of this peak relative to the protonated and deprotonated base indicates the concentration does not change during the reaction. The peak at -5.2 ppm is attributed to the loss of triphenylphosphine portion of the Wittig base, a result of trace moisture.[4]

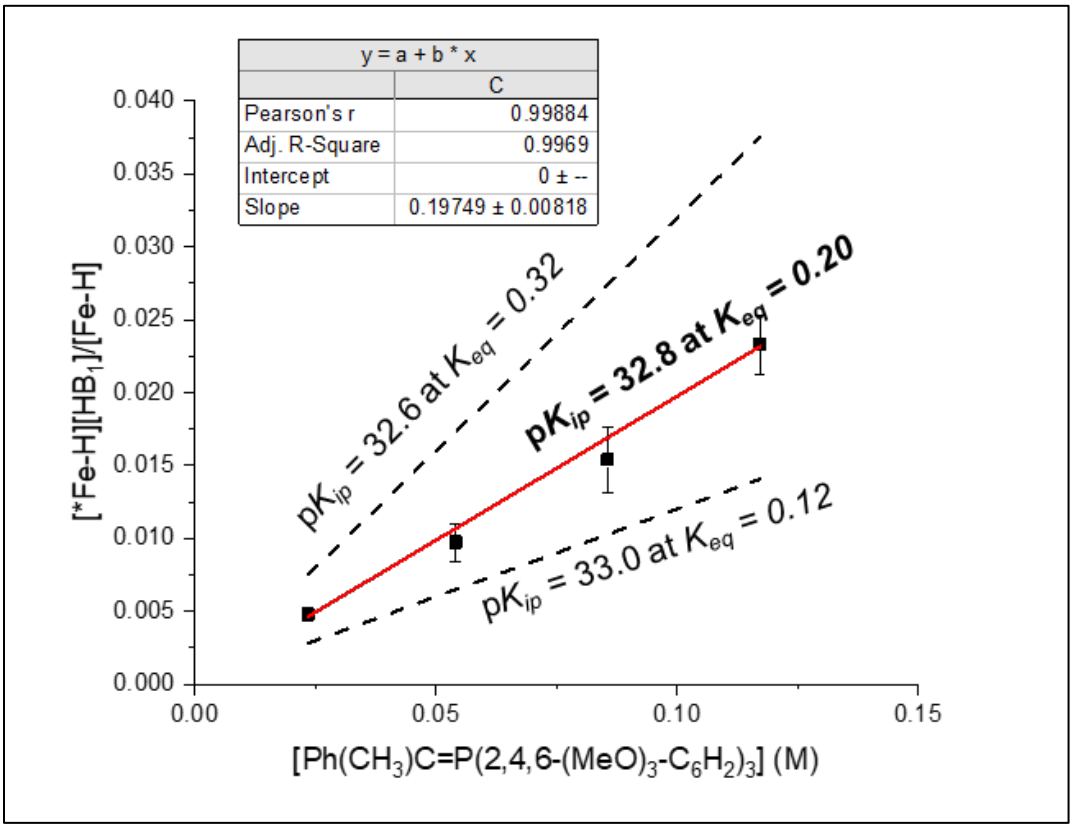

Figure S36. Plot of $\frac{[^{*}\mathbf{Fe-H}][\mathbf{HB}]}{[\mathbf{Fe-H}]}$ vs. [**Ph(CH$_3$)C=P(2,4,6-(MeO)$_3$-C$_6$H$_2$)$_3$**], giving a K_{eq} value of 0.20 ± 0.01 yielding a pK_{ip} of 32.8 ± 0.2 for **[(PNP)(CO)(H)Fe-H**. Dashed lines show the expected fit for the upper and lower pK_{ip} bounds of the error.

D. pK_{ip} of (PNP)(CO)(H)Ru-H.

In a typical experiment, 278 µL of a 17 mM stock solution of **(*PNP)(CO)(H)Ru** (5 µmol) in THF was added to a Teflon valved J Young NMR Tube. The tube was placed on the Schlenk line and freeze-pump-thawed three times to remove dissolved gases, after which the atmosphere replaced with H_2. The reaction was warmed to room temp and placed on a rocker to mix for two hours; the formation of **(PNP)(CO)(H)Ru-H** was confirmed via $^{31}P\{^1H\}$ NMR spectroscopy. The tube was returned to the glovebox, frozen in a cold well with lN2, and varying equivalents (0.5, 0.75, 1, 1.25, and 1.5) of the Wittig Base, **Ph(CH$_3$)C=P(2,4,6-(MeO)$_3$-C$_6$H$_2$)$_3$**, were added from a 35 mM stock solution in THF. After combination, the $^{31}P\{^1H\}$ NMR spectrum was recorded. The reactions were repeated in triplicate so that the overall pK_{ip} is determined from three independent trials.

A final pK_{ip} = 31.4 ± 0.2 was obtained for **(PNP)(CO)(H)Ru-H**.

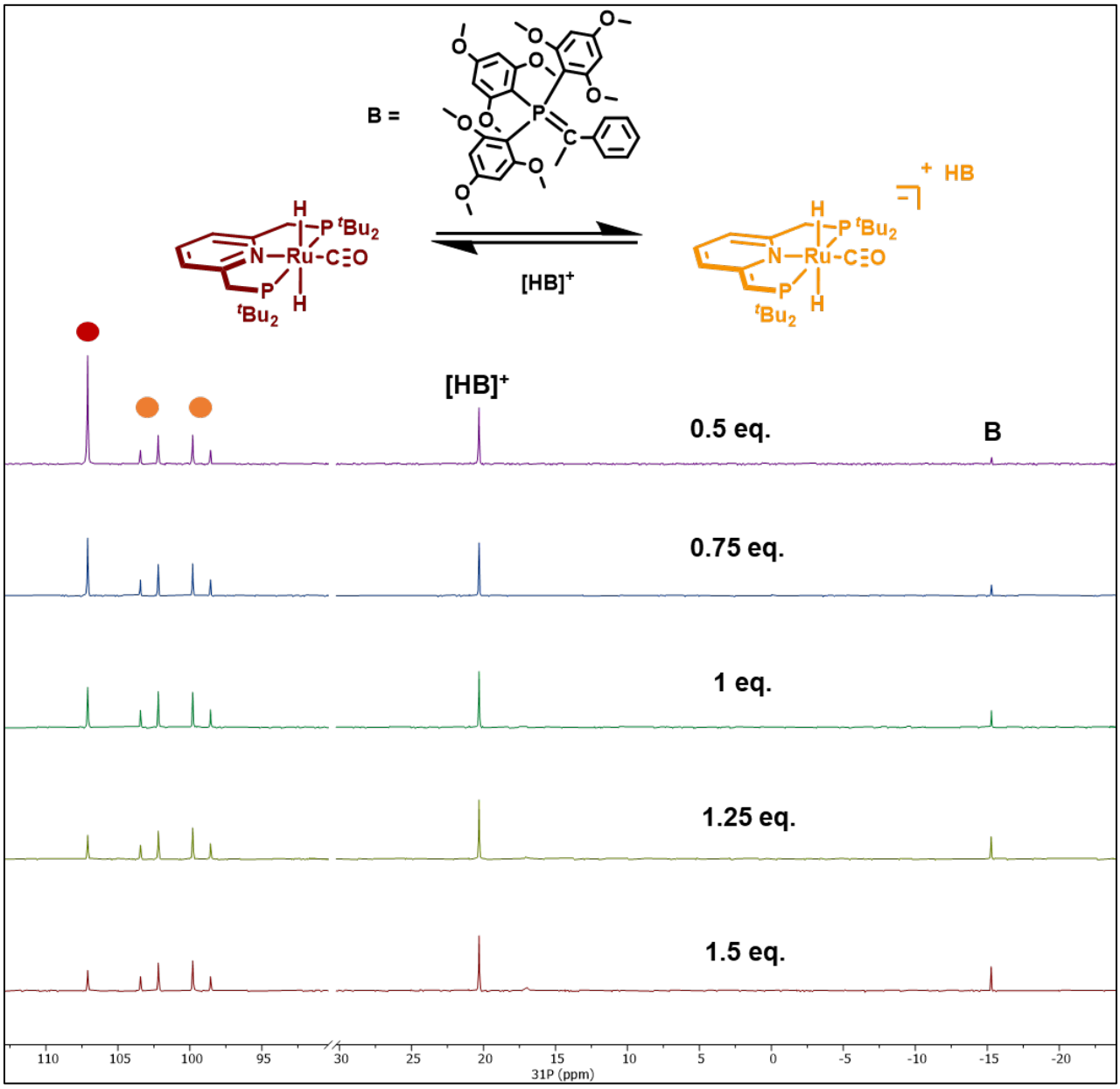

Figure S37. $^{31}P\{^{1}H\}$ NMR spectra (202 MHz, 298K, THF) of **Ph(CH_3)C=P(2,4,6-($MeO)_3$-$C_6H_2)_3$** addition **to (PNP)(CO)(H)Ru-H**. Integration of all four species were used to determine the equilibrium concentration of reactants.

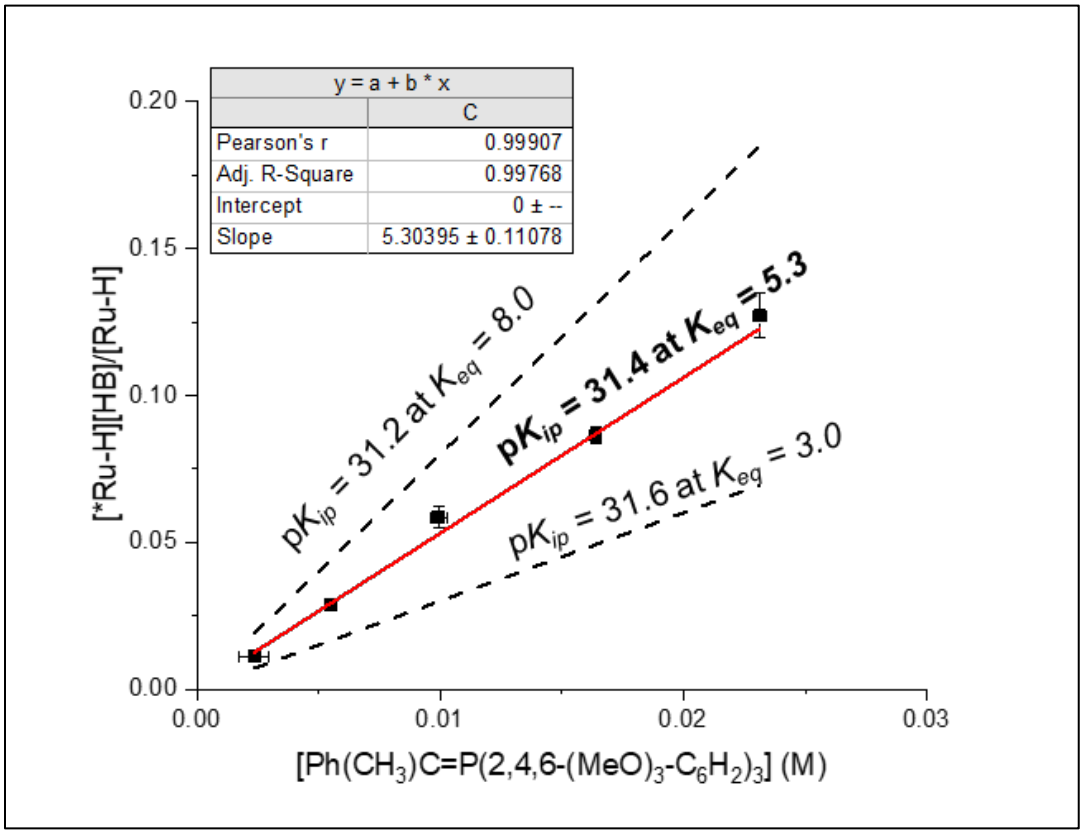

Figure S38. Plot of $\frac{[(^{*}\mathbf{Ru-H}][\mathbf{HB}]}{[\mathbf{Ru-H}]}$ vs. [**Ph(CH$_3$)C=P(2,4,6-(MeO)$_3$-C$_6$H$_2$)$_3$**], giving a K_{eq} value of 5.3 ± 0.1 yielding a pK_{ip} of 31.4 ± 0.2 for **(PNP)(CO)(H)Ru-H**. Dashed lines show the expected fit for the upper and lower pK_{ip} bounds of the error.

E. Attempt to Measure pK_{ip} of (PNP)Co-H.

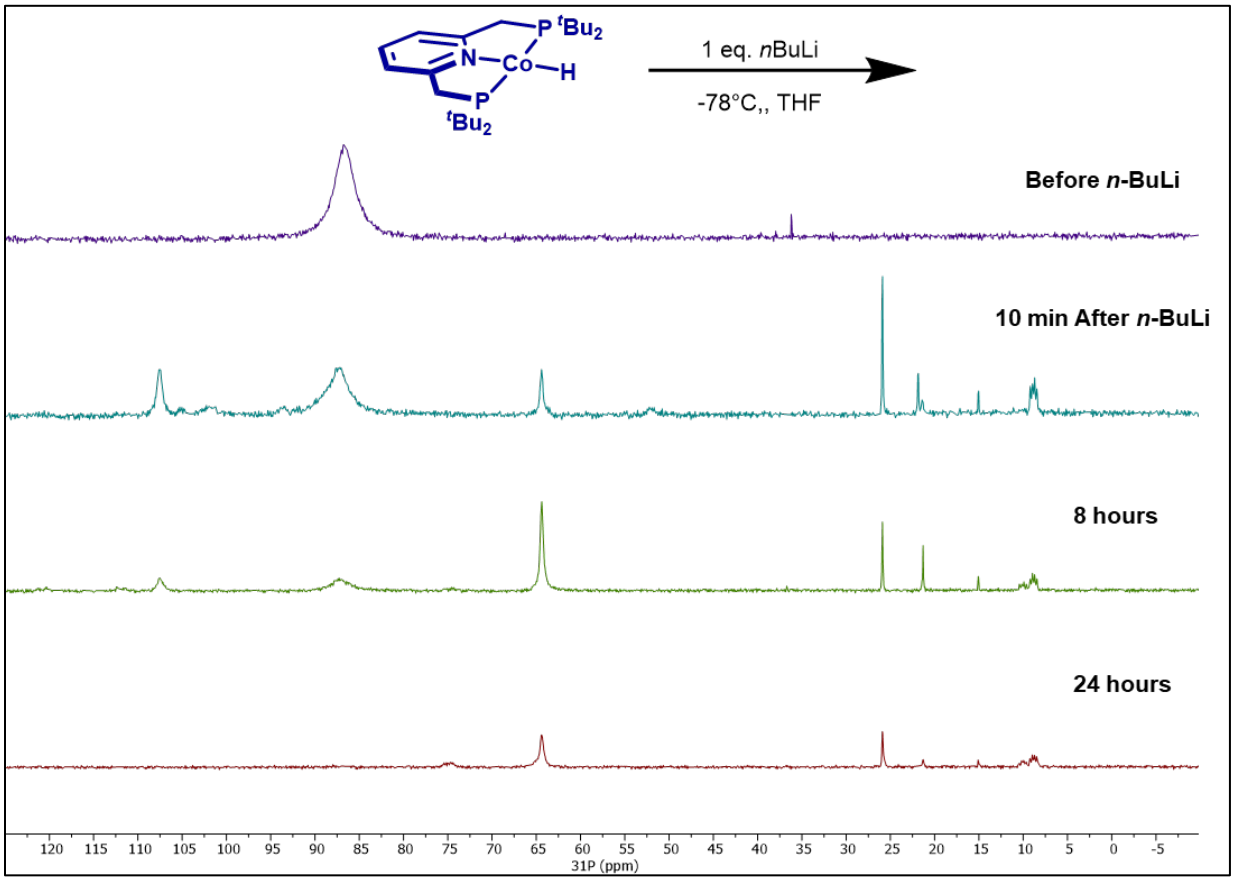

Figure S39. $^{31}P\{^{1}H\}$ NMR spectra (202 MHz, 298K, THF) of *n*-BuLi (23 µmol, 9 µL of 2.5M solution in hexanes) addition to **(PNP)Co-H** (10 mg, 23 µmol, 38 mM in THF) at -78°C. Upon addition of *n*-BuLi, a color change from dark red to black/grey occurred. After 24 hours, dark precipitates were observed in the reaction mixture. A mixture of products was observed in the $^{31}P\{^{1}H\}$ NMR spectra which were not readily identifiable. Since reversible deprotonation and protonation of **(PNP)Co-H** did not occur, the pK_{ip} of **(PNP)Co-H** was not able to be measured.

F. Estimation of pK_α.

Ion-pairing can impact pK_a measurements in THF, which gives rise to pK_{ip} and pK_α. Consider the following equilibrium (eq 4) between a base (B), and an acid (designated MH^+) that is ion-paired to A^-.[4] For clarity, the proton is shown in red.

$$B + (MH^+)(A^-) \underset{\rightleftharpoons}{K_d^{MA}} B + MH^+ + A^- \underset{\rightleftharpoons}{K} M + BH^+ + A^- \underset{\rightleftharpoons}{(K_d^{BA})^{-1}} M + (BH^+)(A^-) \quad (4)$$

The equilibrium that corresponds to the proton transfer, K, gives rise to pK_α, which is f the free-ion pK_a according to eq 5.

$$\log K = \mathrm{p}K_\alpha BH^+ - \mathrm{p}K_\alpha MH^+ \quad (5)$$

However, the equilibrium that is observed during titrations corresponds to $\frac{K_d^{MA} \cdot K}{K_d^{BA}}$, where K_d^{MA} and K_d^{BA} corresponds to the dissociation constants of the respective ion-pairs. Hence, the *observed* equilibrium corresponds to the difference in ion-paired acidities, pK_{ip} (eq 6)

$$\mathrm{p}K_{ip}BH^+ - \mathrm{p}K_{ip}MH^+ = \log\frac{(K_d^{MA})K}{K_d^{BA}} \quad (6)$$

Combining the two expressions (eq 5 and 6) gives eq 7:

$$\Delta\mathrm{p}K_{ip} = \mathrm{p}K_\alpha BH^+ - \mathrm{p}K_\alpha MH^+ + \log\frac{K_d^{MA}}{K_d^{BA}} \quad (7)$$

Rearranging eq 7 allows for the determination of pK_α (eq 8).

$$\mathrm{p}K_\alpha MH^+ = \mathrm{p}K_\alpha BH^+ - \Delta\mathrm{p}K_{ip} + \log\frac{K_d^{MA}}{K_d^{BA}} \quad (8)$$

Unless noted, reported pK_as in THF correspond to pK_{ip} values. As we do not know the dissociation constants, the pK_a values reported in the text correspond to pK_{ip}, not pK_α. The dissociation constants can be estimated from the Fuoss equation[25] (eq 9):

$$\mathrm{K_d} = \frac{3000 \cdot \mathrm{e^b}}{4 \cdot \pi \cdot \mathrm{N} \cdot \mathrm{a^3}} \quad (9)$$

This gives the dissociation constant in units of mM^{-1}, so multiplication by a factor of 1000 gives the dissociation constant in units of M^{-1}. Here, e is exponential, N is Avogadro's number, a is the inter-ion distance in cm, and b is the following eq (10):

$$\mathrm{b} = \frac{-e^2}{\mathrm{a} \cdot \epsilon \cdot k \cdot \mathrm{T}} \quad (10)$$

In this expression, *e* is the charge of an electron (4.8×10^{-10} esu), a is the inter-ion distance in cm, ε is the dielectric constant (7.58 for THF), *k* is Boltzmann's constant (1.38×10^{-16} erg/deg), and T is temperature in Kelvin.

To evaluate K_d, the following ion radii are employed:

Ion	Ionic-radii / Å	Reference	Notes/Assumptions
$^{t\text{Bu}}P_1(pyrr)_3H^+$	4	24	
4-MeO-$C_6H_4P_1(pyrr)H^+$	4	24	
$(CH_3)_2C{=}PPh_3H^+$ (WH^+)	4.6	4	
$Ph(CH_3)C{=}P(2,4,6\text{-}(MeO)_3\text{-}C_6H_2)_3H^+$ (BH^+)	6.4	4	
$[(PNP)Co\text{-}N_2]^+$	3.6	12	From the average diameter measured from CDC 1879930 (5.4, 7.4, 8.7); all other cationic metal fragments assumed to have the same radii.
BPh_4^-	4.4	26	
BF_4^-	2.5	27	
$BAr^F{}_4^-$	5.1	12	Measured from CDC 1879930

Thus, pK_α can be estimated. Errors reported are from propagation of uncertainties in pK_{ip} values; the error for the pK_{ip} values for the bases is assumed to be ± 0.2. Combined with the errors for the metal complexes (± 0.2), the uncertainty in the pK_α values are ± 0.3. In the main text, we triple this uncertainty to emphasize that we do not know the uncertainty in the values of K_d.

<table>
<tr><td colspan="6">$[(PNP)Co-N_2][BAr^F_4] + {}^{t}BuP_1 \overset{K_d^{MA}}{\rightleftharpoons} [(PNP)Co-N_2]^+ + [BAr^F_4]^- + {}^{t}BuP_1 \overset{K}{\rightleftharpoons}$
$({}^{*}PNP)Co-N_2 + [BAr^F_4]^- + [H\ {}^{t}BuP_1]^+ \overset{(K_d^{BA})^{-1}}{\rightleftharpoons} ({}^{*}PNP)Co-N_2 + [H\ {}^{t}BuP_1][BAr^F_4]$</td></tr>
<tr><td>$K_d^{MA} = 0.12M$</td><td>$(K_d^{BA}) = 0.16M$</td><td>pK_α[H ^{t}BuP$_1$]$^+$ = 20.2[a]</td><td>pK_{ip}[H ^{t}BuP$_1$]$^+$ = 20.2[a]</td><td>pK_{ip}[(PNP)Co − N$_2$]$^+$ = 20.4</td><td>pK_α[(PNP)Co − N$_2$]$^+$ = 20.3</td></tr>
<tr><td colspan="6">$[(PNP)(CO)(H)Fe][BAr^F_4] + {}^{t}BuP_1 \overset{K_d^{MA}}{\rightleftharpoons} [(PNP)(CO)(H)Fe]^+ + [BAr^F_4]^- + {}^{t}BuP_1 \overset{K}{\rightleftharpoons}$
$({}^{*}PNP)(CO)(H)Fe + [BAr^F_4]^- + [H\ {}^{t}BuP_1]^+ \overset{(K_d^{BA})^{-1}}{\rightleftharpoons} ({}^{*}PNP)(CO)(H)Fe + [H\ {}^{t}BuP_1][BAr^F_4]$</td></tr>
<tr><td>$K_d^{MA} = 0.12M$</td><td>$(K_d^{BA}) = 0.16M$</td><td>pK_α[H ^{t}BuP$_1$]$^+$ = 20.2[a]</td><td>pK_{ip}[H ^{t}BuP$_1$]$^+$ = 20.2[a]</td><td>pK_{ip}[(PNP)(CO)(H)Fe]$^+$ = 19.8</td><td>pK_α[(PNP)(CO)(H)Fe]$^+$ = 19.7</td></tr>
<tr><td colspan="6">$[(PNP)(CO)_2Mn][BAr^F_4] + OMeP_1 \overset{K_d^{MA}}{\rightleftharpoons} [(PNP)(CO)_2Mn]^+ + [BAr^F_4]^- + OMeP_1 \overset{K}{\rightleftharpoons}$
$({}^{*}PNP)(CO)_2Mn + [BAr^F_4]^- + [OMeP_1H]^+ \overset{(K_d^{BA})^{-1}}{\rightleftharpoons} ({}^{*}PNP)(CO)_2Mn + [OMeP_1H][BAr^F_4]$</td></tr>
<tr><td>$K_d^{MA} = 0.12M$</td><td>$(K_d^{BA}) = 0.16M$</td><td>pK_α[OMeP$_1$H]$^+$ = 16.8[a]</td><td>pK_{ip}[OMeP$_1$H]$^+$ = 16.8[a]</td><td>pK_{ip}[(PNP)(CO)$_2$Mn]$^+$ = 18.8[b]</td><td>pK_α[(PNP)(CO)$_2$Mn]$^+$ = 18.9</td></tr>
<tr><td colspan="6">$[(PNP)(CO)_2Mn][BF_4] + OMeP_1 \overset{K_d^{MA}}{\rightleftharpoons} [(PNP)(CO)_2Mn]^+ + [BF_4]^- + OMeP_1 \overset{K}{\rightleftharpoons}$</td></tr>
</table>

$(\,^{*}\mathrm{PNP})(\mathrm{CO})_2\mathrm{Mn} + [\mathrm{BF_4}]^- + [\mathrm{OMeP_1H}]^+ \underset{\rightleftharpoons}{(K_d^{BA})^{-1}} (\,^{*}\mathrm{PNP})(\mathrm{CO})_2\mathrm{Mn} + [\mathrm{OMeP_1H}][\mathrm{BF_4}]$					
$K_d^{MA} = 0.0096M$	$(K_d^{BA}) = 0.017M$	$\mathrm{p}K_\alpha[\mathrm{OMeP_1H}]^+ = 16.8$[a]	$\mathrm{p}K_{ip}[\mathrm{OMeP_1H}]^+ = 16.8$[a]	$\mathrm{p}K_{ip}[(\mathrm{PNP})(\mathrm{CO})_2\mathrm{Mn}]^+ = 18.8$[b]	$\mathrm{p}K_\alpha[(\mathrm{PNP})(\mathrm{CO})_2\mathrm{Mn}]^+ = 18.6$
$(\,^{*}\mathrm{PNP})(\mathrm{CO})(\mathrm{H})\mathrm{Ru} + [\mathrm{H}\,^{t}\mathrm{BuP_1}][\mathrm{BF_4}] \underset{\rightleftharpoons}{K_d^{BA}} (\,^{*}\mathrm{PNP})(\mathrm{CO})(\mathrm{H})\mathrm{Ru} + [\mathrm{BF_4}]^- + [\mathrm{H}\,^{t}\mathrm{BuP_1}]^+ \underset{\rightleftharpoons}{K} [(\mathrm{PNP})(\mathrm{CO})(\mathrm{H})\mathrm{Ru}]^+ + [\mathrm{BF_4}]^- + {}^{t}\mathrm{BuP_1} \underset{\rightleftharpoons}{(K_d^{MA})^{-1}} [(\mathrm{PNP})(\mathrm{CO})(\mathrm{H})\mathrm{Ru}][\mathrm{BF_4}] + {}^{t}\mathrm{BuP_1}$					
$K_d^{BA} = 0.017M$	$K_d^{MA} = 0.0096M$	$\mathrm{p}K_\alpha[\mathrm{H}\,^{t}\mathrm{BuP_1}]^+ = 20.2$[a]	$\mathrm{p}K_{ip}[\mathrm{H}\,^{t}\mathrm{BuP_1}]^+ = 20.2$[a]	$\mathrm{p}K_{ip}[(\mathrm{PNP})(\mathrm{CO})(\mathrm{H})\mathrm{Ru}]^+ = 20.7$[c]	$\mathrm{p}K_\alpha[(\mathrm{PNP})(\mathrm{CO})(\mathrm{H})\mathrm{Ru}]^+ = 20.5$

[a]Ref 24. [b]Ref 28. [c]Ref 13.

In the above titrations, a neutral base reacts with a cationic acid. For the titrations of the neutral M-H, a neutral acid reacts with a neutral base to give an ion-pair (eq 11):

$$\mathrm{HM} + \mathrm{B} \underset{\rightleftharpoons}{K} [\mathrm{M}]^- + [\mathrm{BH}]^+ \underset{\rightleftharpoons}{(K_d)^{-1}} [\mathrm{M}][\mathrm{BH}] \tag{11}$$

The observed equilibrium corresponds to the difference in the ion-paired acidities (eq 12).

$$\mathrm{p}K_{ip}BH^+ - \mathrm{p}K_{ip}MH^+ = \log\frac{K}{K_d} \tag{12}$$

This is related to the difference in pK_α according to eq 13.

$$\Delta\mathrm{p}K_{ip} = \mathrm{p}K_\alpha BH^+ - \mathrm{p}K_\alpha MH^+ - \log K_d \tag{13}$$

Rearranging eq 13 allows for the determination of pK_α (eq 14).

$$\mathrm{p}K_\alpha MH^+ = \mathrm{p}K_\alpha BH^+ - \Delta\mathrm{p}K_{ip} - \log K_d \tag{14}$$

From this analysis, the pK_α were determined for the neutral M-H.

$(\mathrm{PNP})(\mathrm{CO})(\mathrm{H})_2\mathrm{M} + \mathrm{B} \underset{\rightleftharpoons}{K} [(\,^{*}\mathrm{PNP})(\mathrm{CO})(\mathrm{H})_2\mathrm{M}]^- + [\mathrm{BH}]^+ \underset{\rightleftharpoons}{(K_d)^{-1}} [(\,^{*}\mathrm{PNP})(\mathrm{CO})(\mathrm{H})_2\mathrm{M}][\mathrm{BH}]$				
$K_d = 0.055M$	$\mathrm{p}K_\alpha[\mathrm{BH}]^+ = 33.0$[a]	$\mathrm{p}K_{ip}[\mathrm{BH}]^+ = 32.1$[a]	$\mathrm{p}K_{ip}(\mathrm{PNP})(\mathrm{CO})(\mathrm{H})_2\mathrm{Fe} = 32.8$	$\mathrm{p}K_\alpha(\mathrm{PNP})(\mathrm{CO})(\mathrm{H})_2\mathrm{Fe} = 35.0$
$K_d = 0.055M$	$\mathrm{p}K_\alpha[\mathrm{BH}]^+ = 33.0$[a]	$\mathrm{p}K_{ip}[\mathrm{BH}]^+ = 32.1$[a]	$\mathrm{p}K_{ip}(\mathrm{PNP})(\mathrm{CO})(\mathrm{H})_2\mathrm{Ru} = 31.4$	$\mathrm{p}K_\alpha(\mathrm{PNP})(\mathrm{CO})(\mathrm{H})_2\mathrm{Ru} = 33.6$
$(\mathrm{PNP})(\mathrm{CO})_2(\mathrm{H})\mathrm{Mn} + \mathrm{W} \underset{\rightleftharpoons}{K} [(\,^{*}\mathrm{PNP})(\mathrm{CO})(\mathrm{H})_2\mathrm{M}]^- + [\mathrm{WH}]^+ \underset{\rightleftharpoons}{(K_d)^{-1}} [(\,^{*}\mathrm{PNP})(\mathrm{CO})_2(\mathrm{H})\mathrm{Mn}][\mathrm{WH}]$				
$K_d = 0.088M$	$\mathrm{p}K_\alpha[\mathrm{WH}]^+ = 28.9$[a]	$\mathrm{p}K_{ip}[\mathrm{WH}]^+ = 28.7$[a]	$\mathrm{p}K_{ip}(\mathrm{PNP})(\mathrm{CO})_2(\mathrm{H})\mathrm{Mn} = 31.2$[b]	$\mathrm{p}K_\alpha(\mathrm{PNP})(\mathrm{CO})_2(\mathrm{H})\mathrm{Mn} = 32.5$

[a]Ref 4. [b]Ref 28.

Note, if titrations were done in the reverse direction, more ion-pairing terms would have to be taken into account and hence introduces more uncertainty (eq 15).

$$[\mathrm{M}][\mathrm{A}] + [\mathrm{BH}][\mathrm{C}] \underset{}{\overset{K_d^{MA}}{\rightleftharpoons}} [\mathrm{M}]^- + [\mathrm{A}]^+ + [\mathrm{BH}][\mathrm{C}] \underset{}{\overset{K_d^{BC}}{\rightleftharpoons}} [\mathrm{M}]^- + [\mathrm{A}]^+ + [\mathrm{BH}]^+ + [\mathrm{C}]^-$$

$$\underset{}{\overset{K}{\rightleftharpoons}} \mathrm{MH} + [\mathrm{A}]^+ + B + [\mathrm{C}]^- \underset{}{\overset{(K_d^{CA})^{-1}}{\rightleftharpoons}} \mathrm{MH} + [\mathrm{A}][\mathrm{C}] + B \qquad (15)$$

Eq 15 assumes that all ion pairs remain in solution.

G. Estimation of p*K*$_a$s.

Morris has established an empirical formula to estimate the p*K*$_a$ of a transition metal hydride or dihydrogen complex in THF (eq 16).[29]

$$\mathrm{pK_a^{THF}} = \sum \mathrm{A_L} + \mathrm{C_{charge}} + \mathrm{C_{nd}} + \mathrm{C_{d6}} \qquad (16)$$

In this equation, the ligand constants (A_L) of the conjugate base are summed, C_{charge} is a constant that depends on the charge of the conjugate base, C_{nd} is a constant that depends on the periodic row, and C_{d6} is a constant that depends on the d-electron count and geometry change upon deprotonation.

ligand	**A_L**	**charge of conjugate base**	**C_{charge}**
hydride, H^-	0.2	1	-15
carbonyl, CO	-4.1	0	0
PR_3 (aliphatic)	4.9	-1	30
N donors (including py)	4	**row**	**C_{nd}**
geometry	**C_{d6}**	3	0
d^6 oct -> lower coord. conjugate base	6	4	0
all else	0	5	2

This analysis predicts the p*K*$_a$s for the hydrides or putative H_2 intermediates shown in the main text. For completion, the ligand p*K*$_a$s are also estimated, though the empirical formula has not been used on ligand deprotonations. Our results above indicate that the formula cannot be used for ligand deprotonations in systems that undergo MLC. Figure S40 shows how the parameters are summed and S41 the values obtained.

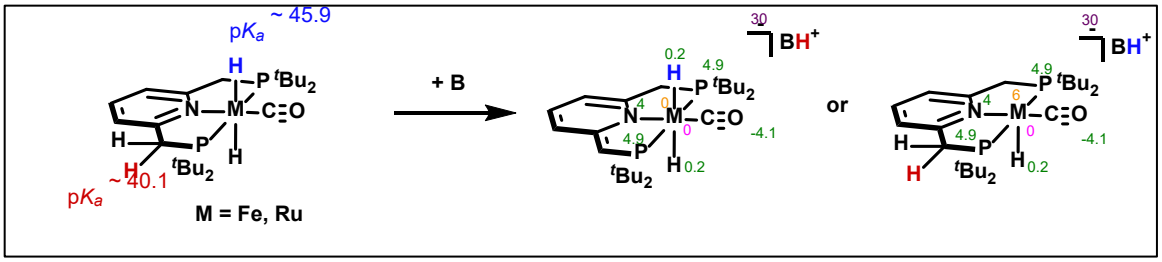

Figure S40. Method for p*K*$_a$ estimation for M-H (blue) and the ligand p*K*$_a$ (red). Legend: A_L constants (green), C_{charge} (purple), C_{d6} (orange), C_{nd} (pink) on the conjugate bases of a di-hydride.

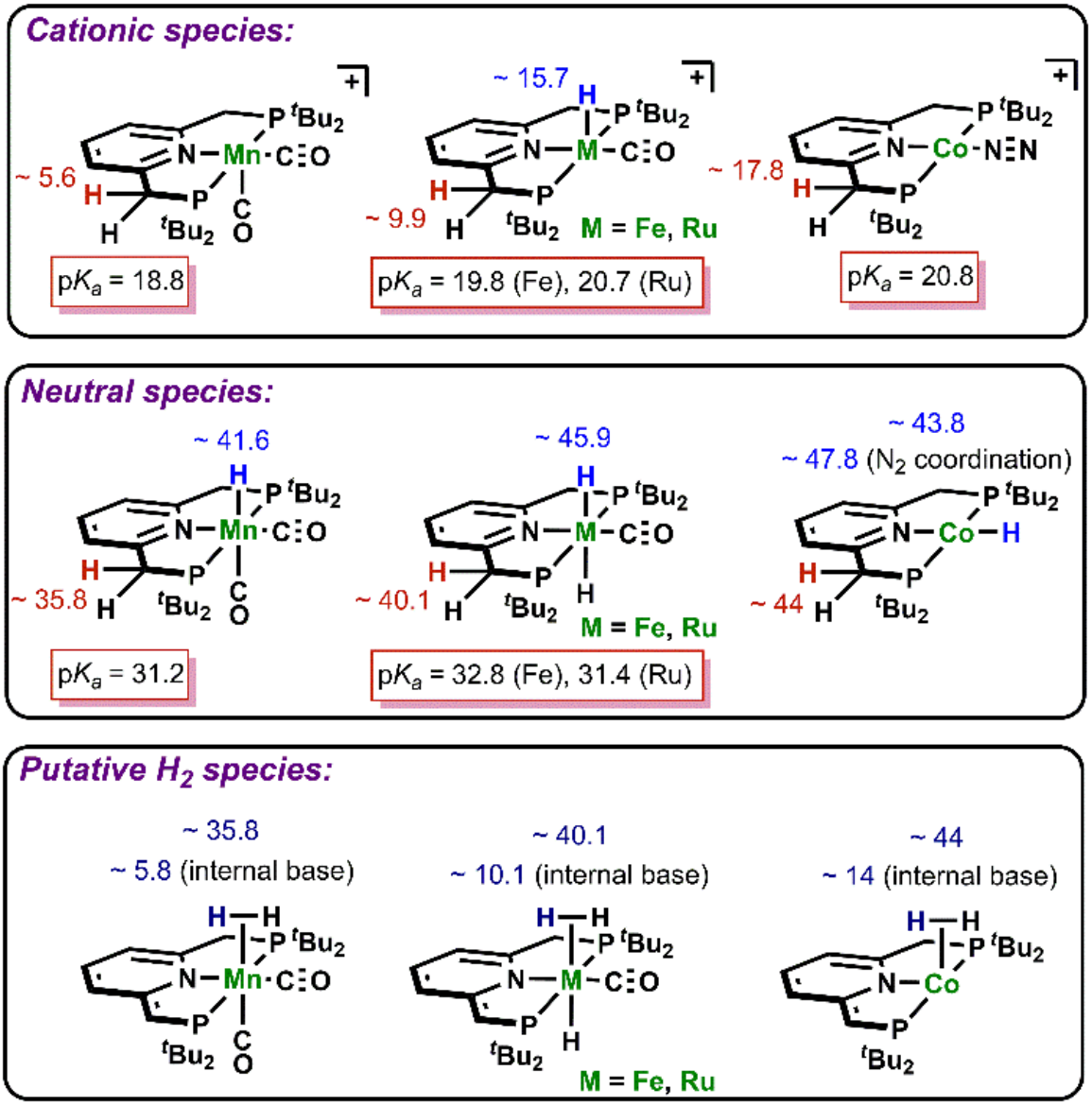

Figure S41. Observed pK_as for the ligand (boxed) and estimated ligand (red), hydride (blue), and dihydrogen (dark blue) pK_as using eq 16.

Section 4: Thermodynamic Measurements

A. Equilibrium of (*PNP)Co-N_2 with HCOOH (formic acid).

A 26 mM stock solution of **(*PNP)Co-N_2** in THF was diluted to 100, 150, 200, and 250 μM in a 5 mL volumetric flask with THF. The solutions were placed into a Teflon sealed UV-Vis cuvette and the spectrum recorded. To each sample was added 1 equiv. of anhydrous formic acid (0.11 M solution in THF). The cuvette was sealed, placed on a rocking table for several minutes to equilibrate and the spectrum recorded. Monitoring the equilibrium by UV-vis spectroscopy indicates that equilibrium is reached within 5 minutes.

The concentration of **(*PNP)Co-N_2** and **(PNP)Co-OCHO** were determined from the absorbance at λ = 765 nm. At λ = 765 nm the molar absorptivity for **(*PNP)Co-N_2** is 16 L mol^{-1} cm^{-1} and for **(PNP)Co-OCHO** it is 936 L mol^{-1} cm^{-1}. The equilibrium constant is defined in eq. 17. The reactions were repeated in triplicate so that $K_{eq,\ HCOOH}$ is determined from three independent trials.

$$K_{eq} = \frac{[(\mathrm{PNP})\mathrm{Co{-}OCHO}]}{[(^{*}\mathrm{PNP})\mathrm{Co{-}N_2}][\mathrm{HCOOH}]} \tag{17}$$

The slope of [Co-OCHO]/[*Co-N_2] vs. [HCOOH] yields $K_{eq,\ HCOOH}$. A final value of $K_{eq,\ HCOOH}$ = 40,000 ± 1100 M^{-1} is obtained giving ΔG_{HCOOH} = -6.3 ± 0.3 kcal/mol.

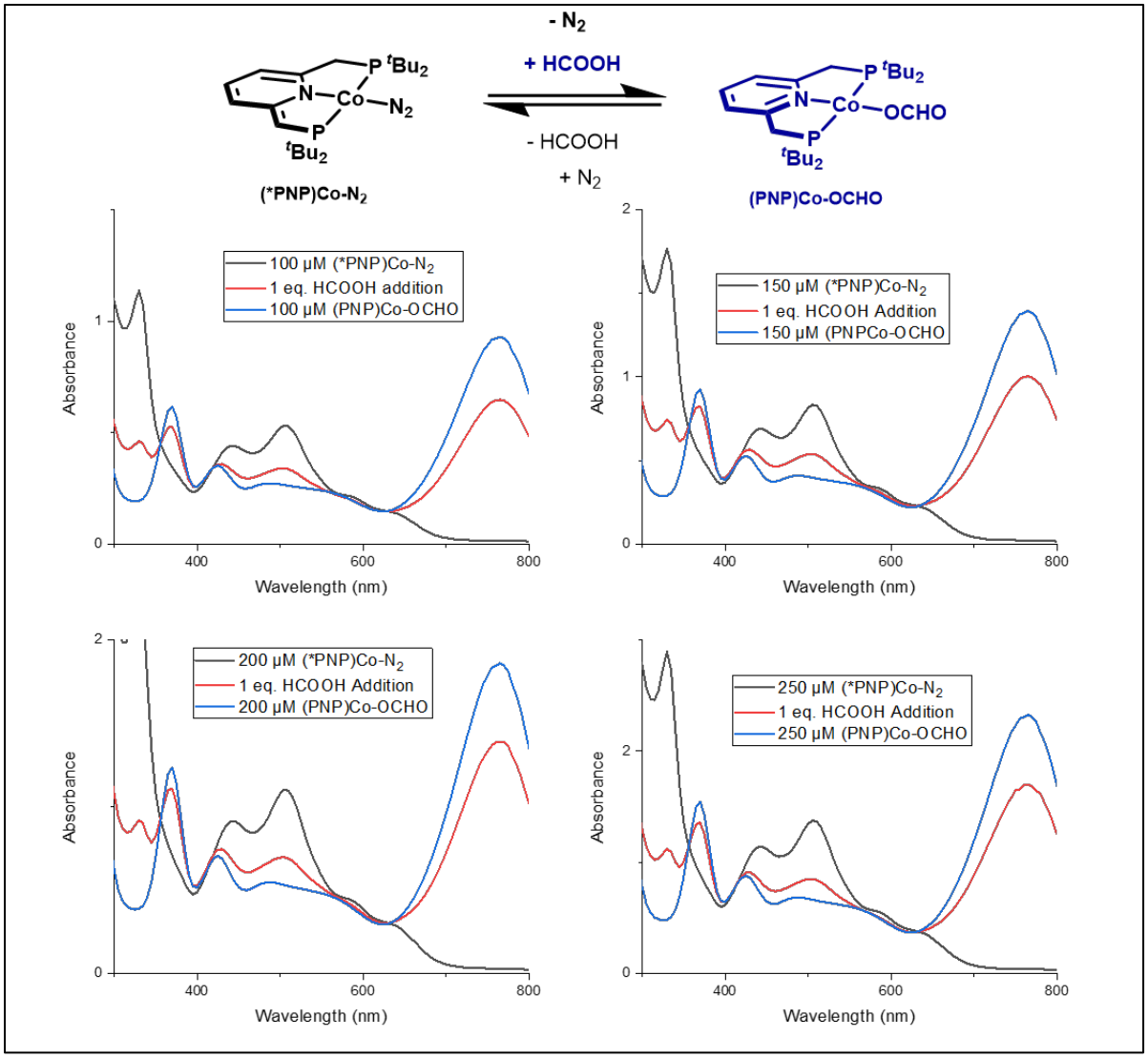

Figure S42. UV-Vis spectra of HCOOH addition to **(*PNP)Co-N_2** at varying concentrations overlaid with the expected product absorption spectra, **(PNP)Co-OCHO**, and the starting material product spectra. A final value of K_{eq} = 40,000 ± 1100 M^{-1} is obtained giving ΔG_{HCOOH} = -6.3 ± 0.3 kcal/mol.

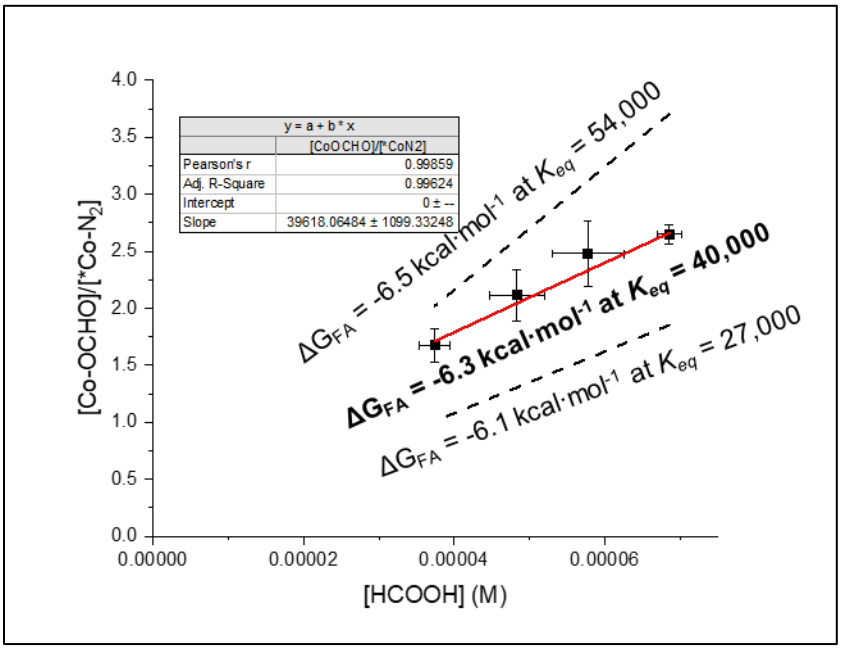

Figure S43. The slope of [Co-OCHO]/[*Co-N_2] vs. [HCOOH] yields $K_{eq,\ HCOOH}$. A final value of $K_{eq,\ HCOOH}$ = 40,000 ± 1100 M^{-1} is obtained giving ΔG_{HCOOH} = -6.3 ± 0.2 kcal·mol^{-1}. The propagated error (from the error in the fit of the linear fit) for ΔG_{HCOOH} is only 0.1 kcal·mol^{-1}. To ensure measurements were within error of the linear fit, the error in ΔG_{HCOOH} was doubled to 0.2 kcal·mol^{-1}. Dashed lines correspond to K_{eq} values derived from the error of ΔG_{HCOOH} (±0.2).

B. Attempt to Measure Equilibrium of (*PNP)(CO)(H)Fe with HCOOH.

Attempts to obtain the formic acid equilibrium with **(*PNP)(CO)(H)Fe** were done in a manner analogous to that for **(*PNP)Co-N_2**. However, addition of formic acid to **(*PNP)(CO)(H)Fe** does not cleanly generate **(PNP)(CO)(H)Fe-OCHO**. Instead, a mixture of products is observed, as shown in Figure S40, due to CO_2 elimination from the **(PNP)(CO)(H)Fe-OCHO** species.[22] Addition of CO_2 to the mixture does not cleanly regenerate **(PNP)(CO)(H)Fe-OCHO**, instead a peak at 36.2 ppm is observed indicating the presence of free ligand.

Experimental: 63 µL of a 14 mM stock solution of **(*PNP)(CO)(H)Fe** (1 µmol) in THF was added to a Teflon valved J Young NMR tube followed by an additional 354 µL of THF. The tube was placed in the cold well and frozen with lN_2. To the frozen reaction mixture was added 30 µL of a 30 mM stock solution of formic acid (1 µmol) in THF to give a concentration of 2 mM for both species. The J Young tube was removed from the cold well and thawed giving a color change from dark blue to yellow. The $^{31}P\{^1H\}$ NMR spectrum was recorded immediately after thawing (Figure S44). The J Young tube was placed on the Schlenk line and 0.85 atm of CO_2 added; the $^{31}P\{^1H\}$ NMR spectrum was recorded two hours after CO_2 addition (Figure S44).

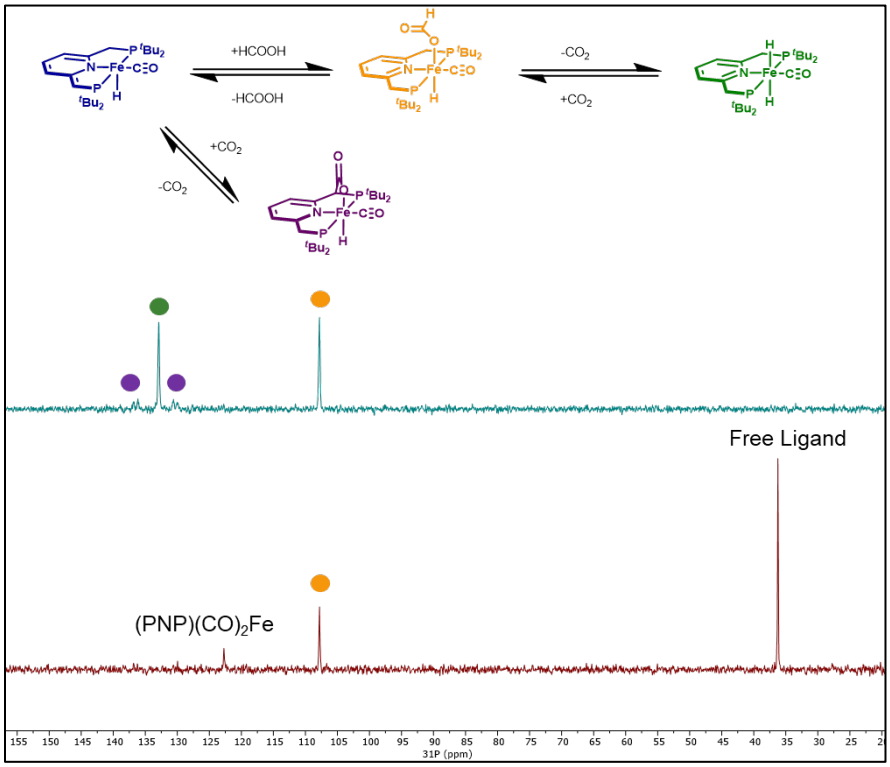

Figure S44. Overlay of $^{31}P\{^1H\}$ NMR spectra (202 MHz, 298K, THF). **Top:** immediately after formic acid addition to **(*PNP)(CO)(H)Fe**. **Bottom:** 2 hours after CO_2 addition.

C. Attempt to Measure Equilibrium of (*PNP)Co-N_2 with H_2.

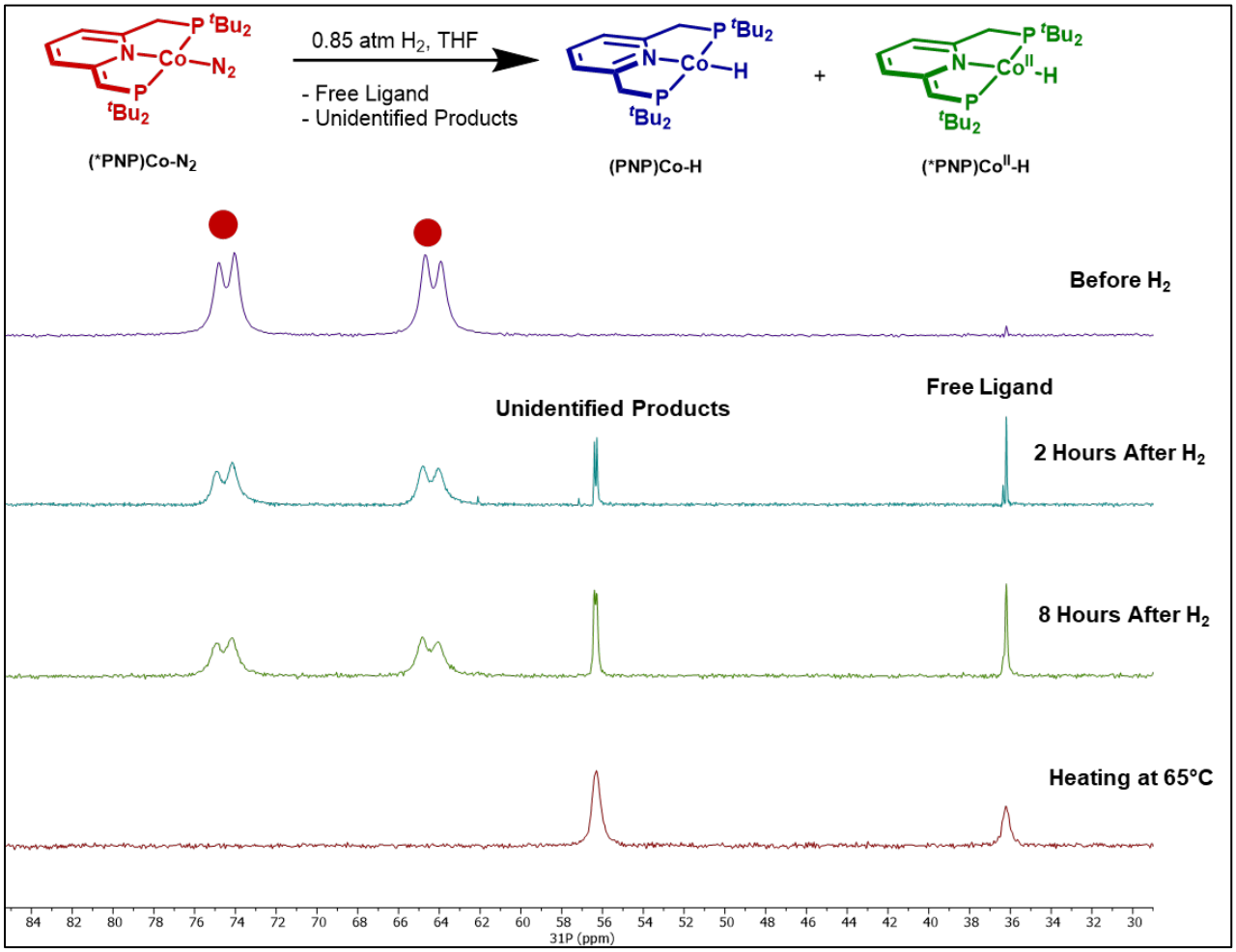

Figure S45. Stacked $^{31}P\{^{1}H\}$ NMR spectra (202 MHz, 298K, THF) of H_2 addition to **(*PNP)Co-N_2** in THF. From top to bottom: **(*PNP)Co-N_2** before H_2 addition**,** 2 hours after H_2 addition, 8 hours after H_2 addition, and heating at 65°C. **Procedure:** 12 mg of **(*PNP)Co-N_2** was dissolved in 0.6 mL of THF and placed into a J Young NMR tube. The tube containing the red solution was placed on the schlenk line and freeze-pump-thawed three times before adding H_2 at room temperature. After the reaction, the solution slowly became darker. 8 hours after H_2 addition, the reaction was placed at 65°C for 16 hours giving a dark brown/black product.

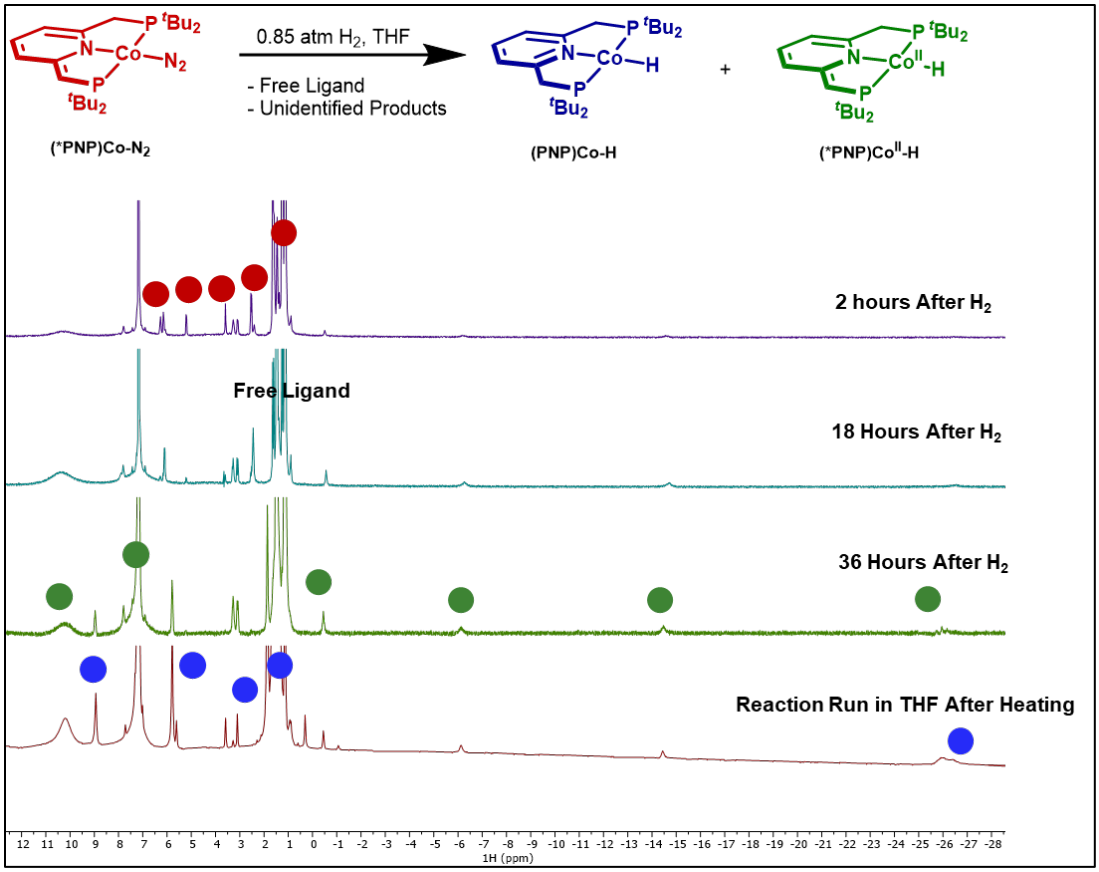

Figure S46. Stacked ^{1}H NMR spectra (300 MHz, 298K, C_6D_6 **)** of H_2 addition to **(*PNP)Co-N_2** to give **(PNP)Co-H** and the paramagnetic **(PNP)Co^{II}-H** along with free ligand for in C_6D_6. From top to bottom: 2 hours, 18 hours, and 36 hours after H_2 addition. The spectrum on the bottom is from the reaction shown in Figure S49. **Experimental:** 6 mg of (*PNP)Co-N_2 was dissolved in 0.6 mL of C_6D_6 and placed into a J Young NMR tube. The tube containing the red solution was placed on the schlenk line and freeze-pump-thawed three times before adding H_2 at room temperature. After the reaction, the solution slowly became darker.

D. Equilibrium of (*PNP)(CO)(H)Fe with H_2.

In a typical experiment, 67 µL of a 19 mM THF stock solution **(*PNP)(CO)(H)Fe** was placed into a Teflon sealed UV-Vis cuvette equipped with an attached round bottom flask (Figure S47).[13] To the attached round bottom was added 5 mL of THF measured in a volumetric flask. The apparatus was removed from the glovebox, and a 3.97 mL gas addition bulb was attached; the joints were heat sealed with H-grease (Figure S47). The THF was frozen with lN_2 and the entire apparatus evacuated for one minute (note: THF is removed from the **(*PNP)(CO)(H)Fe** solution in the cuvette; freeze-pump-thawing of **(*PNP)Fe(H)(CO)** solutions in THF lead to decomposition). After two freeze-pump-thaw cycles, the gas addition bulb was sealed from the cuvette and H_2 added to the gas addition bulb; 35 (10 eq.), 70 (20 eq.), and 105 (30 eq.) mmHg of H_2 were added to the gas addition bulb. The bulb was then closed to the Schlenk line, the degassed THF transferred to the cuvette, and finally the gas addition bulb opened to the blue **(*PNP)(CO)(H)Fe** solution. The total volume of the apparatus (excluding the solution) after H_2 addition, is 27.9 mL. The solution was stirred, and once no more changes were observed in the UV-vis spectrum (scans collected every minute), the solution was assumed to be at equilibrium.

Figure S47. Teflon sealed UV-Vis cuvette with attached round bottom flask, affixed with 4 mL gas addition bulb.

As described in Section 2B, **(*PNP)(CO)(H)Fe** may bind THF at room temperature, giving a 13% error in the molecular weight calculation. As the equilibrium constant is obtained from a ratio of two Fe species, the error cancels out. As shown in Figure S50, samples of **(*PNP)(CO)(H)Fe** contain trace impurities (<1%).

The molar absorptivity of **(PNP)(CO)(H)Fe-H** was obtained through the addition of 0.85 atm of H_2 to a solution of **(*PNP)(CO)(H)Fe** via the procedure described above using a 250 mL gas addition bulb. **(PNP)(CO)(H)Fe-H**, a yellow solution, has a molar absorptivity of 12 L mol^{-1} cm^{-1} at λ = 655 nm. whereas **(*PNP)(CO)(H)Fe**, a blue solution, has a molar absorptivity of 248 L mol^{-1} cm^{-1}, allowing for the determination of the concentration of both species.[13] The amount of **(PNP)(CO)(H)Fe-H** is determined by mass balance, under the assumption **(*PNP)(CO)(H)Fe** only reacts with H_2 to form **(PNP)(CO)(H)Fe-H** (Figure S50). The pressure of gas at equilibrium is described by eq 18.

$$p_{H2} = \frac{P_1 \cdot V_1}{V_2} - \frac{nRT}{V_2} \quad (18)$$

In eq 18, P_1 is the pressure of gas added to the calibrated bulb, V_1 is the volume of the calibrated bulb, V_2 is the volume of the calibrated bulb, connection to cuvette, and cuvette (minus the solution), and n is the moles of **(PNP)(CO)(H)Fe-H** at equilibrium.

Equilibrium measurements were done in triplicate.

The slope of [FeH]/[*Fe] vs. P_{H2} corresponds to K_{eq}. Using data at 655 nm, a value of K_{eq} = 600 ± 100 atm^{-1} is obtained for H_2 addition to **(*PNP)(CO)(H)Fe**, corresponding to ΔG^{o} = -3.8 ± 0.3 $kcal \cdot mol^{-1}$.

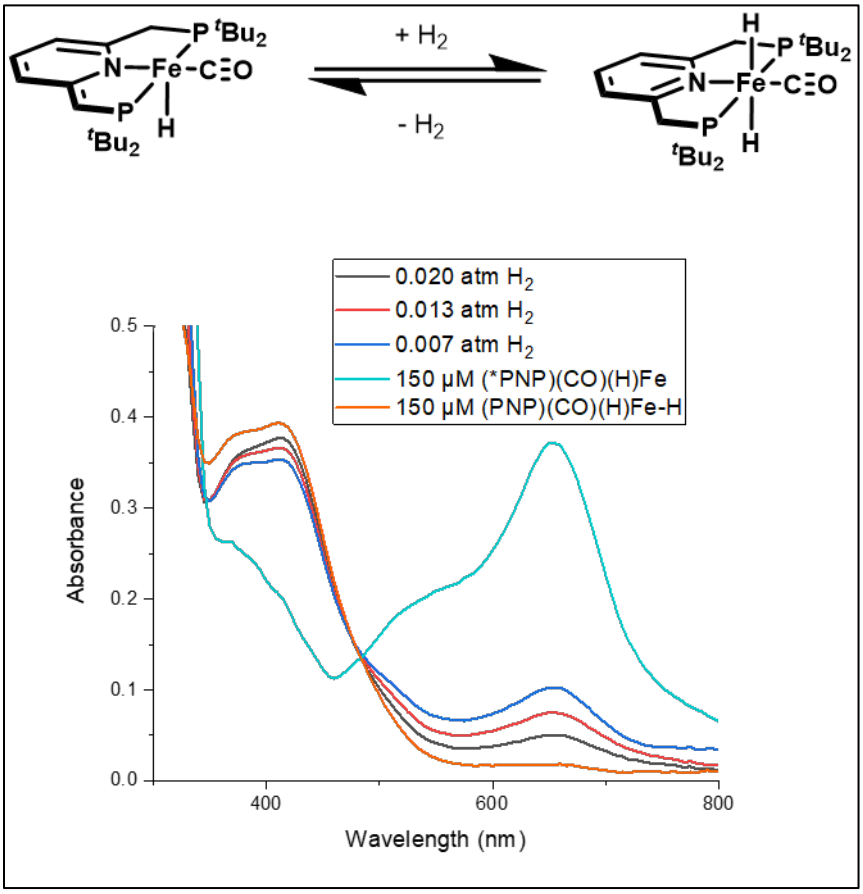

Figure S48. Overlay of UV-Vis spectra of (*PNP)(CO)(H)Fe under varying atmospheres of H_2.

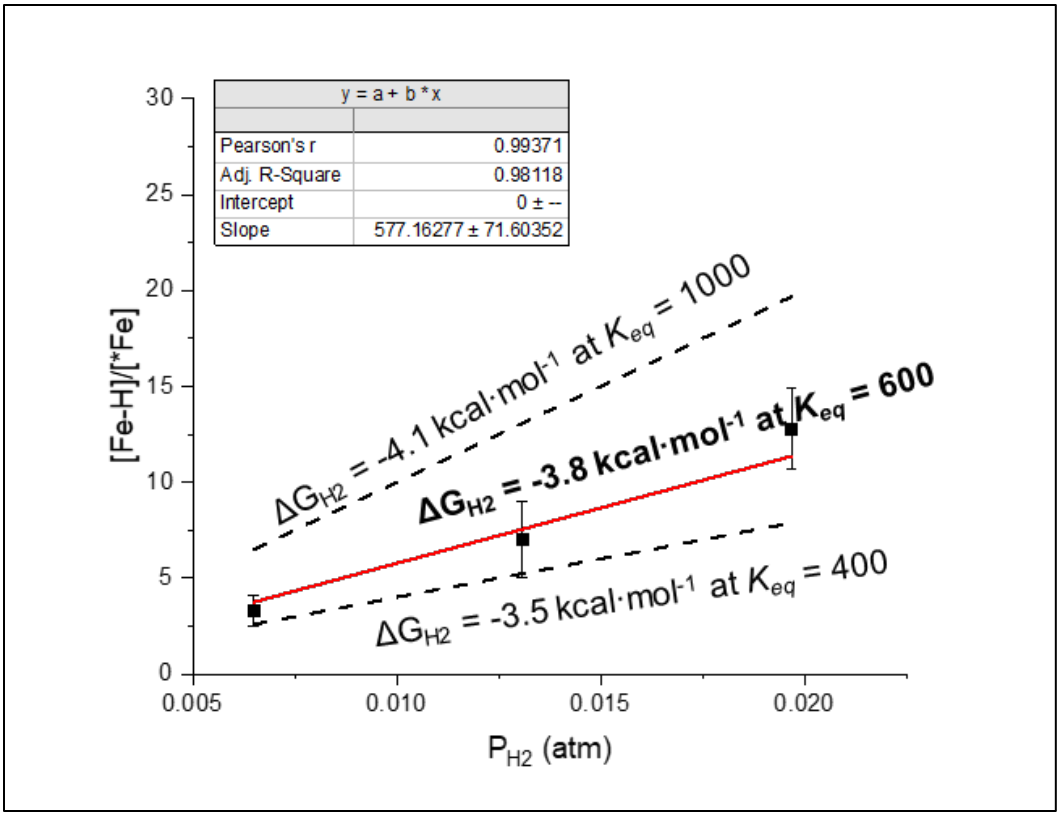

Figure S49. The slope of [Fe-H]/[*Fe] vs. P_{H2} yields $K_{eq,\ H2}$. A final value of $K_{eq,\ H2}$ = 600 ± 100 atm^{-1} is obtained giving ΔG_{H2} = -3.8 ± 0.3 $kcal \cdot mol^{-1}$. The propagated error (from the error in the fit of the linear fit) for ΔG_{H2} is only 0.1 $kcal \cdot mol^{-1}$. To ensure measurements were within error of the linear fit, the error in ΔG_{H2} was tripled to 0.3 $kcal \cdot mol^{-1}$. Dashed lines correspond to K_{eq} values derived from the error of ΔG_{H2} (±0.2).

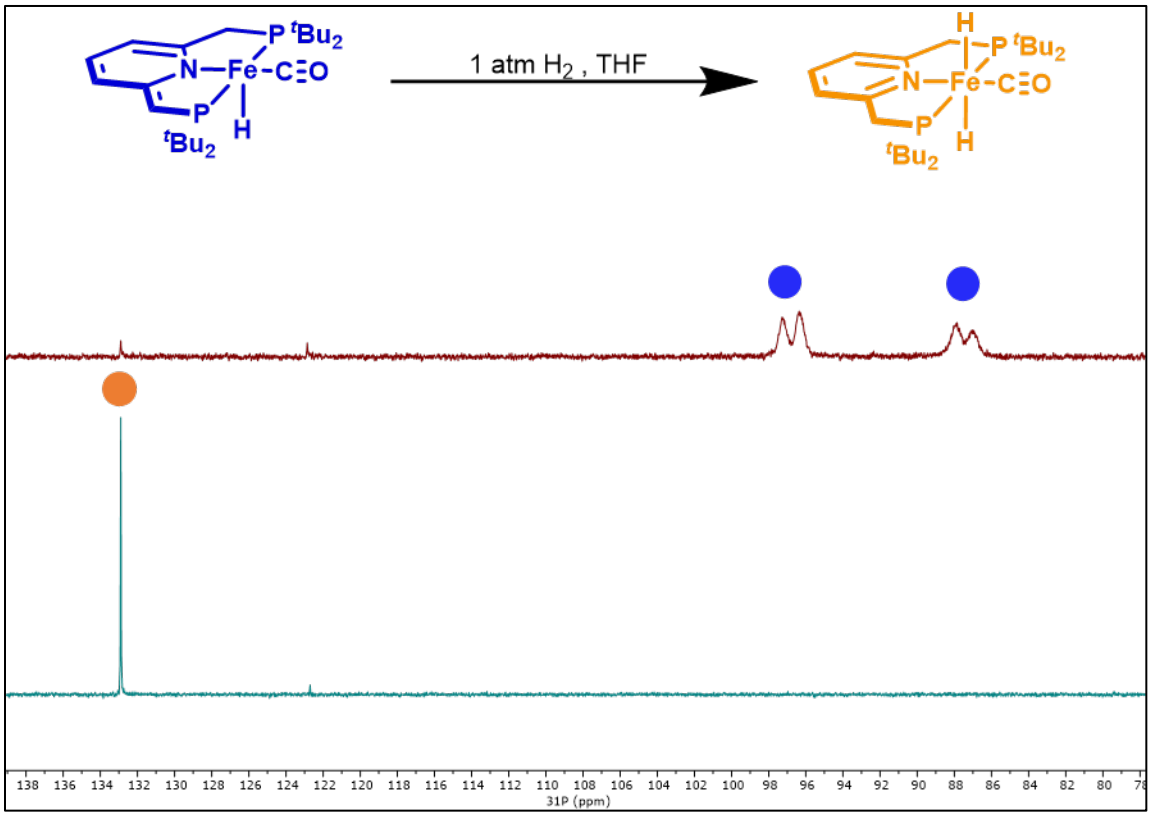

Figure S50. $^{31}P\{^{1}H\}$ NMR spectra (202 MHz, 298K, THF) of H_2 addition to **(*PNP)(CO)(H)Fe** in THF. **Top:** before H_2 addition. **Bottom**: 10 minutes after H_2 addition. **Experimental: (*PNP)(CO)(H)Fe (**8 mg, 17 μmol) was dissolved in 0.7 mL of THF and placed into a J Young NMR tube. The tube was placed on the Schlenk line, and the atmosphere evacuated and replaced with H_2 while the solution was frozen with IN_2. The reaction was warmed to room temp, where an immediate color change from dark blue to orange/yellow occurred.

E. (PNP)Co + (PNP)Ru Hydride Transfer Equilibrium.

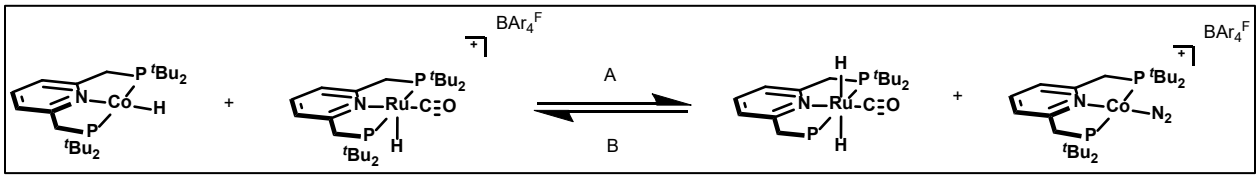

Reaction A (under N_2): In the forward reaction, hydride transfer from **(PNP)Co-H** to **[(PNP)(CO)(H)Ru][BAr$_4^F$]** occurs. In a typical experiment, 142 µL of a 23 mM stock solution of **(PNP)Co-H** (3 µmol) in THF and 332 µL of a 10 mM stock solution of **[(PNP)(CO)(H)Ru][BAr$_4^F$]** (3 µmol) in THF were transferred to a J Young NMR tube along with 76 µL of a 44 mM stock solution of triphenyl phosphate (3 µmol) as an internal standard. After combination, the reaction was monitored via $^{31}P\{^1H\}$ NMR spectroscopy. The starting materials **[(PNP)(CO)(H)Ru][BAr$_4^F$]** and **(PNP)Co-H** gives peaks at 83.8 ppm and 89 ppm (broad), respectively. The product **(PNP)(CO)(H)Ru-H** is observed as a singlet at 107.1 ppm, whereas the product **[(PNP)Co-N$_2$][BAr$_4^F$]** is observed as broad peak centered at 69 ppm. After approximately 4 hours, no further changes in the integrations of the observed peaks occur. Three products are observed in the $^{31}P\{^1H\}$ NMR spectra (Figure S51, bottom) after the reaction: **(PNP)(CO)(H)Ru-H**, **(*PNP)(CO)(H)Ru**, and **[(PNP)(CO)(H)Ru][BAr$_4^F$]**. The formation of the dearomatized complex, **(*PNP)(CO)(H)Ru**, is a result of H_2 loss from **(PNP)(CO)(H)Ru-H**.[13] The Co species are not observed; however, $^{31}P\{^1H\}$ NMR spectra of the complexes at similar concentration under the same NMR parameters do not yield observable peaks (see Figure S31). Due to the competing equilibria of H_2 loss from **(PNP)(CO)(H)Ru-H**, an accurate K_{eq} (eq. 19) was unable to be determined.

$$K_{eq} = \frac{[(\mathrm{PNP})\mathrm{Ru}-\mathrm{H}][(\mathrm{PNP})\mathrm{Co}]}{[(\mathrm{PNP})\mathrm{Ru}][(\mathrm{PNP})\mathrm{Co}-\mathrm{H}]} \quad (19)$$

Reaction A (under H_2): To prevent competing H_2 equilibria, the hydride transfer experiment was repeated as above, except the J Young tube was placed on the Schlenk line and 0.85 atm of H_2 added (Figure S51, top). When performing the reaction under H_2, peaks for **(*PNP)(CO)(H)Ru** are not observed.

Before determining $K_{eq,\ HT}$ under 0.85 atm of H_2, separate experiments were performed between the four metal complexes and H_2 to rule out competing reactivity with H_2. 0.85 atm of H_2 was added to J Young NMR tubes containing **[(PNP)(CO)(H)Ru][BAr$_4^F$]**, **[(PNP)Co-N$_2$][BAr$_4^F$]**, or **(PNP)Co-H**. No changes were observed in the respective $^{31}P\{^1H\}$ NMR spectra upon addition of H_2. Furthermore, solution IR (under N_2) in THF of **[(PNP)(CO)(H)Ru][BAr$_4^F$]** did not reveal a shift in the -*CO* stretch or the N_2 stretch of **[(PNP)Co-N$_2$][BAr$_4^F$]**.

The hydride transfer reaction was repeated in THF-d_8 and observed over the course of several days. As shown in Figure S52, only peaks for the products are observed, no peaks are observed which would indicate the formation of undesired byproducts, such as paramagnetic **(PNP)Co^{II}-H**, in the ^1H NMR spectrum.[10]

Repeating the hydride transfer reaction in duplicate under H_2 gives K_{eq} = 2.4 ± 0.8, and ΔG = -0.5 ± 0.2 kcal/mol. Since ΔG_{H^-} = 44.6 ± 0.6 kcal/mol for **(PNP)(CO)(H)Ru-H**,[13] ΔG_{H^-} = 44.1 ± 0.7 kcal/mol for **(PNP)Co-H**.

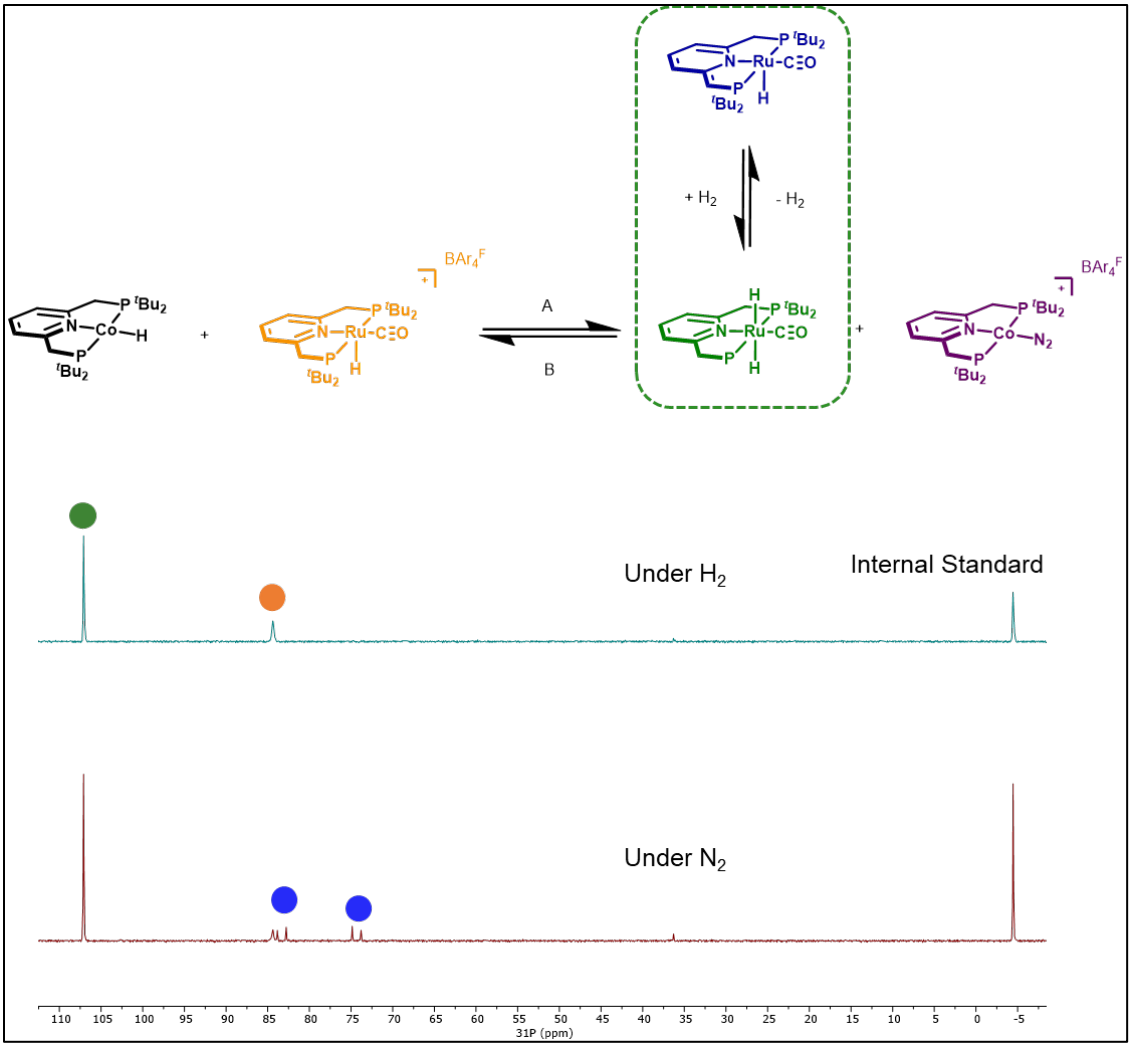

Figure S51. $^{31}P\{^{1}H\}$ NMR spectra (202 MHz, 298K, THF) of the hydride transfer reaction between **(PNP)Co-H** and **[(PNP)(CO)(H)Ru][BAr$_4^F$]**. **Top:** Hydride transfer under H_2 atmosphere after 4 hours. **Bottom:** Hydride transfer under N_2 atmosphere after 4 hours.

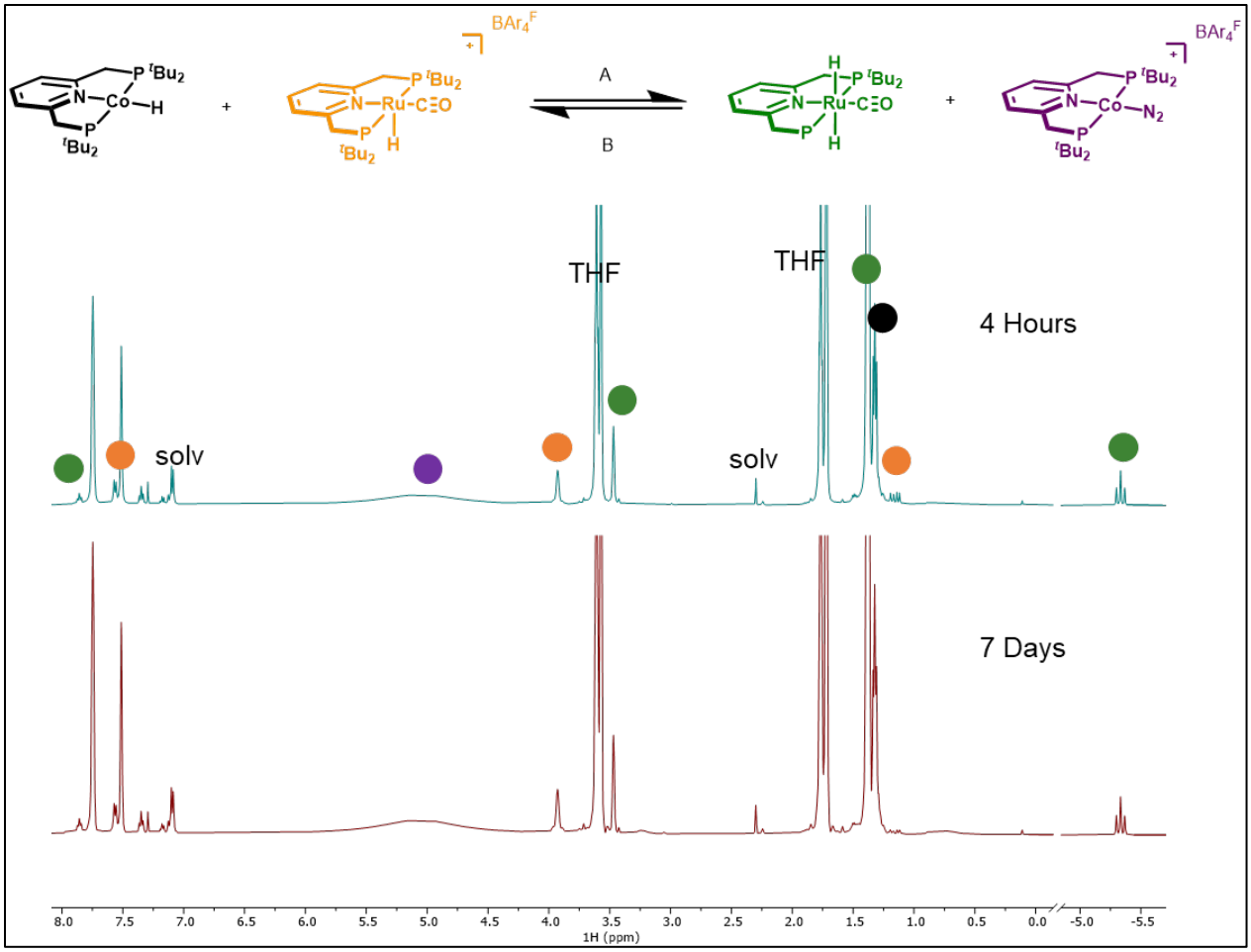

Figure S52. ^{1}H NMR spectra (500 MHz, 298K, THF) of the hydride transfer reaction between **(PNP)Co-H** and **[(PNP)(CO)(H)Ru][BAr$_4^F$]** in THF-d_8. **Top:** 4 hours after combination. **Bottom:** 7 days after combination. The Chirik group recently reported the dynamic exchange of N_2/THF in **[(PNP)Co-N$_2$][BAr$_4^F$]** causing broadening in the ^{1}H NMR spectrum.[10,12]

Reaction B:

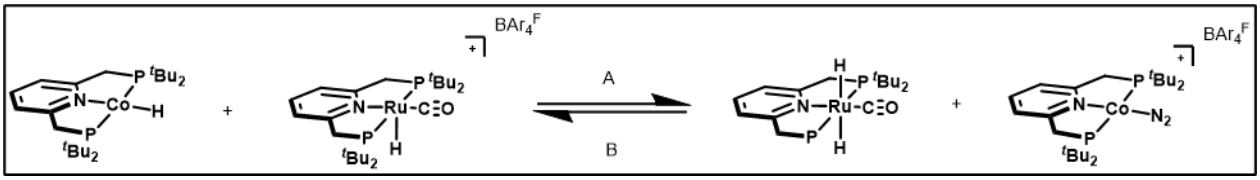

To demonstrate the reversibility of the reaction, the equilibrium between **(PNP)(CO)(H)Ru-H** and **[(PNP)Co-N_2][BAr_4^F]** was monitored. In a typical experiment, 100 µL of a 15 mM stock solution of **(*PNP)(CO)(H)Ru** (2 µmol) in THF was added to a Teflon valved J Young NMR Tube. The tube was placed on the Schlenk line and freeze-pump-thawed three times to remove dissolved gases, after which the atmosphere was replaced with H_2. The reaction was warmed to room temp and placed on a rocker to mix for two hours; the formation of **(PNP)(CO)(H)Ru-H** was confirmed via $^{31}P\{^1H\}$ NMR spectroscopy. The tube was returned to the glovebox, frozen in the cold well with IN_2, and 210 µL of a 7 mM stock solution of **[(PNP)Co-N_2][(BAr_4^F]** (2 µmol) in THF was added along with 35 µL of a 44 mM stock solution of triphenylphosphate (2 µmol) in THF as an internal standard. The reaction was monitored via $^{31}P\{^1H\}$ NMR with a relaxation delay of 10s (d1 = 10s). After 4 hours, no further changes were observed in the integration of the internal standard relative to **(PNP)(CO)(H)Ru-H**. The reaction was repeated with 2 and 4 equiv. of **[(PNP)Co-N_2][BAr_4^F]**. Assuming mass balance, the concentration of the other three species can be determined from the amount of **(PNP)(CO)Ru-H** present (concentration determined from internal standard). The equilibrium expression is given by eq. 20, and rearrangement to eq. 21 allows for K_{eq} to be determined from the slope of the plot $\frac{[(\mathrm{PNP})\mathrm{Ru}][(\mathrm{PNP})\mathrm{Co-H}]}{[(\mathrm{PNP})\mathrm{Ru-H}]}$ vs. [(PNP)Co-N_2].

$$K_{eq} = \frac{[(\mathrm{PNP})\mathrm{Ru}][(\mathrm{PNP})\mathrm{Co-H}]}{[(\mathrm{PNP})\mathrm{Ru-H}][(\mathrm{PNP})\mathrm{Co-N_2}]} \quad (20)$$

$$[(\mathrm{PNP})\mathrm{Co-N_2}] \cdot K_{eq} = \frac{[(\mathrm{PNP})\mathrm{Ru}][(\mathrm{PNP})\mathrm{Co-H}]}{[(\mathrm{PNP})\mathrm{Ru-H}]} \quad (21)$$

The slope of [(PNP)Ru][Co-H]/[Ru-H] vs. [(PNP)Co-N_2] yields K_{eq} = 0.076 ± 0.004 giving ΔG_{rxn} = 1.5 ± 0.3 kcal/mol. Since ΔG_{H^-} = 44.6 ± 0.6 kcal/mol for **(PNP)(CO)(H)Ru-H**,[13] ΔG_{H^-} = 43.1 ± 0.7 kcal/mol for **(PNP)Co-H**.

Taking the average values obtained from reactions A and B gives a final value of ΔG_{H^-} = 43.6 ± 0.5 kcal/mol for **(PNP)Co-H**.

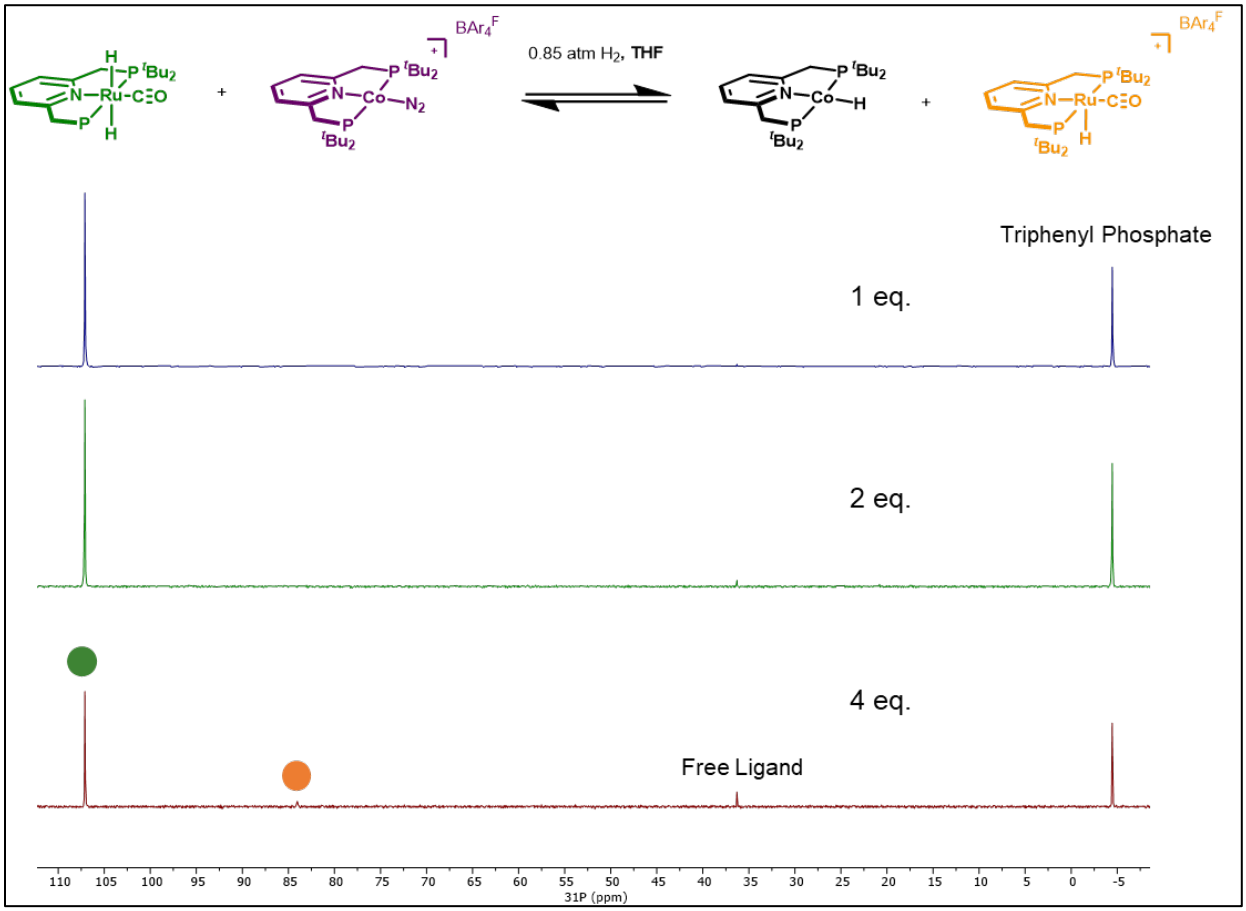

Figure S53. $^{31}P\{^{1}H\}$ NMR spectra (202 MHz, 298K, THF) in THF showing various ratios of **[(PNP)Co-N_2][BAr_4^F]** and **(PNP)(CO)(H)Ru-H**.

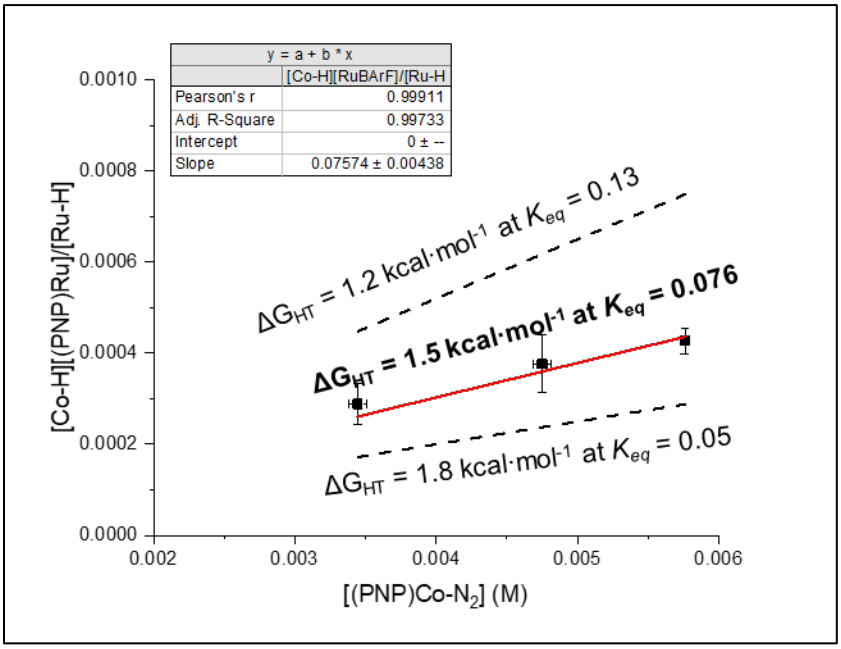

Figure S54. The slope of [(PNP)Ru][Co-H]/[Ru-H] vs. [(PNP)Co-N_2] yields K_{eq} = 0.076 ± 0.004 giving ΔG_{HT} = 1.5 ± 0.3 kcal·mol^{-1}. The propagated error (from the error in the fit of the linear fit) for ΔG_{HT} is only 0.1 kcal·mol^{-1}. To ensure measurements were within error of the linear fit, the error in ΔG_{HT} was tripled to 0.3 kcal·mol^{-1}. Dashed lines correspond to K_{eq} values derived from the error of ΔG_{HT} (±0.3).

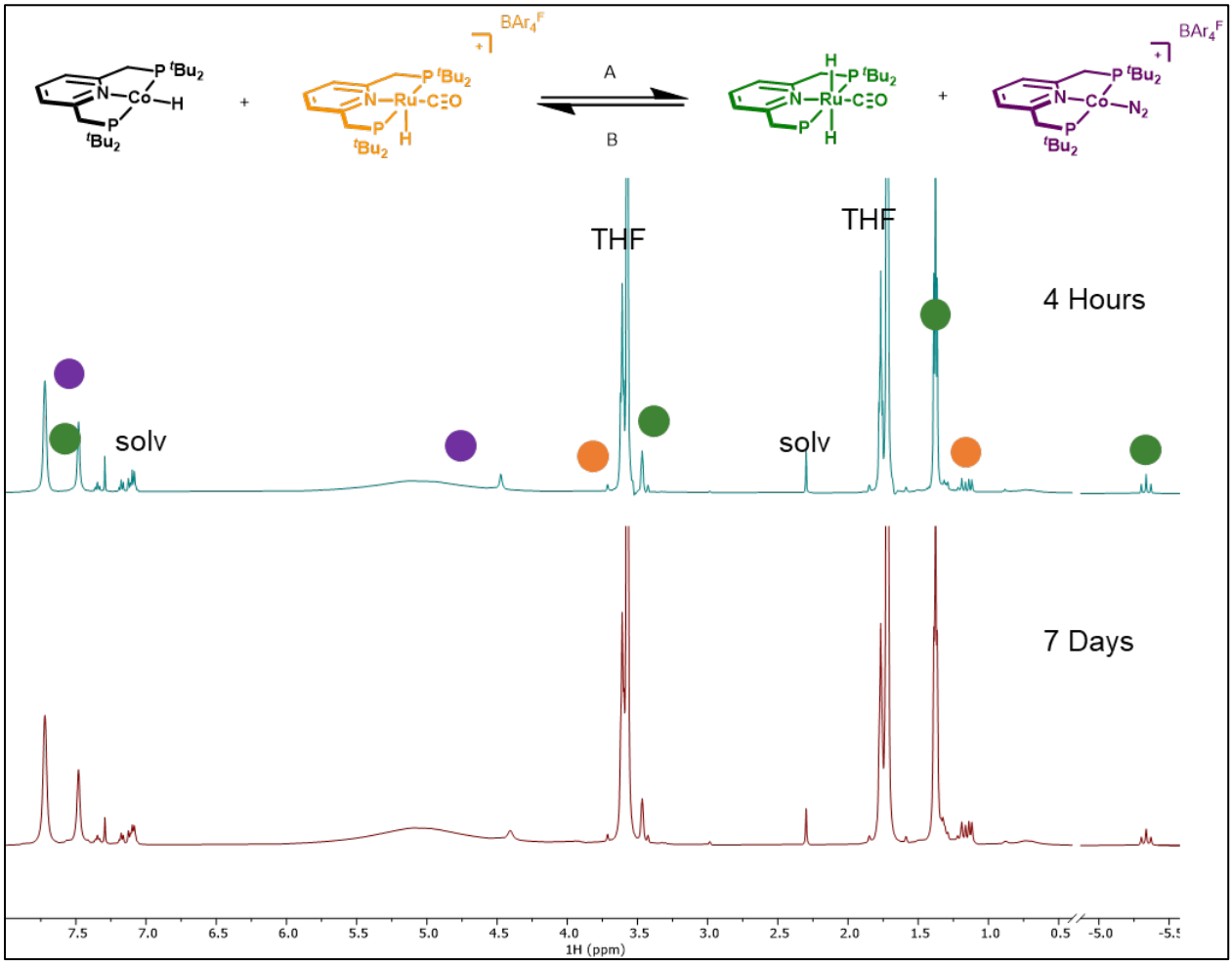

Figure S55. ^{1}H NMR spectra (500 MHz, 298K, THF) of the hydride transfer reaction between **(PNP)(CO)(H)Ru-H** and **[(PNP)Co-N$_2$][Bar$_4^F$]** in THF-d_8. **Top:** 4 hours after combination. **Bottom:** 7 days after combination.

F. Extrapolation to Determine $\Delta G_{H2,addn}$ for (*PNP)Co-N_2.

Addition of H_2 to **(*PNP)Co-N_2** does not cleanly generate **(PNP)Co-H** (Figures S42-43), therefore, $\Delta G_{H2,addn}$ was extrapolated from the thermochemical cycle shown in Scheme 1 (eq. 22-24).

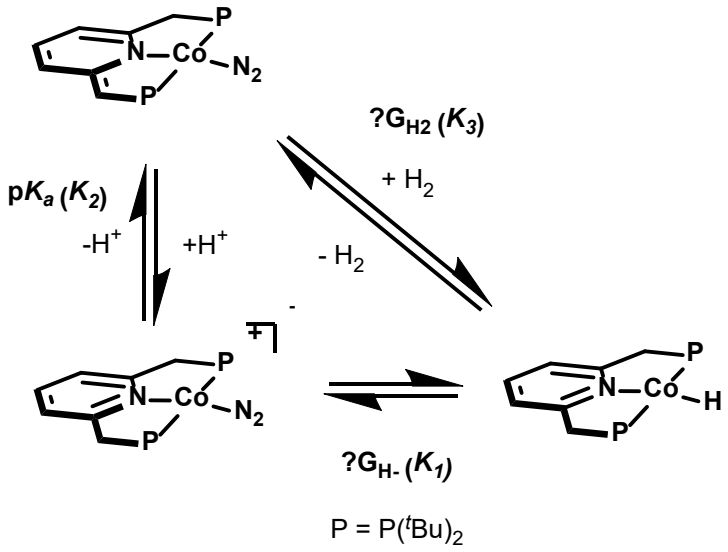

Scheme 1. Thermochemical cycle relating ΔG_{H2} and ΔG_{H^-} (hydricity).

From the hydricity of 43.6 ± 0.5 kcal·mol^{-1} (eq. 22) found in section 4D, pK_{ip} = 20.4 ± 0.2 (ΔG = 27.8 ± 0.3 kcal·mol^{-1}, eq. 23, section 3A), and ΔG_{HDE} = 68.7 kcal·mol^{-1} (eq. 24),[30] $\Delta G_{H2,\ addn}$ = -2.7 ± 0.6 kcal·mol^{-1} (eq. 25) for **(*PNP)Co-N_2**.

$(\mathbf{PNP})\mathbf{Co}^{+} + \mathbf{H}^{-} \rightleftarrows (\mathbf{PNP})\mathbf{Co}-\mathbf{H}$	-(ΔG_{H^-})	(22)
$(^{*}\mathbf{PNP})\mathbf{Co} + \mathbf{H}^{+} \rightleftarrows (\mathbf{PNP})\mathbf{Co}^{+}$	-(ΔG_{K2})	(23)
$\mathbf{H_2} \rightleftarrows \mathbf{H}^{+} + \mathbf{H}^{-}$	ΔG_{HDE}	(24)
$(^{*}\mathbf{PNP})\mathbf{Co} + \mathbf{H_2} \rightleftarrows (\mathbf{PNP})\mathbf{Co}-\mathbf{H}$	ΔG_{H2}	(25)

G. Effective Hydricity of (PNP)Co-H.

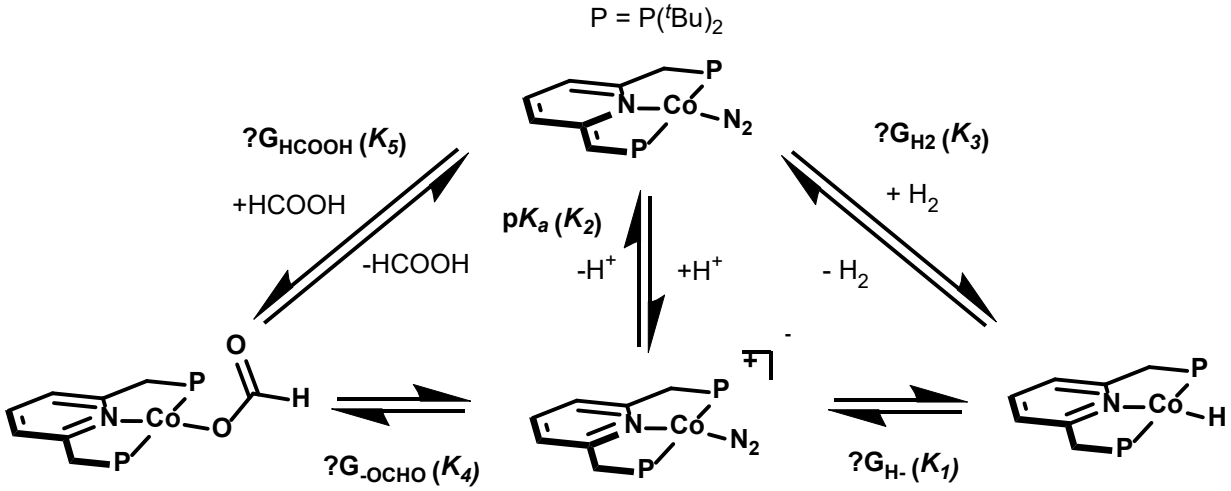

Scheme 2. Thermochemical cycle used to determine the effective hydricity ($\Delta G_{H^-,\,eff}$) of **(PNP)Co-H**.

The effective hydricity ($\Delta G_{H^-,\,eff}$) is the summation of K_1 and K_4 as shown in scheme 2. Since the hydricity, ΔG_{H^-} = 43.7 ± 0.5 kcal·mol^{-1}, was found in section 4D, $\Delta G_{H^-,\,eff}$ can be found through measurement of $\Delta G_{\text{-OCHO}}$ (K_4). Direct loss of the formate anion from **(PNP)Co-OCHO** is not observed, however, $\Delta G_{\text{-OCHO}}$ can be extrapolated from the series of equations shown below (eq. 26-28).

From ΔG_{HCOOH} = -6.3 ± 0.3 kcal·mol^{-1} (eq. 26, section 4A), pK_{ip} = 20.4 ± 0.2 (ΔG = 27.8 ± 0.3 kcal·mol^{-1}, eq. 27, section 3A), and the pK_a of formic acid[13] (K_6, ΔG = 28.4 ± 0.8 kcal·mol^{-1}, eq. 28), $\Delta G_{\text{-OCHO}}$ = -6.9 ± 0.9 kcal·mol^{-1} (eq. 29).

Thus, $\Delta G_{H^-,\,eff}$ = 36.7 ± 1.0 kcal·mol^{-1} for **(PNP)Co-H** in the reduction of CO_2 to formate.

$(^{*}\mathbf{PNP})\mathbf{Co} + \mathbf{HCOOH} \rightleftarrows (\mathbf{PNP})\mathbf{Co}-\mathbf{OCHO}$	ΔG_{HCOOH}	(26)
$(\mathbf{PNP})\mathbf{Co}^{+} \rightleftarrows (^{*}\mathbf{PNP})\mathbf{Co} + \mathbf{H}^{+}$	ΔG_{K2}	(27)
$\mathbf{OCHO}^{-} + \mathbf{H}^{+} \rightleftarrows \mathbf{HCOOH}$	-(ΔG_{K6})	(28)[13]
$(\mathbf{PNP})\mathbf{Co}^{+} + \mathbf{OCHO}^{-} \rightleftarrows (\mathbf{PNP})\mathbf{Co}-\mathbf{OCHO}$	$\Delta G_{\text{-OCHO}}$	(29)

H. Summary of Thermodynamic Values.

Equation	Value	Section
$[(\mathrm{PNP})\mathrm{Co}-\mathrm{N_2}][\mathrm{BAr_4^F}] \rightleftarrows (^*\mathrm{PNP})\mathrm{Co}-\mathrm{N_2} + \mathrm{H^+}$	pK_{ip} = 20.4 ± 0.2	3A
$[(\mathrm{PNP})(\mathrm{CO})(\mathrm{H})\mathrm{Fe}][\mathrm{BAr_4^F}] \rightleftarrows (^*\mathrm{PNP})(\mathrm{CO})(\mathrm{H})\mathrm{Fe} + \mathrm{H^+}$	pK_{ip} = 19.8 ± 0.2	3B
$(\mathrm{PNP})(\mathrm{CO})(\mathrm{H})\mathrm{Fe}-\mathrm{H} \rightleftarrows [(^*\mathrm{PNP})(\mathrm{CO})(\mathrm{H})\mathrm{Fe}-\mathrm{H}][\mathrm{Li}] + \mathrm{H^+}$	pK_{ip} = 32.8 ± 0.2	3C
$(\mathrm{PNP})(\mathrm{CO})(\mathrm{H})\mathrm{Ru}-\mathrm{H} \rightleftarrows [(^*\mathrm{PNP})(\mathrm{CO})(\mathrm{H})\mathrm{Ru}-\mathrm{H}][\mathrm{Li}] + \mathrm{H^+}$	pK_{ip} = 31.4 ± 0.2	3D
$(^*\mathrm{PNP})\mathrm{Co}-\mathrm{N_2} + \mathrm{HCOOH} \rightleftarrows (\mathrm{PNP})\mathrm{Co}-\mathrm{OCHO}$	ΔG_{HCOOH} = -6.3 ± 0.3 kcal·mol^{-1}	4A
$(\mathrm{PNP})\mathrm{Co^+} + \mathrm{OCHO^-} \rightleftarrows (\mathrm{PNP})\mathrm{Co}-\mathrm{OCHO}$	$\Delta G_{\text{-OCHO}}$ = -6.9 ± 0.9 kcal·mol^{-1}	4G
$(^*\mathrm{PNP})\mathrm{Co} + \mathrm{H_2} \rightleftarrows (\mathrm{PNP})\mathrm{Co}-\mathrm{H}$	ΔG_{H2} = -2.7 ± 0.6 kcal·mol^{-1}	4F
$(^*\mathrm{PNP})(\mathrm{CO})(\mathrm{H})\mathrm{Fe} + \mathrm{H_2} \rightleftarrows (\mathrm{PNP})(\mathrm{CO})(\mathrm{H})\mathrm{Fe}-\mathrm{H}$	ΔG_{H2} = -3.8 ± 0.3 kcal·mol^{-1}	4D
$[(\mathrm{PNP})\mathrm{Co}-\mathrm{N_2}][\mathrm{BAr_4^F}] + (\mathrm{PNP})(\mathrm{CO})(\mathrm{H})\mathrm{Ru}-\mathrm{H} \rightleftarrows (\mathrm{PNP})\mathrm{Co}-\mathrm{H} + [(\mathrm{PNP})(\mathrm{CO})(\mathrm{H})\mathrm{Ru}][\mathrm{BAr_4^F}]$	ΔG_{HT} = 1.5 ± 0.3 kcal·mol^{-1}	4E
$(\mathrm{PNP})\mathrm{Co}-\mathrm{H} + [(\mathrm{PNP})(\mathrm{CO})(\mathrm{H})\mathrm{Ru}][\mathrm{BAr_4^F}] \rightleftarrows [(\mathrm{PNP})\mathrm{Co}-\mathrm{N_2}][\mathrm{BAr_4^F}] + (\mathrm{PNP})(\mathrm{CO})(\mathrm{H})\mathrm{Ru}-\mathrm{H}$	ΔG_{HT} = -1.6 ± 0.1 kcal·mol^{-1}	4E
$(\mathrm{PNP})\mathrm{Co}-\mathrm{H} \rightleftarrows (\mathrm{PNP})\mathrm{Co^+} + \mathrm{H^-}$	ΔG_{H-} = 43.6 ± 0.5 kcal·mol^{-1}	4E
$(\mathrm{PNP})(\mathrm{CO})(\mathrm{H})\mathrm{Fe}-\mathrm{H} \rightleftarrows (\mathrm{PNP})(\mathrm{CO})(\mathrm{H})\mathrm{Fe^+} + \mathrm{H^-}$	ΔG_{H-} = 45.5 ± 0.4 kcal·mol^{-1}	*
$[(^*\mathrm{PNP})(\mathrm{CO})(\mathrm{H})\mathrm{Fe}-\mathrm{H}][\mathrm{Li}] \rightleftarrows (^*\mathrm{PNP})(\mathrm{CO})(\mathrm{H})\mathrm{Fe} + \mathrm{H^-} + \mathrm{Li^+}$	ΔG_{H-} = 27.7 ± 0.4 kcal·mol^{-1}	* **
$[(^*\mathrm{PNP})(\mathrm{CO})(\mathrm{H})\mathrm{Ru}-\mathrm{H}][\mathrm{Li}] \rightleftarrows (^*\mathrm{PNP})(\mathrm{CO})(\mathrm{H})\mathrm{Ru} + \mathrm{H^-} + \mathrm{Li^+}$	ΔG_{H-} = 30.0 ± 0.3 kcal·mol^{-1}	* **

*Values are extrapolated, see main text for equations.

**Values assume ion-pairing, and hence pK_{ip} were used to determine the hydricity. To estimate the hydricity in the absence of ion-pairing, the pK_a should be employed.

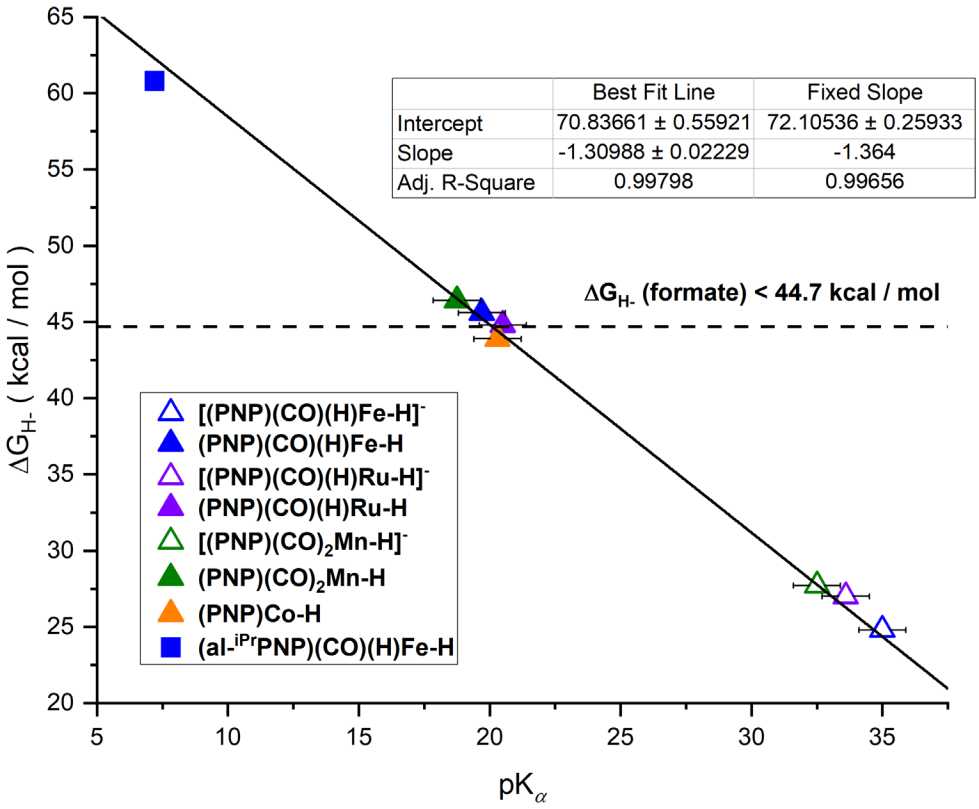

Figure S56. Plot of hydricity versus pK_α. See main text for references. Black line corresponds to the fixed slope equation.

I. Correlation of pK_a or ΔG_{H-} with ΔG_{H2} for $[Ni(PR_2NR'_2)_2H]^+$ complexes.

Dubois and co-workers have developed and extensively studied the thermodynamic parameters of $P^R_2N^R_2$-ligated Ni complexes (in MeCN).[31] The pK_a, equilibrium with H_2, and hydricity are all related akin to the complexes described in the text, as follows:

$[H\mathrm{Ni}^{II}(P^R_2N^{R'}_2)_2]^+ + H^+ \rightleftharpoons [\mathrm{Ni}^0(P^R_2N^{R'}NH^{R'})_2]^{2+}$	$-1.364pK_a$	Eq 30
$[\mathrm{Ni}^0(P^R_2N^{R'}NH^{R'})_2]^{2+} \rightleftharpoons [\mathrm{Ni}^{II}(P^R_2N^{R'}_2)_2]^{2+} + H_2$	$-\Delta G_{H2}$	Eq 31
$H_2 \rightleftharpoons H^+ + H^-$	$\Delta G_{H2(het)} = 76.0\ \mathrm{kcal \cdot mol^{-1}}$ (ref [32])	Eq 32
$[H\mathrm{Ni}^{II}(P^R_2N^{R'}_2)_2]^+ \rightleftharpoons [\mathrm{Ni}^{II}(P^R_2N^{R'}_2)_2]^{2+} + H^-$	$\Delta G_{H-} = -1.364pK_a - \Delta G_{H2} + 76.0$	Eq 33

Note, protonation of the ligand (eq 30) is concomitant with a second protonation, whereby the Ni-H is the proton source and the Ni(II) is reduced to Ni(0). Because other thermochemical cycles can be used to obtain the hydricity, not all reported complexes have the pertinent thermochemical data to directly compare with the system of the main text. In the table below, the pertinent thermochemical data for all complexes are presented. In some instances, two of the three thermochemical parameters were given in the original report, and the equations above were used to deduce the third. This data is used to generate the plots of Figures S52-S53.

R	R'	Hydricity (kcal·mol^{-1})	pK_a[d]	ΔG_{H2} (kcal·mol^{-1})	References
Cy	Ph	63.7[a]	(6.0)[e]	4.1	31,33
Cy	^{t}Bu	61.0[b]	(16.8)[e]	-7.9	34
Cy	Bn	60.9[c]	13.4	-3.1	35-36
Ph	Ph	59.1[a]	6.0	8.8	33 (8.8 not 9 from ref 33,35)
Ph	Bn	57.2[a]	11.8	2.7	35
Bn	Ph	59.4[a]	(6.0)[e]	8.4	33
2-phenylethyl	Ph	57.8[a]	(6.0)[e]	10	33
2,4,4-trimethylpentyl	Ph	57.6[a]	(6.0)[e]	10.2	33
^{n}Bu	Ph	57.1[a]	(6.0)[e]	10.7	33
Me	Ph	54.0[a]	6.0	13.8	37
Cy	$CH_2C_6H_4OMe$	58.8[b]	(15.2)[e]	-3.6	36,38
Cy	BnCOOMe	61.3[b]	12.5	-2.4	36,38
Cy	Bn-Ala-OMe	60.8[b]	12.8	-2.3	36,38
Cy	Bn-Phe-OMe	60.8[b]	12.5	-1.9	36,38

Table 1. Thermochemical parameters for $[HNi(P^R_2N^{R'}_2)_2]^+$. [a]Hydricity measured via H_2 heterolysis.[32] [b]Hydricity measured via potential-pK_a.[32] [c]Hydricity measured via pK_a-H_2 addition.[32] [d]pK_a corresponds to eq 30. [e]Values in parentheses were calculated from eqs 30-33.

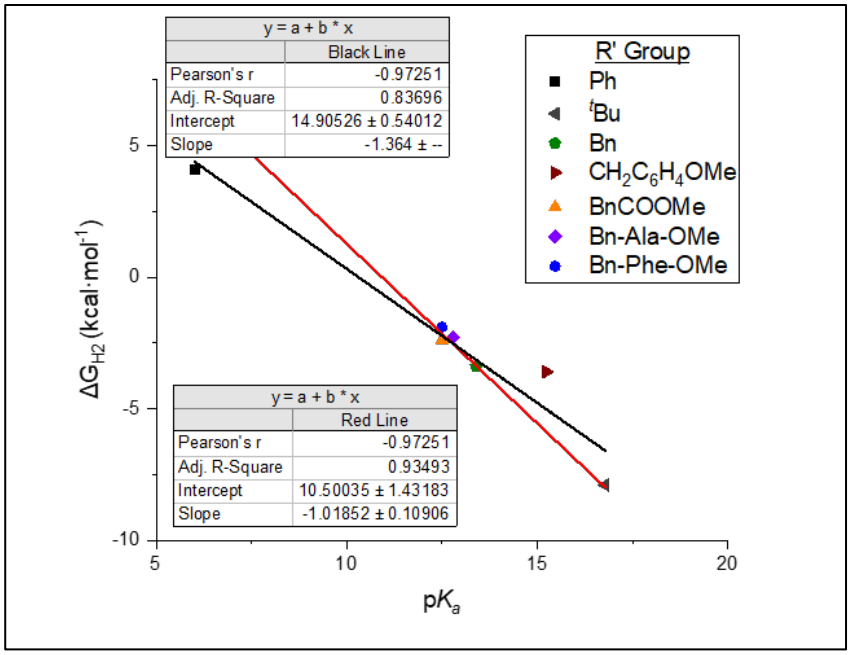

Figure S57. Plot of ΔG_{H2} vs. pK_a for **[HNi(P$^{R}_2$N$^{R'}_2$)$_2$]$^+$** (R = Cy) as the R' group on the amine is varied. Two fits of the data are shown: the red line corresponds to a linear fit of the data, and the black line corresponds to a linear fit of the data with a fixed slope of -1.364.

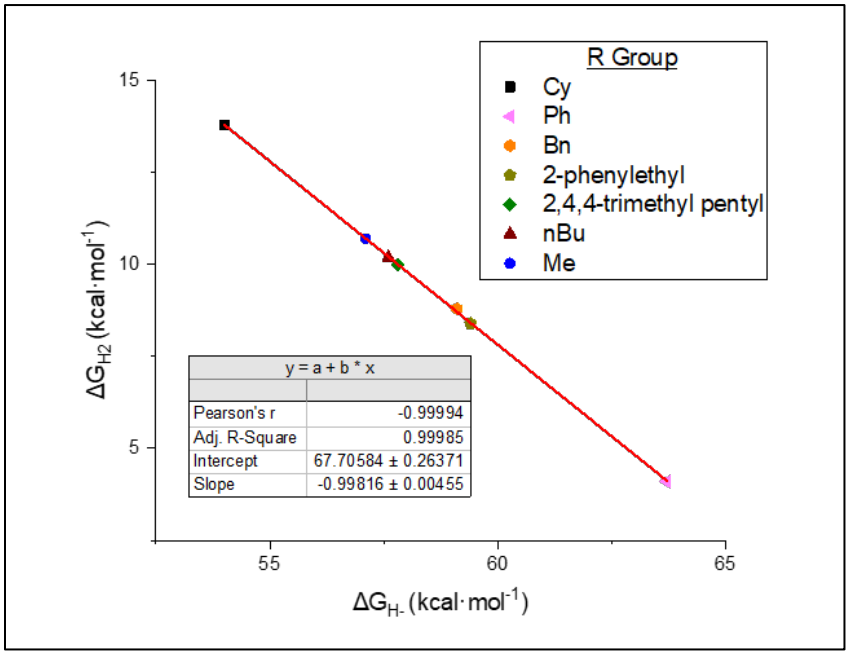

Figure S58. Plot of ΔG_{H2} vs. ΔG_{H-} for **[HNi(P$^{R}_2$N$^{R'}_2$)$_2$]$^+$ (R' = Ph)** as the R group on the phosphine is varied.

J. Thermochemical Data For (^{al}PNP)Fe(H)(CO) System.

The pK_a, hydricity, and equilibrium with H_2 for the species shown below has recently been published.[39]

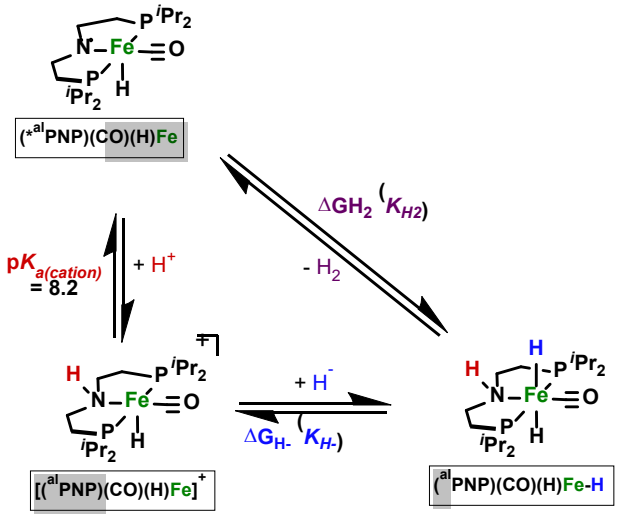

Figure S59. Thermochemical parameters of a related Fe species. The published pK_a corresponds to a pK_{ip}.

The equilibrium with H_2 took into account the solution concentration of H_2, and hence differs from the K_{eq} values we measure, which correspond to an equilibrium under 1 atm of H_2. Using the data in Table S1 of reference [39], a van't Hoff plot can be constructed under ideal conditions of 1 atm H_2 pressure (Figure S56). At 298 K, this gives a value of -1.9 kcal·mol^{-1} for ΔG_{H2}. This gives a hydricity value of 59.3 kcal·mol^{-1}.

The pK_α is determined as described earlier, using data from [26]. This gives a pK_α value of 7.2. Using this value, and -1.9 kcal·mol^{-1} for ΔG_{H2} gives a hydricity value of 60.8 kcal·mol^{-1}.

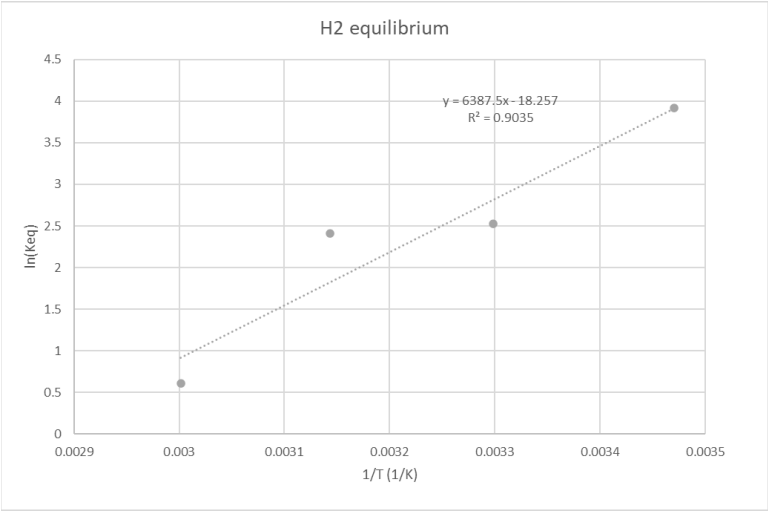

Figure S60. Van't Hoff plot for K_{H2}. Data from reference [39].

Section 5: References

(1) Yakelis, N. A.; Bergman, R. G., *Organometallics* **2005,** *24*, 3579-3581.
(2) Brookhart, M.; Grant, B.; A. F. Volpe, J., *Organometallics* **1992,** *11*, 3920-3922.
(3) Del Castillo, T. J.; Thompson, N. B.; Peters, J. C., *J. Am. Chem. Soc.* **2016,** *138*, 5341-50.
(4) Saame, J.; Rodima, T.; Tshepelevitsh, S.; Kutt, A.; Kaljurand, I.; Haljasorg, T.; Koppel, I. A.; Leito, I., *J. Org. Chem.* **2016,** *81*, 7349-61.
(5) Kawatsura, M.; Hartwig, J. F., *Organometallics* **2001,** *20*, 1960-1964.
(6) Bauer, J. O.; Leitus, G.; Ben-David, Y.; Milstein, D., *ACS Catal.* **2016,** *6*, 8415-8419.
(7) Gnanaprakasam, B.; Zhang, J.; Milstein, D., *Angew. Chem. Int. Ed. Engl.* **2010,** *49*, 1468-71.
(8) Anaby, A.; Butschke, B.; Ben-David, Y.; Shimon, L. J. W.; Leitus, G.; Feller, M.; Milstein, D., *Organometallics* **2014,** *33*, 3716-3726.
(9) Langer, R.; Diskin-Posner, Y.; Leitus, G.; Shimon, L. J. W.; Ben-David, Y.; Milstein, D., *Angew. Chem. Int. Ed.* **2011,** *50*, 9948-9952.
(10) Semproni, S. P.; Milsmann, C.; Chirik, P. J., *J. Am. Chem. Soc.* **2014,** *136*, 9211-24.
(11) Scheuermann, M. L.; Semproni, S. P.; Pappas, I.; Chirik, P. J., *Inorg. Chem.* **2014,** *53*, 9463-5.
(12) Rummelt, S. M.; Zhong, H.; Léonard, N. G.; Semproni, S. P.; Chirik, P. J., *Organometallics* **2019,** *38*, 1081-1090.
(13) Mathis, C. L.; Geary, J.; Ardon, Y.; Reese, M. S.; Philliber, M. A.; VanderLinden, R. T.; Saouma, C. T., *J. Am. Chem. Soc.* **2019,** *141*, 14317-14328.
(14) Jeletic, M. S.; Hulley, E. B.; Helm, M. L.; Mock, M. T.; Appel, A. M.; Wiedner, E. S.; Linehan, J. C., *ACS Catalysis* **2017,** *7*, 6008-6017.
(15) Krause, L.; Herbst-Irmer, R.; Sheldrick, G. M.; Stalke, D., *J. Appl. Cryst.* **2015,** *48*, 3-10.
(16) Sheldrick, G. M., *Acta Cryst.* **2015,** *71*, 3-8.
(17) Sheldrick, G. M., *Acta Cryst.* **2015,** *71*, 3-8.
(18) Müller, P., *Crystallography Reviews* **2009,** *15*, 57-83.
(19) Khaskin, E.; Iron, M. A.; Shimon, L. J. W.; Zhang, J.; Milstein, D., *J. Am. Chem. Soc.* **2010,** *132*, 8542-8543.
(20) Langer, R.; Leitus, G.; Ben-David, Y.; Milstein, D., *Angew. Chem. Int. Ed.* **2011,** *50*, 2120-2124.
(21) Mock, M. T.; Pierpont, A. W.; Egbert, J. D.; O'Hagan, M.; Chen, S.; Bullock, R. M.; Dougherty, W. G.; Kassel, W. S.; Rousseau, R., *Inorg. Chem.* **2015,** *54*, 4827-39.
(22) Zell, T.; Butschke, B.; Ben-David, Y.; Milstein, D., *Chem. Eur. J.* **2013,** *19*, 8068-72.
(23) Crossland, J. L.; Tyler, D. R., *Coordination Chemistry Reviews* **2010,** *254*, 1883-1894.
(24) Kaljurand, I.; Rodima, T.; Pihl, A.; Mäemets, V.; Leito, I.; Koppel, I. A.; Mishima, M., *J. Org. Chem.* **2003,** *68*, 9988-9993.
(25) Fuoss, R. M., *J. Am. Chem. Soc.* **1958,** *80*, 5059-5061.
(26) Rodima, T.; Kaljurand, I.; Pihl, A.; Mäemets, V.; Leito, I.; Koppel, I. A., *J. Org. Chem.* **2002,** *67*, 1873-1881.
(27) Abdur-Rashid, K.; Fong, T. P.; Greaves, B.; Gusev, D. G.; Hinman, J. G.; Landau, S. E.; Lough, A. J.; Morris, R. H., *J. Am. Chem. Soc.* **2000,** *122*, 9155-9171.
(28) Schlenker, K.; Christensen, E. G.; Zhanserkeev, A. A.; McDonald, G. R.; Yang, E. L.; Lutz, K. T.; Steele, R. P.; Vanderlinden, R. T.; Saouma, C. T., *Acs Catalysis* **2021,** *11*, 8358–8369.
(29) Morris, R. H., *J. Am. Chem. Soc.* **2014,** *136*, 1948-59.
(30) Brereton, K. R.; Jadrich, C. N.; Stratakes, B. M.; Miller, A. J. M., *Organometallics* **2019,** *38*, 3104-3110.
(31) Galan, B. R.; Schoffel, J.; Linehan, J. C.; Seu, C.; Appel, A. M.; Roberts, J. A.; Helm, M. L.; Kilgore, U. J.; Yang, J. Y.; DuBois, D. L.; Kubiak, C. P., *J. Am. Chem. Soc.* **2011,** *133*, 12767-79.

(32) Wiedner, E. S.; Chambers, M. B.; Pitman, C. L.; Bullock, R. M.; Miller, A. J.; Appel, A. M., *Chem Rev* **2016,** *116*, 8655-92.
(33) Kilgore, U. J.; Stewart, M. P.; Helm, M. L.; Dougherty, W. G.; Kassel, W. S.; DuBois, M. R.; DuBois, D. L.; Bullock, R. M., *Inorg. Chem.* **2011,** *50*, 10908-18.
(34) Yang, J. Y.; Smith, S. E.; Liu, T.; Dougherty, W. G.; Hoffert, W. A.; Kassel, W. S.; Rakowski DuBois, M.; DuBois, D. L.; Bullock, R. M., *J. Am. Chem. Soc.* **2013,** *135*, 9700-12.
(35) Fraze, K.; Wilson, A. D.; Appel, A. M.; DuBois, M. R.; DuBois, D. L., *Organometallics* **2007,** *26*, 3918-3924.
(36) Lense, S.; Ho, M.-H.; Chen, S.; Jain, A.; Raugei, S.; Linehan, J. C.; Roberts, J. A. S.; Appel, A. M.; Shaw, W., *Organometallics* **2012,** *31*, 6719-6731.
(37) Wiese, S.; Kilgore, U. J.; DuBois, D. L.; Bullock, R. M., *ACS Catalysis* **2012,** *2*, 720-727.
(38) Jain, A.; Lense, S.; Linehan, J. C.; Raugei, S.; Cho, H.; DuBois, D. L.; Shaw, W. J., *Inorg. Chem.* **2011,** *50*, 4073-85.
(39) Curley, J. B.; Smith, N. E.; Bernskoetter, W. H.; Ertem, M. Z.; Hazari, N.; Mercado, B. Q.; Townsend, T. M.; Wang, X., *ACS Catalysis* **2021,** *11*, 10631-10646.